

**WEAR BEHAVIOUR OF COATED CARBIDE TOOLS
DURING MACHINING OF Ti6Al4V AEROSPACE ALLOY**

**WEAR BEHAVIOUR OF COATED CARBIDE TOOLS DURING MACHINING
OF Ti6Al4V AEROSPACE ALLOY**

By

Mohammad Shariful Islam Chowdhury, B.Sc, M.Sc.

(Mechanical Engineering, Islamic University of Technology, Bangladesh)

A Thesis

Submitted to the School of Graduate Studies

in Partial Fulfilment of the Requirements

for the Degree

Master of Applied Science

McMaster University, Hamilton, Ontario

© Copyright by Mohammad Shariful Islam Chowdhury, July 2016

MASTER OF APPLIED SCIENCE (2016)

(Mechanical Engineering)

McMaster University

Hamilton, Ontario

**TITLE: WEAR BEHAVIOUR OF COATED CARBIDE TOOLS
DURING MACHINING OF Ti6Al4V AEROSPACE ALLOY**

AUTHOR: Mohammad Shariful Islam Chowdhury, B.Sc., M.Sc.

SUPERVISOR: Dr. Stephen C. Veldhuis
Department of Mechanical Engineering
McMaster University

NUMBER OF PAGES: xvii, 152

Abstract

Titanium alloys are increasingly becoming the material of choice for a wide range of applications. They have found their way into aerospace, biomedical and automotive industries due to their superior properties such as good strength-to-weight ratio, high corrosion resistance and bio-compatibility. However, machining of titanium alloys has proven difficult over the years owing to several inherent properties of these materials. Titanium has a very strong chemical affinity and, therefore, has a tendency to weld or stick to the cutting tool during machining, which results in chipping and premature tool failure. Their low thermal conductivity causes high temperatures to be generated at the tool/workpiece interface, affecting tool life adversely. Additionally, their high strength at elevated temperature and low modulus of elasticity further impairs their machinability. Researchers have yet to find an effective strategy to overcome these challenges and improve the tool life during the machining of titanium alloys. The present research aims to find suitable tool coatings that will increase tool life during the machining Ti6Al4V, a prominent titanium alloy.

The alloy Ti6Al4V make up 60% of all titanium production [1]. Thus, the present research is focused on this alloy. Standard industrial practice for machining titanium alloys still revolves around the use of uncoated cemented carbide tools, although recently TiAlN coatings are being recommended by tool manufacturers. However, both uncoated and TiAlN coated cemented carbide tools have yet to achieve the desired tool life and

productivity. Hence, a variety of coatings have been investigated in this research study and are compared with uncoated and TiAlN coated carbide tools to find a more effective tool coating that will improve tool life during the machining of Ti6Al4V.

The coatings tested were chosen with the expectation that beneficial tribofilms could be generated on a tool's surface due to the coatings' self-adaptability characteristics under the cutting conditions experienced during machining. If the coating is properly engineered, these tribofilms have the potential to improve tool life significantly [2]. Experimental studies were carried out and the results showed that TiB₂, CrN/WN and CrN/ZrN coated cemented carbide tools outperformed standard uncoated and TiAlN coated tools during Ti6Al4V machining. Detailed analysis of the best coatings revealed the beneficial tribofilms that each coating generated and how they affected tool wear.

Effect of deposition parameters on TiB₂ (best coating) and chip breaker profile of the tools were also studied. Results showed that tools with positive chip breaker profile gave a better tool life and that low hardness TiB₂ coating obtained through varying deposition parameters was more suitable for machining Ti6Al4V alloy compared to harder variants of TiB₂ coating. End milling tests with TiB₂ coated tools revealed that the coating was not as effective at increasing tool life as it was in turning.

Acknowledgements

First and foremost, I would like to express my deepest gratitude to my supervisor Dr. Stephen C. Veldhuis for his continuous guidance, helpful suggestions and supervision at all stages of this thesis work. I am thankful to him for giving me the opportunity to be a part of the McMaster Manufacturing Research Institute (MMRI).

Additionally, I would like to express my heartfelt gratitude to Dr. German Fox-Rabinovich for his constructive suggestions and detailed guidance in every step of this research work. I would like to thank and acknowledge the MMRI team, especially Terry Wagg, Dr. Maryam Aramesh, Dr. Julia Dosbaeva, Shahereen Chowdhury, Jeremy Boyd, Simon Oomen-Hurst and my fellow students for their guidance and help in everyday tasks.

I would also like to extend my special thanks to Dr. Kenji Yamamoto, Senior Researcher at Kobe Steel Ltd., for all his help and suggestions with the coating selection. Thanks also to Danielle Covelli, Research Lab Technician, Biointerfaces Institute, McMaster University and Victoria Jarvis, XRD2/XRD3 Specialist, MAX Diffraction Facility, McMaster University for their help with XPS and XRD experimental studies and analyses.

Finally, I thank my wife, my son and my family for their understanding, patience and support. None of this would have been possible without their endless love, sacrifice and support over the years.

Although I have given my best effort to complete this thesis paper, I seek excuse for any mistake in this report.

Table of Contents

Abstract	iii
Acknowledgements	v
List of Figures	ix
List of Tables	xiv
Nomenclature	xvii
Chapter 1: Introduction	1
1.1 Motivation	1
1.2 Research Objectives	3
1.3 Thesis Outline	3
Chapter 2: Literature Review	5
2.1 Machining.....	5
2.1.1 Common Machining Terminologies	6
2.2 Tool Wear.....	7
2.2.1 Types of Tool Wear	8
2.2.2 Tool Wear Mechanisms	12
2.3 Coating	13
2.3.1 Necessity of Coatings and Coating Techniques.....	13
2.3.2 Classification of Hard PVD Coatings	16

2.3.3	Tribofilms	21
2.4	Titanium alloys.....	21
2.4.1	Classification of Titanium Alloys.....	22
2.4.2	Machinability Issues of Titanium Alloys.....	26
2.4.3	Cutting Tools and Substrate Material used in Titanium Machining.....	35
2.4.4	Wear Mechanisms of Cemented Carbide Tools in Titanium Machining	41
2.4.5	Application of Coated Carbide Tools in Titanium Machining	47
Chapter 3:	Experimental Details	53
3.1	Introduction	53
3.2	Cutting Tool and Workpiece Properties.....	53
3.3	Experimental Setup for Cutting and Process Parameters.....	56
3.4	Experimental Methodology.....	60
3.5	Tool Life Study	62
3.6	Tool Coatings	64
3.6.1	Coating Details.....	64
3.6.2	Techniques for Coating Investigation.....	66
3.7	Chip Analysis	68
Chapter 4:	Results and Discussion.....	69
4.1	Identification of a Benchmark Tool for Turning Operations	69

4.2	Identification of Coated Turning Tools Outperforming Benchmark	73
4.3	Material Characterization of Most Effective Coatings	76
4.3.1	TiB ₂ Coated Tool	77
4.3.2	CrN/WN Coated Tool	99
4.4	Further Machinability Analysis of TiB ₂ Coated Turning Tool.	110
4.5	Investigation of the Effect of Chip Breaker Profile and Coating Hardness on the Performance of TiB ₂ Coated Tool.....	116
4.5.1	Chip Breaker Profile.....	117
4.5.2	Effect of Coating Hardness.....	127
4.6	Tool Wear Studies for End Milling Operation.....	129
	Chapter 5: Conclusion.....	135
	Chapter 6: Future Work	140
	References	142

List of Figures

<i>Figure 1: Usage of titanium in aircraft engine over the years [based on [2]]</i>	2
<i>Figure 2: Cross-sectional view of machining process [based on [84]]</i>	5
<i>Figure 3: Four factors influencing tool wear [based on [3]]</i>	8
<i>Figure 4: Typical stages in flank wear [based on [85]]</i>	9
<i>Figure 5: Types of tool wear [reprinted from [86] with permission]</i>	11
<i>Figure 6: Impacts of coating during cutting [based on [86]]</i>	14
<i>Figure 7: Influences and requirements of substrate and coating [based on [87]]</i>	15
<i>Figure 8: Two allotropic forms of titanium (a) Body centered cubic (β structure) (b) Hexagonally closely packed (α) structure [based on [21]]</i>	23
<i>Figure 9: Distribution of thermal load when machining Ti6Al4V and Steel CK45 [based on [16]]</i>	28
<i>Figure 10: Strength-density behaviour comparison between two titanium alloys and three steel as a function of temperature [reprinted from [21]with permission Taylor and Francis LLC,(http://www.tandfonline.com)]</i>	31
<i>Figure 11: Micrographs of saw toothed chips showing longitudinal mid-sections</i>	32
<i>Figure 12: Sequential events illustrating serrated chip formation during titanium machining [reprinted from [25] with permission from Elsevier]</i>	34
<i>Figure 13: Characteristic hot hardness of some tool material [reprinted from [88] with permission]</i>	36

<i>Figure 14: Relationship between adhesion area and cutting speed during dry milling of Ti6Al4V machining at feed: 0.1mm/tooth and depth of cut: 0.5 mm using K10 tool [Based on [47]]</i>	43
<i>Figure 15: Turning inserts used: (a) Geometry of the insert (b) CNMG432 roughing insert (c) CNMP432 roughing insert (d) CNGG432FS finishing insert</i>	53
<i>Figure 16: Chip Breaker profile: (a) CNMG432 (b) CNMP432</i>	54
<i>Figure 17: 4 Flute Fullerton Square End Mill</i>	55
<i>Figure 18: MCLN-5° Kennametal Kenloc™ Tool Holder</i>	56
<i>Figure 19: Experimental setup for turning operation</i>	57
<i>Figure 20: Dynamometer setup for collecting force readings during turning</i>	58
<i>Figure 21: Experimental setup for milling operation</i>	59
<i>Figure 22: Experimental Flow Chart</i>	61
<i>Figure 23: Microscopes used for tool wear studies (a) Mitutoyo Toolmaker Microscope (b) Nikon AZ100 Multizoom Microscope</i>	63
<i>Figure 24: Mounted chips</i>	68
<i>Figure 25: Tool wear curve for rough turning of uncoated and TiAlN coated tools</i>	70
<i>Figure 26: 3D images of worn tool after 1000 m cut: (a) uncoated insert</i>	70
<i>Figure 27: SEM image and EDS elemental maps of the worn rake surface of uncoated tool</i>	71
<i>Figure 28: SEM image and EDS elemental maps of the worn rake surface of TiAlN coated tool</i>	71
<i>Figure 29: XPS of rake surface of uncoated tool</i>	72

<i>Figure 30: Tool wear curve of uncoated and several coated tools for rough turning operation.....</i>	<i>74</i>
<i>Figure 31: Tool wear curve of uncoated and several coated tools for finish turning operation.....</i>	<i>75</i>
<i>Figure 32: 3D images of worn tool after 1000 m cut: (a) uncoated insert (b) TiB₂ coated insert [Provided by Kobe Steel Ltd.]</i>	<i>77</i>
<i>Figure 33: Tool wear curve for uncoated and TiB₂ coated tool for roughing operation..</i>	<i>78</i>
<i>Figure 34: Tool wear curve for uncoated and TiB₂ coated tool for finishing operation...</i>	<i>78</i>
<i>Figure 35: SEM images of rake surfaces of worn inserts after 3000 m cut: (a) Uncoated stool (b) TiB₂ coated tool</i>	<i>85</i>
<i>Figure 36: High Resolution XPS after 3 min Ar etching time on the built up of rake surface of uncoated tool after 3000 m cut.....</i>	<i>86</i>
<i>Figure 37: High Resolution XPS after 3 min Ar etching time on the built up of rake surface of TiB₂ coated tool after 3000 m cut</i>	<i>87</i>
<i>Figure 38: High Resolution XPS after 8 min Ar etching time on the built up of rake surface of uncoated tool after 3000 m cut.....</i>	<i>90</i>
<i>Figure 39: High Resolution XPS after 8 min Ar etching time on the built up of rake surface of TiB₂ coated tool after 3000 m cut</i>	<i>91</i>
<i>Figure 41: Average friction coefficients of various oxides [Based on [82]].....</i>	<i>96</i>
<i>Figure 40: SEM image and EDS elemental maps of the worn rake surface of TiB₂ tool..</i>	<i>96</i>
<i>Figure 42: High Resolution XPS after 3 min Ar etching time on flank surface of TiB₂ coated tool after 1000 m cut</i>	<i>97</i>

<i>Figure 43: High Resolution XPS after 3 min Ar etching time on rake surface of TiB₂ coated tool after 1000 m cut</i>	<i>98</i>
<i>Figure 44: 3D images of worn tool after 3000 m cut: (a) uncoated insert (b) CrN/WN coated insert.....</i>	<i>99</i>
<i>Figure 45: Tool wear curve for uncoated and CrN/WN coated tool for roughing operation.....</i>	<i>100</i>
<i>Figure 46: Tool wear curve for uncoated and CrN/WN coated tool for finishing operation</i>	<i>100</i>
<i>Figure 47: High Resolution XPS after 5 min Ar etching time on rake surface of CrN/WN coated tool after 1000 m cut</i>	<i>108</i>
<i>Figure 48: Cutting forces measured for 100 m cutting length with uncoated tool.....</i>	<i>111</i>
<i>Figure 49: Cutting forces measured for 100 m cutting length with TiB₂ coated tool</i>	<i>111</i>
<i>Figure 50: SEM image of chips during roughing with uncoated tool: (a) chip shape and (b) chip under-surface morphology</i>	<i>112</i>
<i>Figure 51: SEM image of chips during roughing with TiB₂ coated tool: (a) chip shape and (b) chip under-surface morphology</i>	<i>112</i>
<i>Figure 52: Chip cross-section for roughing tool: (a) Uncoated tool (b) TiB₂ coated tool</i>	<i>114</i>
<i>Figure 53: Tool wear curve for rough turning of uncoated and TiB₂ coated tools with general and positive chip breaker profile</i>	<i>118</i>
<i>Figure 55: Cutting forces measured for 100 m cutting length for TiB₂ coated tool with positive chip breaker profile</i>	<i>124</i>

<i>Figure 54: Cutting forces measured for 100 m cutting length for uncoated tool with positive chip breaker profile</i>	<i>124</i>
<i>Figure 56: SEM image of chips during roughing operation for uncoated tools: (a) general chip breaker profile (b) positive chip breaker profile</i>	<i>125</i>
<i>Figure 57: Chip cross-section for positive chip breaker tool: (a) Uncoated (b) TiB₂ coated tool.....</i>	<i>125</i>
<i>Figure 58: Tool wear curve for rough turning of three different TiB₂ coated tools with positive chip breaker profile</i>	<i>128</i>
<i>Figure 59: Average flank wear of uncoated, TiB₂-LHC and CrN/WN coated tool during end milling operation.....</i>	<i>130</i>
<i>Figure 60: Average rake wear of uncoated, TiB₂-LHC and CrN/WN coated tool during end milling operation.....</i>	<i>131</i>
<i>Figure 61: Average flank chipping of uncoated, TiB₂-LHC and CrN/WN coated tool during end milling operation</i>	<i>131</i>
<i>Figure 62: Average rake chipping of uncoated, TiB₂-LHC and CrN/WN coated tool during end milling operation</i>	<i>132</i>
<i>Figure 63: SEM image of one tooth of the worn four flute end mill tool after 50 m cut: (a) Uncoated (b) TiB₂-LHC coated</i>	<i>132</i>
<i>Figure 64: SEM image of chips during end milling for: (a) uncoated tool (b) TiB₂-LHC coated tool.....</i>	<i>133</i>
<i>Figure 65: SEM image of chip under-surface morphology: (a) Uncoated tool and (b) TiB₂-LHC coated tool</i>	<i>133</i>

List of Tables

<i>Table 1: Softening temperatures of some tool materials [12], [30]</i>	35
<i>Table 2: Effects of additive elements on carbide tools [16]</i>	40
<i>Table 3: Specifications of the Kennametal turning inserts</i>	54
<i>Table 4: Specifications of the Fullerton end mill</i>	55
<i>Table 5: Chemical composition of Ti6Al4V workpiece</i>	55
<i>Table 6: Physical and Mechanical properties of Ti6Al4V workpiece at room temperature</i>	56
<i>Table 7: Cutting parameters for turning operation</i>	57
<i>Table 8: Cutting parameters for end milling operation</i>	59
<i>Table 9: List of coatings investigated and expected tribo-oxides formation</i>	65
<i>Table 10: Optical images of Flank Wear vs. Length of Cut for uncoated and TiB₂ coated worn roughing inserts</i>	79-80
<i>Table 11: Optical images of Rake Wear vs. Length of Cut for uncoated and TiB₂ coated worn roughing inserts</i>	81-82
<i>Table 12: Optical images of Flank Wear vs. Length of Cut for uncoated and TiB₂ coated worn finishing inserts</i>	83
<i>Table 13: Optical images of Rake Wear vs. Length of Cut for uncoated and TiB₂ coated worn finishing inserts</i>	84

<i>Table 14: Relative percentages of the phases present on the built up of the rake surface of uncoated tool after 3000 m cut obtained from High Resolution XPS after 3 min Ar etching time.....</i>	<i>88</i>
<i>Table 15: Relative percentages of the phases present on the built up of the rake surface of TiB₂ coated tool after 3000 m cut obtained from High Resolution XPS after 3 min Ar etching time.....</i>	<i>89</i>
<i>Table 16: Relative percentages of the phases present on the built up of the rake surface of uncoated tool after 3000 m cut obtained from High Resolution XPS after 8 min Ar etching time.....</i>	<i>92</i>
<i>Table 17: Relative percentages of the phases present on the built up of rake surface of TiB₂ coated tool after 3000 m cut obtained from High Resolution XPS after 8 min Ar etching time.....</i>	<i>93</i>
<i>Table 18: Relative percentages of the phases present on the flank surface of TiB₂ coated tool after 1000 m cut obtained from High Resolution XPS after 3 min Ar etching time ...</i>	<i>97</i>
<i>Table 19: Relative percentages of the phases present on the rake surface of TiB₂ coated tool after 1000 m cut obtained from High Resolution XPS after 3 min Ar etching time ...</i>	<i>98</i>
<i>Table 20: Optical images of Flank Wear vs. Length of Cut for uncoated and CrN/WN coated worn roughing inserts</i>	<i>101-102</i>
<i>Table 21: Optical images of Rake Wear vs. Length of Cut for uncoated and CrN/WN coated worn roughing inserts</i>	<i>103-104</i>
<i>Table 22: Optical images of Flank Wear vs. Length of Cut for uncoated and CrN/WN coated worn finishing inserts</i>	<i>105</i>

<i>Table 23: Optical images of Rake Wear vs. Length of Cut for uncoated and CrN/WN coated worn finishing inserts</i>	<i>106</i>
<i>Table 24: Relative percentages of the phases present on the rake surface of CrN/WN tool after 1000 m cut obtained from High Resolution XPS after 5 min Ar etching time.....</i>	<i>109</i>
<i>Table 25: Average cutting forces measured for 100 m cutting length.....</i>	<i>110</i>
<i>Table 26: Calculated chip thickness ratio, shear plane angle and ratio of radial force to tangential force for uncoated and TiB₂ coated tool.....</i>	<i>114</i>
<i>Table 27: Properties of TiB₂ coating</i>	<i>115</i>
<i>Table 28: Optical images of Flank Wear vs. Length of Cut for uncoated tools with general and positive chip breaker profiles for worn roughing inserts</i>	<i>119</i>
<i>Table 29: Optical images of Rake Wear vs. Length of Cut for uncoated tools with general and positive chip breaker profiles for worn roughing inserts</i>	<i>120</i>
<i>Table 30: Optical images of Flank Wear vs. Length of Cut for TiB₂ coated tools with general and positive chip breaker profiles for worn roughing inserts</i>	<i>121</i>
<i>Table 31: Optical images of Rake Wear vs. Length of Cut for TiB₂ coated tools with general and positive chip breaker profiles for worn roughing inserts</i>	<i>122</i>
<i>Table 32: Average cutting forces measured for 100 m cutting length for different chip breaker profiles.....</i>	<i>123</i>
<i>Table 33: Calculated chip thickness ratio, shear plane angle and ratio of radial force to tangential force for different chip breaker profiles</i>	<i>126</i>

Nomenclature

HSS - High-speed steel

CBN - Cubic boron nitride

PCBN – Polycrystalline cubic boron nitride

PCD – Polycrystalline diamond

WC/Co – Tungsten carbide/Cobalt

BUE – Built up edge

f - Feed

V_c – Cutting speed

PVD – Physical vapor deposition

CVD – Chemical vapor deposition

XPS – X-Ray photoelectron spectroscopy

XRD – X-Ray diffraction

SEM – Scanning electron microscopy

EDS – Energy dispersive spectroscopy

Chapter 1: Introduction

1.1 Motivation

Over the years, the use of titanium and its alloys has increased significantly in various industries, especially aerospace, because of their superior properties. Figure 1 shows a comparison of the weight percentage of titanium used in aero-gas turbines from 1960 to 2010[3]. Titanium alloys are also used increasingly for numerous other industrial and commercial applications, such as petroleum refining, surgical implants, and marine applications.

Although machining industries have made noteworthy advances in addressing machinability issues of steel, cast irons and high temperature alloys (e.g., nickel-based alloys), no equivalent progress has been made when it comes to machining titanium and its alloys, owing to their unique characteristics such as low thermal conductivity, high chemical affinity towards tool materials, high temperature strength, low modulus of elasticity, etc. Hence, despite their increased usage, they are still expensive to machine when compared to other metals.

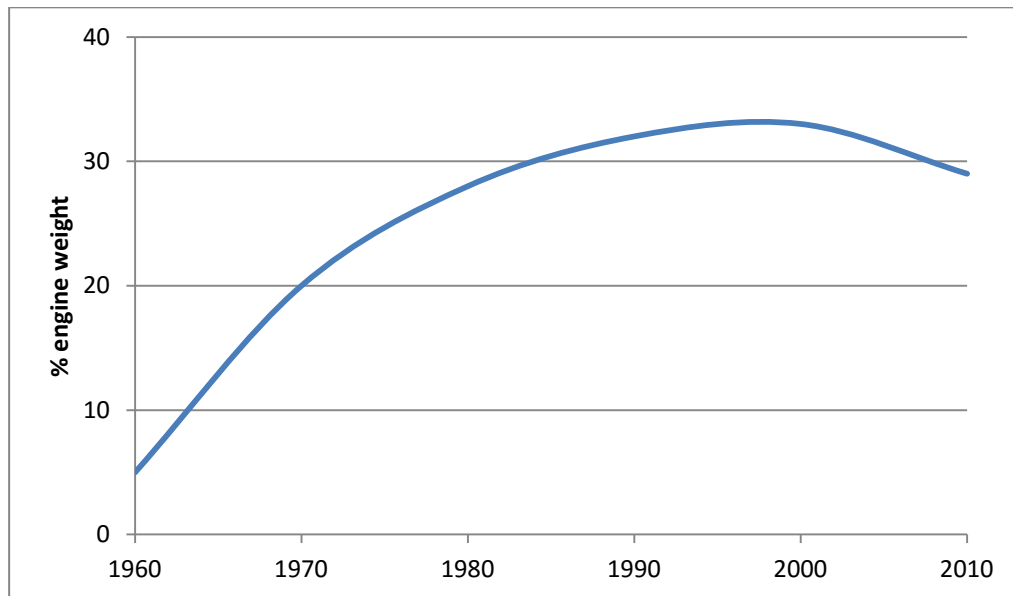


Figure 1: Usage of titanium in aircraft engine over the years[based on[3]]

In the present research, problems associated with titanium machining have been addressed. The research focused on the Ti6Al4V alloy specifically, as it accounts for 60% of all titanium production [1]. Uncoated straight grade cemented carbide tools are still the preferred choice for titanium machining as most coated carbide tools perform worse due to the reactivity of titanium with the coating materials. However, coating technology has advanced considerably over the years and with the evolution of coating deposition technologies, new coating designs have become possible [4]. Hence, the research aim was to find suitable tool coatings that will enhance tool life during machining of TiAl6V4 alloys, thereby reducing production cost and improving product quality.

1.2 Research Objectives

The main objectives of the present research are as follows:

1. Assessing the tool life of several new coating designs during machining of Ti6Al4V, and identify those coatings that enhance tool life in comparison to the industry standard.
2. Study the tribofilms formed on coatings during machining and their effect on tool wear.
3. Investigate why one particular coating performs better than another.
4. Examine the effect of different chip breaker profiles of turning inserts on tool wear and cutting forces.
5. Illustrate that changing deposition parameters of PVD process significantly affect coating properties like hardness which in turn affect tool wear.
6. Investigate whether the coatings that improve tool life for turning operations are effective in milling as well or not.

1.3 Thesis Outline

This thesis is arranged in five chapters. A brief summary of each of the chapters is as follows:

CHAPTER 1: INTRODUCTION – This chapter discusses the motivation behind the research and presents the research objectives.

CHAPTER 2: LITERATURE REVIEW – This chapter provides a detailed overview on different types of tool wear, tool wear mechanisms and tool coatings. A

detailed discussion on different grades of titanium and their alloys along with machinability issues is given. As well as, an extensive review of the research of contemporary scientists in related fields is provided.

CHAPTER 3: EXPERIMENTAL SETUP – This chapter presents a detailed account of the experimental setups for the cutting tests, including the experimental methodology, cutting tools and process parameters used. A list of the different coatings tested in this research along with different techniques used to characterize the coatings is also provided.

CHAPTER 4: RESULTS AND DISCUSSION – This chapter shows the experimental results and provides detailed explanations of the results and analyses that were carried out. This chapter is subdivided into several sections where each section discusses the results of a particular aspect of the research.

CHAPTER 5: CONCLUSION – This chapter summarizes the important findings of the research. The decisions derived based on the results of the study are elaborately stated.

CHAPTER 6: FUTURE WORK – In this chapter, recommendations regarding future research work related to the present study are provided.

Chapter 2: Literature Review

2.1 Machining

Machining, in relation to metal cutting, refers to various controlled metal removal processes that removes excess material from the parent metal in the form of chips to obtain a desired geometry. The most important machining operations are turning, milling and drilling. Cutting action is achieved by means of a relative motion between the tool and the workpiece. Figure 2 shows a cross-sectional view of the machining process.

In the present research, turning and milling operations were used. Turning refers to the machining operation in which a single point cutting tool removes unwanted material from a rotating workpiece to form a cylindrical shape. Whereas in milling, a rotating multi-teeth cutter moves relative to the workpiece to generate plain or straight surface.

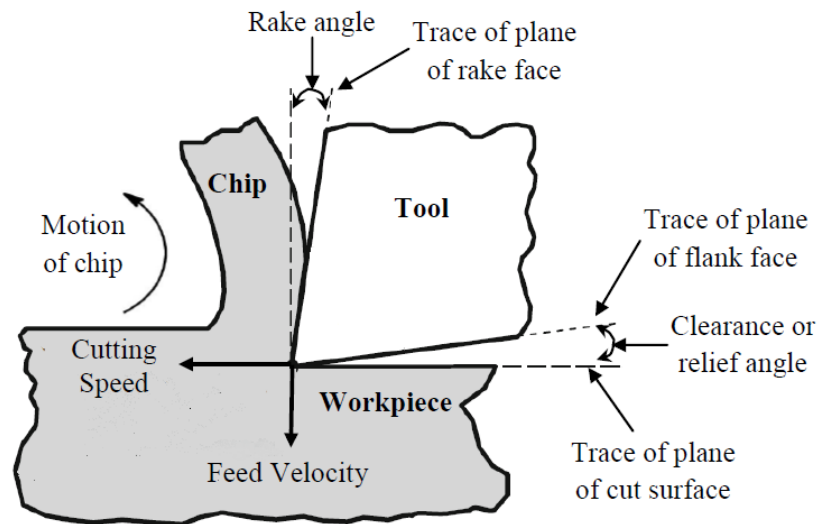


Figure 2: Cross-sectional view of the machining process [based on [86]]

2.1.1 Common Machining Terminologies

The common terminologies used in machining are defined below:

Cutting speed:

Cutting speed is defined as the rate at which the cutting edge of a cutting tool passes over the surface of the workpiece per unit time. Unit: m/min

Feed or Feed rate:

Feed refers to the relative velocity at which the cutting tool is advanced or fed into or across the workpiece. Unit: mm/rev or mm/min

Depth of cut:

Depth of cut refers to the thickness of the material layer removed in one pass by the cutting tool. To avoid confusion depth of cut is more accurately referred to as the uncut chip width. Unit: mm

Rake angle:

Rake angle is the angle between the top or rake face of the cutting tool and the normal to the workpiece at the cutting edge.

Clearance angle or relief angle:

Clearance angle is the angle between the bottom or flank face of the cutting tool and the tangent to the workpiece at the cutting edge.

2.2 Tool Wear

Tool wear is the change in shape of the tool from its original shape, during cutting, resulting from the gradual loss of tool material or deformation [5]. Relative sliding velocity, stresses and temperature generated at the contact surface dictates tool wear and is often described in terms of wear rate (volume loss per unit area per unit time). Tool wear is an inevitable phenomenon in all machining processes. It adversely affects productivity, dimensional accuracy, as well as product quality in most machining processes. So it is of primary concern to reduce tool wear in any machining process.

According to Yen et al. [6], there are four major factors that affect tool wear, which are depicted in Figure 3. Firstly, the physical properties (e.g. hardness, ductility, thermal conductivity) and microstructure of the workpiece material which affect the cutting forces and energy involved in the cutting action. Secondly, the choice of cutting parameters and coolant/lubricant delivery affects the nature of contact at the interface of tool and workpiece and influences the friction coefficient. Thirdly, there is the effect of the tool itself, such as the tool material (substrate and coating) as well as its geometric design, which must be appropriately chosen according to the specific machining operation. Lastly, the stability and dynamics of the machine tool system play a role.

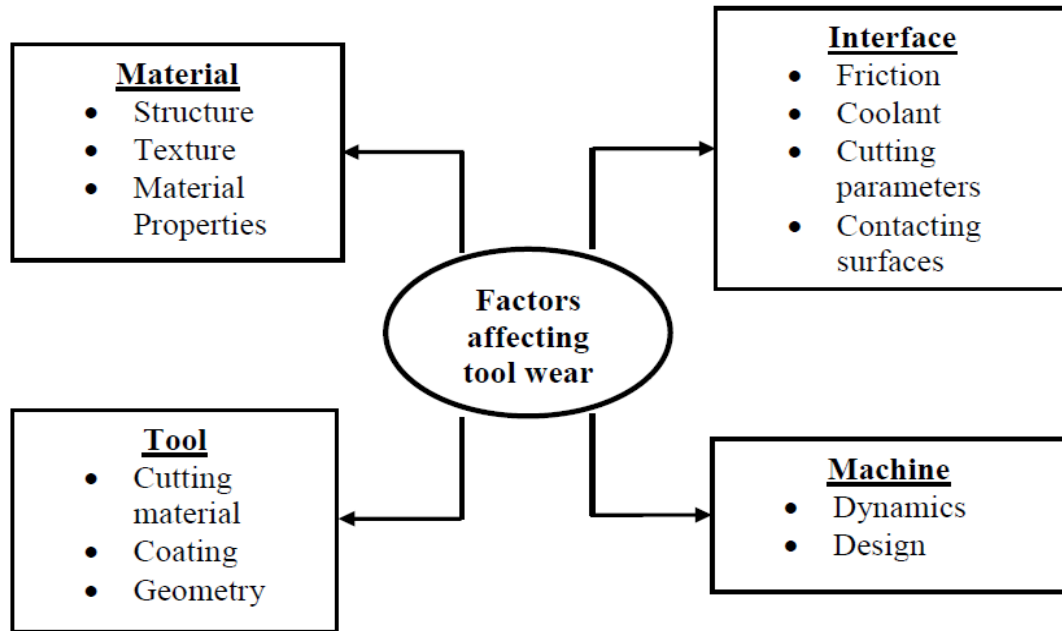


Figure 3: Four factors influencing tool wear [based on [3]]

2.2.1 Types of Tool Wear

According to the ISO standard 3685:1993, there are multiple types of wear. The most important wear types are flank wear and crater wear. The following types of tool wear are typically seen in cutting tools:

Flank Wear:

Flank wear appears in the form of a so-called *wear land* on the flank (relief) face of the tool. Flank wear reduces the relief angle on the clearance face of the tool consequently increasing frictional resistance [7]. It occurs primarily due to abrasive wear mechanisms. It results in reduced dimensional accuracy and poor surface integrity of the machined part. According to ISO 3685:1993 and ISO 8688-2:1989, tool life criterion is set to be 0.3 mm of flank wear. Figure 4 shows the characteristic tool wear curve.

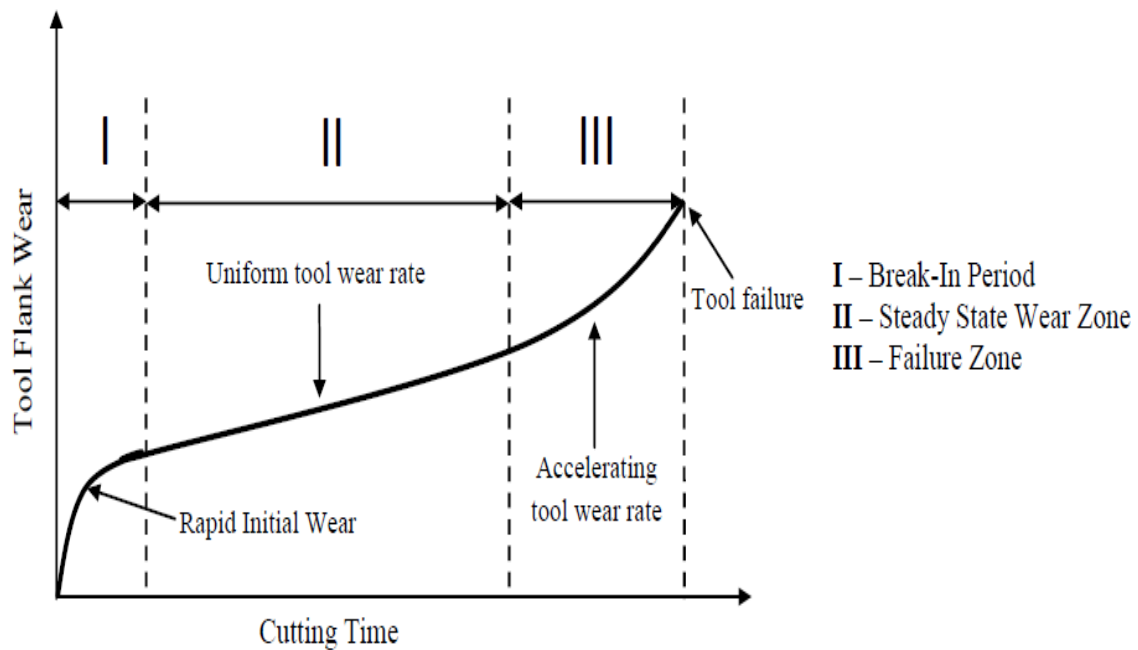


Figure 4: Typical stages in flank wear [based on [87]]

Crater Wear:

Crater wear results as a consequence of the sticking and sliding motion of the chips as they pass over the rake face of the tool at high temperature and stress. Crater wear decreases the strength of the cutting edge, enhancing the likelihood of tool breakage. Diffusion, abrasion and adhesion wear mechanisms typically dictates crater wear. While evaluating rake face wear, the crater depth, K_T , is most widely used.

Notch Wear:

Notch wear is a combined flank and rake face wear formed near the point where the major cutting edge and the workpiece intersect [8]. It is associated with the uncut chip width (depth of cut) selected. The notch or grooving at the outer edge of the wear land is due to oxidation as well as from hard or abrasive particles present on the workpiece. It may also occur due to strain hardening of previously machined surfaces.

Built up edge (BUE):

Built up edge refers to workpiece material adhering to the cutting edge of the tool altering the tool's geometry. BUE is never completely stable. The adhered material breaks off when it reaches a critical size often taking a part of the tool material with it leading to tool chipping.

Thermal and Mechanical fatigue:

These wear types occur due to cyclic loads. These cyclic loads can be either thermal or mechanical in nature. Thermal shocks, originating from alternate heating and cooling of the tool surface, are more prominent in milling due to interrupted nature of the cutting. Fluctuation of mechanical loads results from excessive feed rates. Cyclic loads thus initiates crack propagation along the cutting edge.

Chipping:

Chipping of the tools refers to large discrete particles of the tool material being removed. Discontinuous cutting conditions and built up edge formation promote tool chipping. Chipping occurs due to tools not having the strength to handle cyclic loads. It may also occur as a consequence of the brittleness of the tools.

Plastic Deformation:

Plastic deformation of the cutting edge occurs when the tool is subjected to high temperature and stresses in excess of the yield strength of the tool material. High cutting forces, excessive feed and speed promotes deformation wear.

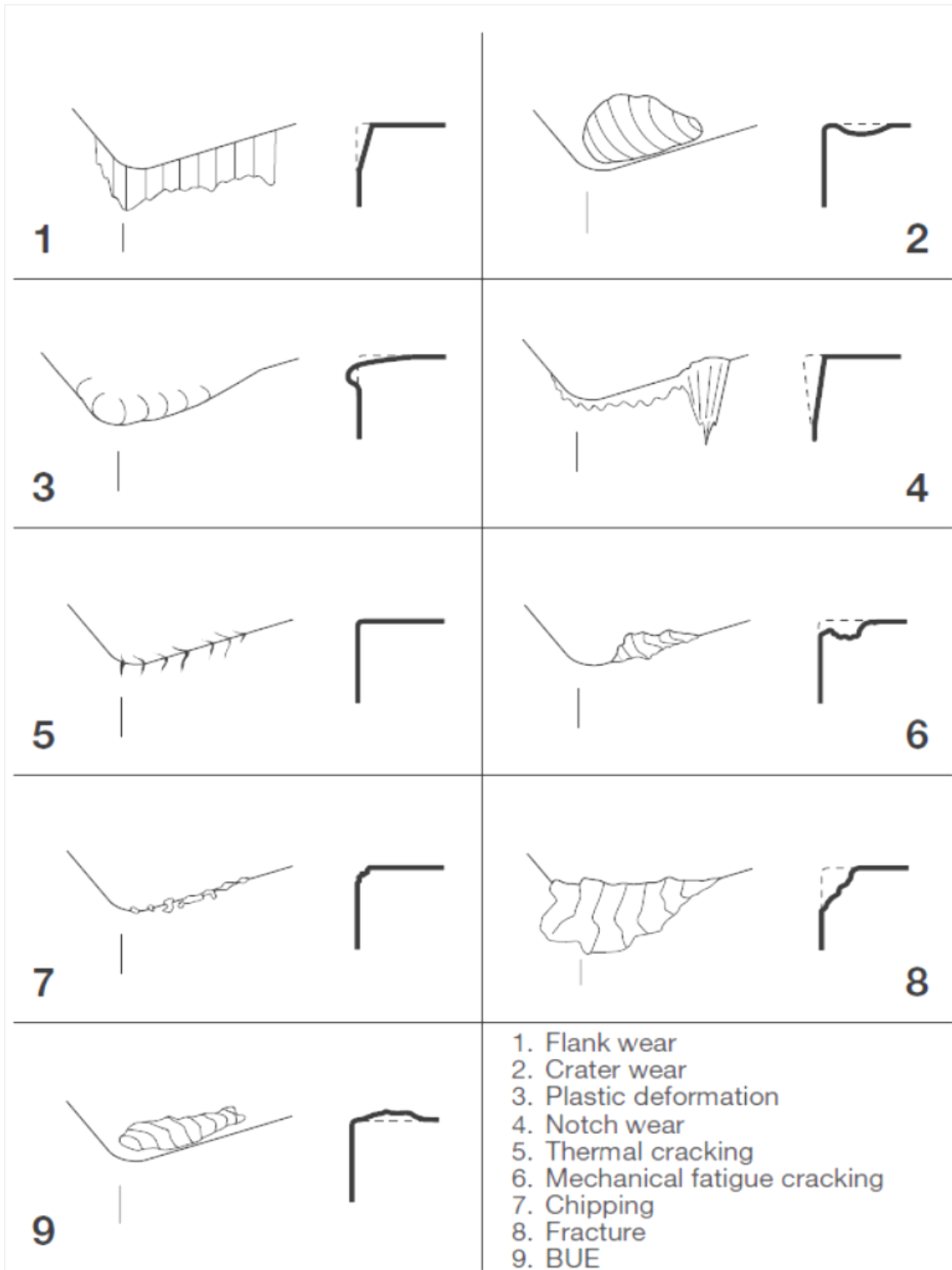


Figure 5: Types of tool wear [reprinted from [88] with permission]

2.2.2 Tool Wear Mechanisms

There are different mechanisms by which wear can occur. The typical mechanisms responsible for wear of cutting tools are briefly described below. The influence of one or more of these mechanisms depends on the specifics of the cutting process (microstructure of the workpiece material, continuous vs. interrupted cutting, maximum temperature/stress acting on the tool).

Abrasive Wear:

Abrasive wear occurs when hard abrasive particles present in the workpiece material scratches or scores the tool surface. Abrasion occurs primarily on the flank face of the tool. Such wear is not uniform in nature and appears at various positions across the land of the tool. Abrasion wear volume is typically higher than adhesion wear volume.

Adhesion Wear:

Due to high temperatures and pressures generated during cutting, workpiece material often adheres to the tool surface. The adhered material breaks off at intervals taking tool fragments along with it. The adhered material is referred to as built up edge when it reaches a significant amount. This form of tool wear is commonly known as adhesion or attrition wear and is attributed to a very rough surface on the tool land and face. It is prevalent on both flank and rake faces. Wear volumes associated with adhesion wear are generally low.

Diffusion Wear:

Diffusion wear occurs due to the chemical interaction between the tool and workpiece. At high temperatures, tool constituents diffuse into the workpiece material or

vice versa resulting in a smooth type of wear. The diffusion rate is dependent on the chemical affinity between the tool and work material, cutting temperature and the concentration gradient. Diffusion rates increase exponentially with temperature.

Oxidation Wear:

Oxidation wear occurs near the tool surface and is due to oxidation of tool constituents like tool binder. At high temperatures and pressures, oxygen reacts with tool material resulting in this type of wear. Oxidation wear typically results in depth-of-cut notch wear, which is a localized, severe wear corresponding to the point of maximum depth of cut (uncut chip width).

Fatigue Wear:

Fatigue wear can be differentiated into two types: mechanical and thermal fatigue. Mechanical fatigue occurs due to alternating compressive and tensile stresses whereas thermal fatigue happens due to cyclic heating and cooling of the tool surface. These cyclic loadings promote crack propagation.

2.3 Coating

2.3.1 Necessity of Coatings and Coating Techniques

Machining in general generates high temperatures during cutting. The heat generated is dissipated into the chip, tool and workpiece. Over the years, coatings have been applied to cutting tools that are able to reduce friction between the tool-chip or tool-workpiece interfaces thereby minimizing cutting temperature. It is important to understand how coatings behave with different tool and work material combinations as

well as the effect they have on cutting temperature generation. Figure 6 illustrates the influences that coatings may have during cutting. Coatings, therefore, should be designed in such a way that they are able to withstand the harsh machining conditions, provide wear resistance and serve as a thermal barrier.

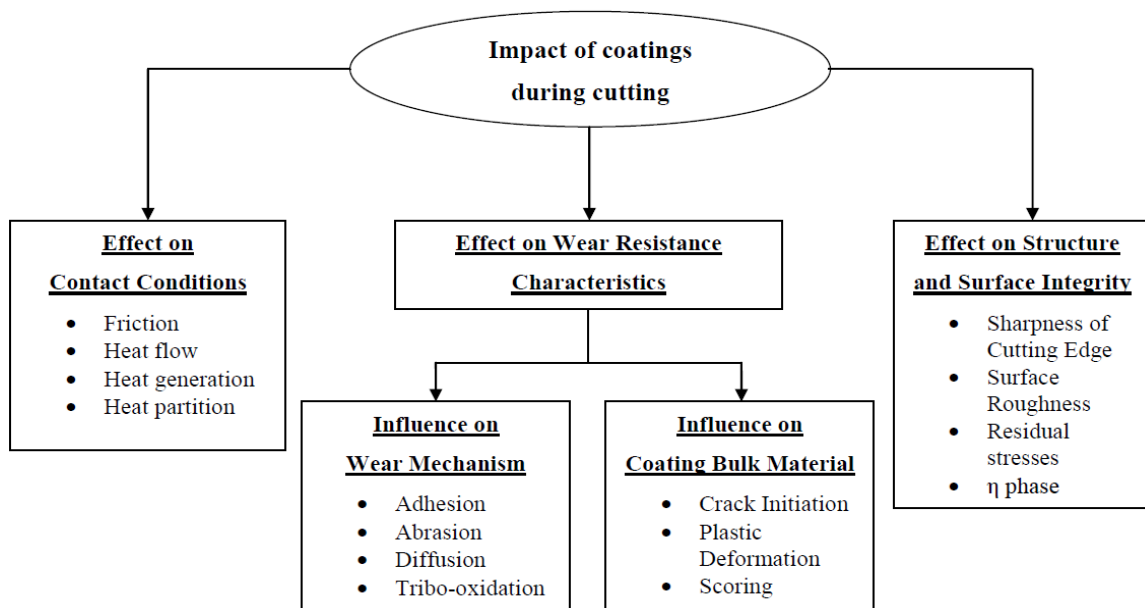


Figure 6: Impacts of coating during cutting [based on [86]]

There are three layers at the interface between the coating and the substrate. The first layer is the interface between the tool substrate and the coating. The chemical and physical compatibility of the coating like thermal coefficient of expansion in addition to the adhesion of the coating with the substrate material is of utmost importance in this layer. The second layer is the coating bulk material. Here, the coating properties are determined by the coating composition and microstructure. The third layer is the top or outer layer of the coating and it is this layer that determines how the coating will interact

with the workpiece or the surrounding environment. Figure 7 shows the influences and requirements of coating and substrate.

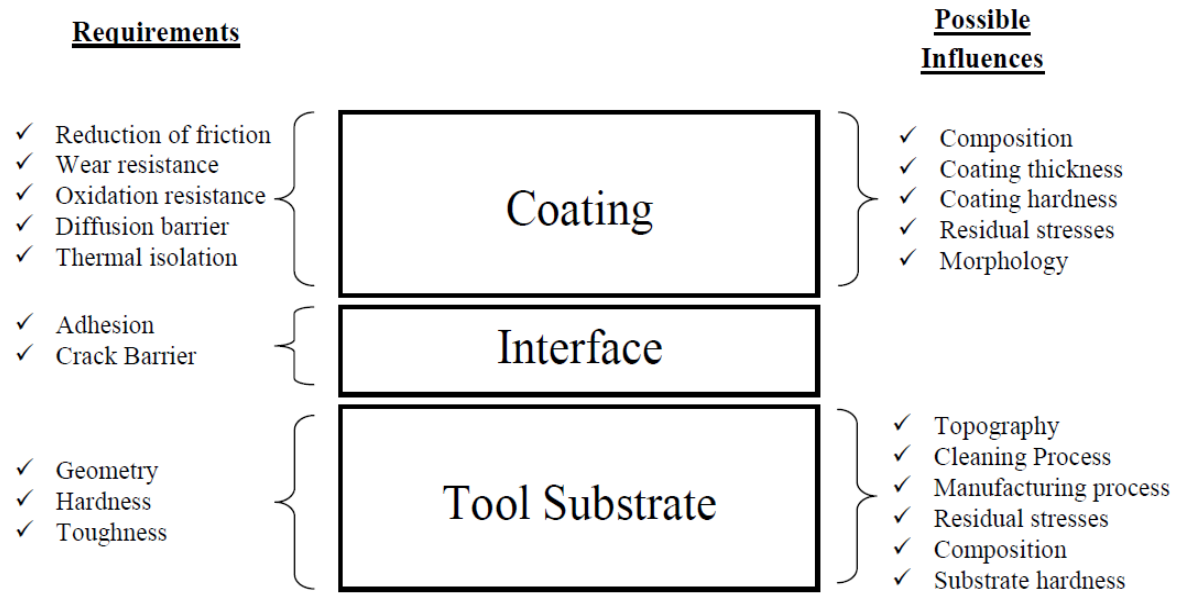


Figure 7: Influences and requirements of substrate and coating [based on [89]]

The two most common coating techniques used for cutting tools are Physical Vapor Deposition (PVD) and Chemical Vapor Deposition (CVD). PVD is a vacuum coating process where the deposited material is separated from a source, also known as a target, through evaporation or sputtering. Vapor particles are transported and condensed forming a film on suitably placed parts. If chemical compounds need to be deposited, this is accomplished either by introducing reactive gases (oxygen, nitrogen or hydrocarbons) containing desired reactants, which then react with the metal from the PVD source, or by using a similar source material [4]. To ensure uniform coating deposition, the tools are constantly rotated in the coating chamber.

CVD is a heat activated process. In this technique, gaseous chemical compounds are introduced in the chamber where they decompose or react with appropriately heated and prepared substrates. Anhydrous and anaerobic environments at sub-atmospheric pressures are often maintained in the chamber. Formation of uniform thick coatings with refined grain structure is dependent on the deposition temperature.

For high material removal rates of abrasive materials in turning, CVD coated tools are more suited as they are able to produce thick coating layers at high deposition rates. PVD coated tools are suitable for medium finish and finish machining processes. PVD coated tools ensure a sharp coated edge due to the capability of the associated process to control coating thicknesses on the edge. Unlike PVD films, CVD coatings chemically interact with substrates causing substrate embrittlement. PVD coated tools also have high intrinsic hardness and exhibit beneficial compressive stresses, enabling them to resist crack initiation. PVD coatings can also be stripped, making resharpener of tools much easier and thereby reducing long term production costs. All the coated tools used in the present research are PVD coated.

2.3.2 Classification of Hard PVD Coatings

Hard PVD coatings can be classified into seven groups. A short description of the different types of hard PVD coatings is given below and has been summarized from references [9]–[11].

➤ **Multi-component Coatings**

These coatings have binary, ternary, quaternary or multiple components in their coating structures. The most common and successful binary component coatings are TiN and TiC. Adding metal and/or metalloid components improves the performance of binary coatings. The addition of varying compositions of aluminium or carbonitrides makes up ternary coatings. Improvements of ternary coatings are dependent on the working conditions. Alloying elements such as Cr, Nb, Zr, Hf, V, Mo, W, Si, etc. are also often added which influences the wear behaviour significantly. Quaternary and further multi-component coatings are primarily achieved by adding elements like V, Y, Si, Cr, W, Zr, Hf, Mo, B to (Ti,Al)N based coatings.

➤ **Multiple-layer Coatings**

These coatings are achieved by assembling coatings with different functional layers. The idea is to incorporate multiple characteristics of the assembled coatings. The outer layers of multi-layer coatings typically provide friction and wear resistances while the inner layers enhance adhesion, arrest cracking, even out stress, support load and stop diffusion. A well-known multi-layer coating is TiC/Al₂O₃/TiN. The TiC layer has a similar thermal coefficient to cemented carbides thereby increasing the adhesion of the coating to the substrate. The low thermal conductivity of the Al₂O₃ layer protects the substrate from heat during cutting while the TiN layer provides good wear resistance.

➤ **Superlattice Coatings**

Superlattice coatings are deposited using a layer sequence deposition technique. The technique involves rotating the samples around different sources effectively exposing the different sources to the substrate. Layer thickness achievable by this technique is in the range of a few nm to approximately 100nm. Maximum hardness for coatings is seen to occur for coatings with 5-20nm coating thickness. The advantages of superlattice coatings include enhanced crack propagation resistance due to the presence of interfaces between layers and increased hardness and strength resulting from reduced grain size. Coatings with lubricant layers incorporated in a superlattice structure outperform coatings with only a top lubricant layer in reducing friction.

➤ **Dispersion/multiphase Coatings**

Dispersion coatings have a second phase of small particles embedded in the coating matrix. These are produced by depositing two different materials that do not form a complete mutual solid solution. The deposited materials thus are very different in type and have dissimilar lattice structures. The characteristics of the coating are dependent on the amount and property of the single phase and general influence of the cutting parameters. Nucleation of the second phase interrupts the columnar growth making these coatings dense and fine grained. Depending on specific cases, dispersion coatings show improved toughness, hardness and tribological properties.

➤ **Nano-structured Coatings**

These coatings have multi layers with each layer having thicknesses of a few nanometers. The coating also includes dispersion particles and structure modulations also in the nanometer scale. Nano-composite coatings such as AlTiN/Si₃N₄ demonstrate exceptionally high hardness. Nano-scaled TiAlCrN/WN and TiAlCrN/NbN coatings, which are characterized as protective and functional tribological coatings, exhibit outstanding tool performance under high speed dry cutting conditions.

➤ **Self-lubricating Coatings**

Self-lubricating coatings consist of a lubricating compound in their structure and are able to improve tribological properties of wear resistant coatings. Self-lubricating characteristics of the coatings can be achieved in two ways. One way is to embed lubricious layers into the coating. Examples of such are TiN-MoS₂ and TiAlN-MoS₂ where MoS₂ provide the lubricious layers. TiN-MoS₂ and TiAlN-MoS₂ are well known low friction coatings. The aforementioned coatings are proficient at low and moderate cutting speeds and thus well suited for stamping tool applications where intensive seizure and galling persists. By functional grading of the embedded lubricious layer, it is possible to further improve such coatings. The limiting factor for these coatings is the thermal stability of the lubricious layer. Another approach is to provide self-lubrication through the generation of lubricious tribofilms in the surface layers of a coating surface in response to cutting conditions. Such ‘self-adaptive’ or ‘smart’ behaviour is discussed further below.

➤ **Self-adaptive/self-organized/smart Coatings**

These coatings are multi-layered coatings that respond in a selective and favourable way to cutting conditions such as temperature, stress, strain and the environment. The layers are able to meet the requirements of the current wear stage of the cutting tool. The operating life of self-adaptive coatings can be divided into running-in stage, self-organizing stage and catastrophic stage in relation to the three phases of tool life.

The performance of such coatings are greatly dependent on the state of the running-in stage as tribological compatibility between the cutting tool and workpiece are not achieved for every mode of the running-in phase. Thus the effectiveness of such coatings depends on preventing critical surface damage during the running-in stage and transforming the tribo-system to its self-organizing mode.

Multi-layered self-adapting coatings should therefore have the following properties:

- Resist intensive surface damage during the running-in stage of wear;
- Be able to form stable compounds at the coating surface during the self-organizing stage of wear;
- Such compounds should protect the tool from thermal, mechanical and/or chemical attack as well as reduce sticking intensity so as to ensure a prolonged stage of stable wear.

2.3.3 Tribofilms

Tribofilms are thin films that form on the interface or worn surface during friction. They are dynamic structures that have different chemical composition as well as tribological and structural characteristics from the underlying bulk material [10], [11]. They have been shown to have a notable influence on frictional characteristics and wear performance of tools. Tribofilms in cutting tools form as a consequence of: (1) structural or chemical transformation of the tool surface layer due to interaction with the environment; or (2) material transfer from the workpiece or chips sticking to the tool surface with further tribo-oxidation. Tribofilms provide thermal barrier (protecting) and lubricating functions [12].

Self-adaptive coatings function by forming beneficial tribofilms through interaction with their environment. The coating system reacts with elements from the environment (mostly oxygen) to form lubricating films or tribo-ceramics with enhanced hardness, strength and thermal barrier characteristics [12]. Although most tribofilms favourably reduce the friction during cutting, some tribofilms like Ti-O are non-beneficial. Hence, selection of coatings should be made considering the tribological compatibility of the tool and the workpiece and the conditions under which they are operating.

2.4 Titanium alloys

Titanium and its alloys are increasingly becoming the material of choice for a wide range of applications. They have found their way into numerous industries due to

their superior properties. Their major application, however, is still the aerospace industry, where they are used in engine parts and airframes [13]–[17]. Titanium alloys makeup 30% and 40% of the total engine mass in commercial and military sectors respectively [18]. They have exceptional corrosion resistance, high wear resistance and fracture resistance, bio-compatibility and high strength-to-weight ratio, which they can retain even at elevated temperatures [13], [15], [19]. Titanium alloys are about 40% lighter than steel while only about 60% heavier than aluminium [20].

2.4.1 Classification of Titanium Alloys

For a better understanding of the effects of machining titanium and its alloys, some basic knowledge of this material family is necessary. This section gives an overview of the metallurgy of titanium and its alloys, and has been summarized from references [13], [16], [17], [19]–[22].

Titanium is an allotropic metal and therefore exists in two crystallographic forms. Figure 8 shows the two allotropic forms of titanium. At temperatures below 882°C, titanium has a hexagonal close packed (hcp) crystal structure referred to as α -phase. This structure has a very limited number of shear or slip planes. At temperatures above 882°C, it has a body centered cubic (bcc) structure referred to as β -phase. This phase is stable until the melting point of titanium at about 1677°C. It also features more slip or shear planes, thereby allowing for more local deformations.

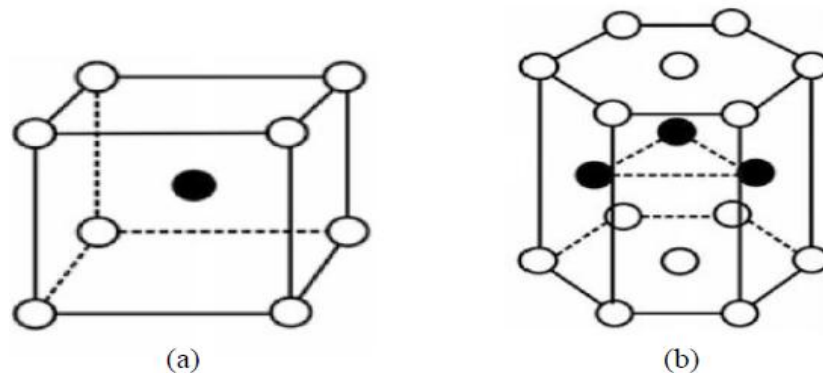


Figure 8: Two allotropic forms of titanium (a) Body centered cubic (β structure)(b) Hexagonally closely packed (α) structure [based on [22]]

Unalloyed titanium has excellent corrosion resistance but low strength and is thus almost never used in practice. The allotropic transformation temperature of titanium can be increased or decreased by alloying which involves adding certain elements. The alloys normally add valuable characteristics to the material while retaining the positive features of the original base metal. The mechanical properties of alloys may be quite distinct from that of the base metal or the individual elements added. Alloying elements that increase the transformation temperature are called α -stabilizers whereas elements that decrease the transformation temperature are referred to as β -stabilizers. Common α -stabilizers are aluminium (Al), oxygen (O), nitrogen (N), gallium (Ga) and carbon (C). Of these Al is very effective in increasing the strength of the α -phase at ambient and elevated temperatures up to about 550°C. The low density of Al also gives added benefits to the strength to weight ratio of the alloy. In commercial alloys, O, N and C are considered to be impurities. However, O is still used as a strengthening agent in several commercial pure-titanium grades to attain various strength and fabricability. Common β -stabilizers are molybdenum (Mo), vanadium (V), nickel (Ni), tantalum (Ta), copper (Cu),

manganese (Mn), chromium (Cr), iron (Fe), cobalt (Co), and hydrogen (H). β -stabilizers enable the β -phase to remain stable even at low temperatures including room temperature. Alloying elements such as tin (Sn), silicon (Si) and zirconium (Zr) that have little influence on the transformation temperature due to their high solubility are called neutral elements. Sn and Zr are able to strengthen the α -phase of titanium. Classification of titanium alloys are based on the alloying condition and the elements added to enhance its properties. Classification is done as follows:

- **α Alloys**

α alloys have a single α phase microstructure containing α -stabilizers and sometimes other neutral elements. They have high creep stability and are able to maintain their tensile strength up to 300°C. They have excellent weldability properties. However, these alloys are not heat treatable. The minimum yield strength ranges from 170 to 480 MPa. Their primary usage is in cryogenic and corrosion resistance applications. A frequently used α alloy is Ti5-212(Ti-5Al-212Sn).

- **Near α Alloys**

These are α alloys consisting of a small amount of β -stabilizers (1–2%). Their microstructure is thus characterized by mainly α phase with little β phase and therefore they behave more like conventional α alloys. Adding β -stabilizers improves their strength and workability. They are able to operate at higher temperatures in the range of 400-520°C. They are primarily used in jet engines where parts are exposed to high

temperatures. Examples of such alloys are Ti 8-1-1 (Ti-8Al-1Mo-1V) and IMI 685 (Ti-6Al-5Zr-0.5Mo-0.25Si).

- **$\alpha+\beta$ Alloys**

In these alloys the amount of β -stabilizers is more (4–6%) than that found in near α alloys. Through heat treatment, the microstructure of these alloys can be varied giving them better mechanical properties. The heat treatment gives them high strength, enabling them to be used at temperatures of 350-400°C. They provide high corrosion resistance compared to low alloy steels and aluminium thereby making them more suitable for use in aerospace applications. Alloys with higher β -stabilizers show better hardenability. The high temperature creep strength, however, is low compared to most near α alloys. Ti 6-4 (Ti6Al4V, designated as IMI 318) and IMI 550(Ti-4Al-2Sn-4Mo-0.5Si) are the most commonly used $\alpha+\beta$ alloys. $\alpha+\beta$ alloys account for 70% of overall titanium production amongst which Ti6Al4V contribute to about 45-60% of total titanium production. Ti6Al4V has been chosen as the workpiece material in the present research due to its high usage in industry.

- **Metastable β Alloys**

Metastable β alloys contain 10-15% β -stabilizers while retaining the β -phase in a metastable state at room temperature. These alloys also include small amounts of α -stabilizers giving them higher strength. They also exhibit high toughness, forgeability and hardenability over a wide temperature range making them ideal for aerospace structural parts.

- **β Alloys**

β alloys consist of large amounts of β -stabilizers (30%). They show high strength, hardenability, creep resistance, fracture toughness and corrosion resistance. They also provide improved forgeability and cold formability characteristics. However, they have higher density and low ductility compared to other alloys. They have a tendency of ductile-brittle transformation restricting their use in cryogenic applications. Their application is thus reduced to applications requiring burn resistance and corrosion resistance. They give an equivalent strength to $\alpha+\beta$ alloys at room temperature, however, at elevated temperature their properties are poor compared to that of $\alpha+\beta$ alloys.

- **Titanium Aluminides**

Titanium aluminide (TiAl), an intermetallic chemical compound, is also used as an alloying compound for titanium to attain superior heat and oxidation resistance characteristics. TiAl consists mainly of three intermetallic compounds: γ -TiAl (Ti₃Al), TiAl₃ and α 2-Ti₃Al. These alloys however show low fracture toughness and poor ductility.

2.4.2 Machinability Issues of Titanium Alloys

Machinability generally refers to the ease or difficulty faced during machining a particular material for a certain set of operating conditions. Machinability of a certain material depends not only on the mechanical properties of the material but also on the machining processes, cutting tools and cutting condition. Tool life, surface roughness,

power consumption, component forces and chip shape provide good insight into the machinability of a material. Machinability is mainly evaluated by assessing tool life, forces generated during cutting and surface finish of the machined part [17], [23].

Titanium alloys are considered to be difficult-to-cut materials owing to their inherent properties. As a result of this, the costs of finished titanium products are high limiting the use of titanium despite its beneficial characteristics. Most of the tool materials that perform well when machining other materials show relatively poor performance in machining titanium and its alloys [17], [24]. The problems associated with titanium machining are discussed below and have been summarized from references [14], [17], [25], [26]:

➤ **Poor Thermal Conductivity**

During machining, energy is consumed to overcome friction between the tool-chip or tool-workpiece interface and also to plastically deform the workpiece to form chips. Nearly all of the energy is converted to heat which in turn raises the cutting zone temperature. Generally, a significant portion of the heat generated is dissipated into the chip, with a small amount dissipating into the workpiece and tool. However, because of the poor thermal conductivity of titanium and its alloys (about 1/6 that of steel), the fast flowing chip and the workpiece are not able to dissipate the heat thereby trapping and intensifying the heat in the cutting zone. As a consequence, almost 80% of the heat is conducted into the tool, which results in rapid tool wear. Figure 9 gives a comparison of thermal load distribution during machining Ti6Al4V and steel CK45. The figure shows that for all tool materials heat dissipated into the tool is considerably higher during

machining of Ti6Al4V when compared to steel CK45. Further machining with a worn tool generates more heat, thereby accelerating tool wear in many instances. Previous research has shown that in titanium machining, the heat affected zone is small and temperature gradients are very steep due to the short tool-chip contact length and thin flow zone between tool and chip (approximately $8\mu\text{m}$ in comparison to $50\mu\text{m}$ while cutting iron under the same cutting conditions). This can cause the temperature in the cutting zone to reach levels as high as 1100°C .

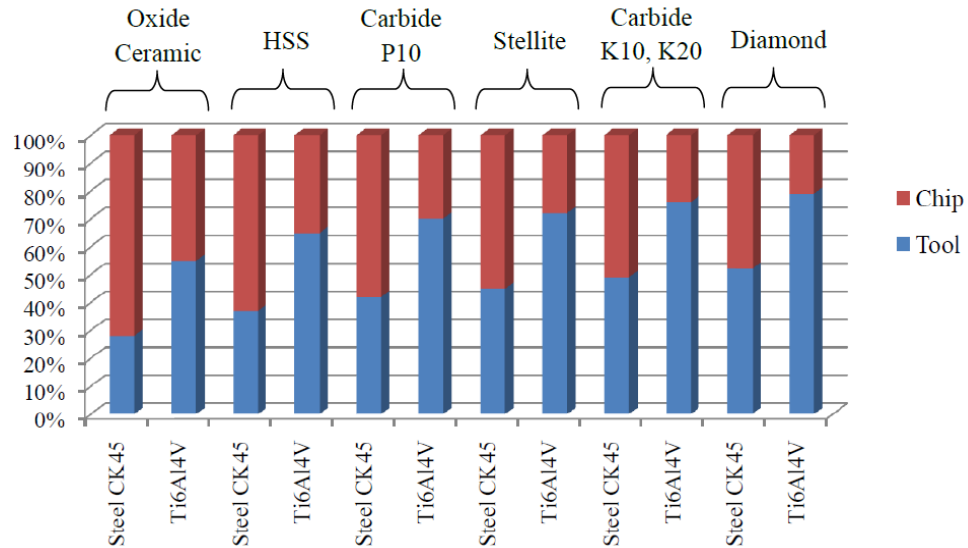


Figure 9: Distribution of thermal load when machining Ti6Al4V and Steel CK45 [based on [17]]

➤ **Low Modulus of Elasticity**

Titanium has high elasticity making it ideal for use in applications requiring flexibility while limiting crack formation. However, this characteristic is problematic during machining. Titanium has a low modulus of elasticity compared to other metals, meaning that it deflects more per unit force/stress. Thus, when subjected to pressure from

contacting cutting tool edge, titanium has a greater spring-back effect causing rubbing of the cutting edge instigating premature flank wear and chipping. Titanium deflects nearly twice as much as steel under the same cutting pressure.

The presence of a BUE at the tool edge when machining titanium, a common occurrence, has been observed to increase the perpendicular forces acting on the workpiece by at least three to four times. This high thrust force coupled with low modulus of elasticity causes the workpiece to deflect and spring away from the tool. This results in rubbing of the cutting edge against the workpiece instead of cutting causing an increase in friction raising the temperature at the cutting zone further. The deflections also often produce chatter. Rubbing and chatter causes poor dimensional accuracy and surface quality of the finished product.

➤ **Chemical Reactivity**

Titanium and its alloys are relatively chemically inert making them suitable for medical implant applications. However, at temperatures above 500°C, they become very reactive and react with almost all tool materials. Due to the high chemical reactivity and adhesive characteristics of titanium at high temperatures, intensive sticking on the tool is commonly observed in the form of built up edge. This high chemical reactivity coupled with built up edge formation also provides an ideal platform for chemical dissolution or diffusion between tool and workpiece material to take place causing rapid tool wear.

➤ **Hardening due to Diffusion and Plastic Deformation**

Hardening characteristics of titanium and its alloys make them very difficult-to-machine. Titanium work hardens or strain hardens during machining and is also hardened due to diffusion of oxygen and nitrogen. As previously mentioned, the temperature at the cutting zone can reach as high as 1100°C due to poor thermal conductivity of titanium. At high temperature most materials experience thermal softening and undergo a reduction in strength. This is often a desired effect in machining as it decreases the cutting forces and energy required for cutting given that mechanical characteristics of the material or the tool are not severely affected. However, this is not the case with titanium machining. Titanium retains its strength even at high temperatures. Though this characteristic is helpful for certain applications, it poses a great challenge during machining. Due to its ability to maintain high strength at elevated temperatures, higher cutting power is needed to plastically deform titanium to produce chips. This high cutting power and its resultant plastic deformation hardens the machined surface, a phenomenon commonly referred to as strain hardening or work hardening. Both diffusion and plastic deformation that takes place during titanium machining influences hardening of titanium; however, the latter is the dominant one. Figure 10 compares the strength-density behaviour of two titanium alloys and three different grades of steel.

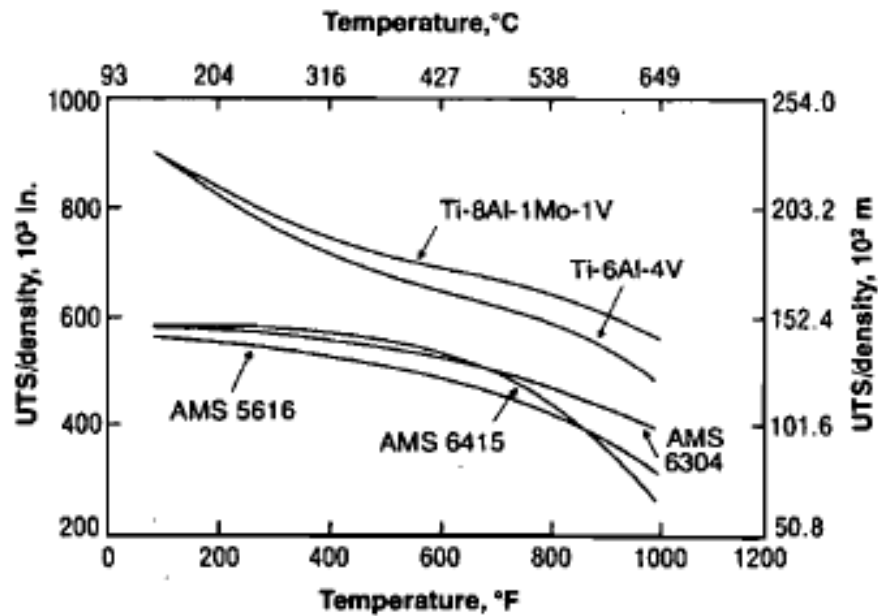


Figure 10: Strength-density behaviour comparison between two titanium alloys and three steel as a function of temperature [reprinted from [22] with permission from Taylor and Francis LLC,(<http://www.tandfonline.com>)]

➤ Mechanism of Chip Formation

Chip formation during titanium machining is somewhat unique. The distinct characteristics of titanium chips are that they are serrated, cyclic and of segmented geometry with shear-localized zones. Serrated or segmented chips are mainly formed as a consequence of adiabatic shear band formation, generally started by local shear deformation, or crack propagation from the external surface of the chip. Figure 11 shows a segmented chip typically observed in titanium machining.

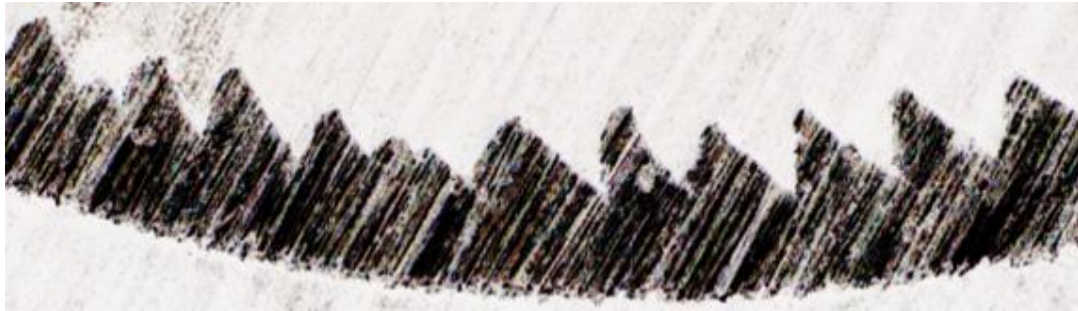


Figure 11: Micrographs of saw toothed chips showing longitudinal mid-sections

Komanduri and Von Turkovich [26] gave one of the detailed descriptions of the chip formation mechanism during titanium machining. Their explanation was based on video footage of chip formation at low and high cutting speeds of orthogonal cutting as well as micrographs of the cross-section of the chips. Figure 12 demonstrates the sequential events taking place during chip formation in titanium machining. Their findings are summarized below.

Unlike the continuous chips seen in machining steel where strain and deformation are uniformly distributed, with noted exception at the secondary zone (tool-chip interface); segmented chips formed during titanium machining demonstrate thin zones with highly concentrated intensive strain separating the segments. Sequential events resulting in catastrophically shear-failed chips can be divided into two stages. The first stage comprises of plastic instability of the workpiece material resulting in strain localization taking place in the primary shear zone along a narrow band. This commences at the cutting edge and advances with upward concavity towards the free surface. The outside of the shear failed chip looks like a crack while on the inside a highly deformed band persists which looks like a white band if metallurgically etched. The second stage

consists of steady flattening of the remaining wedge-shaped or inclined surface of the workpiece material as the cutting tool pushes against the inclined face of the workpiece, forming chip segments with no substantial deformation. As a result, chip thickness will be similar to the depth of cut for orthogonal machining. The white layer in between the segments, as seen in the chip cross-section in general, signifies the highly concentrated shear bands formed during this stage. Relative motion between the adiabatic shear-failed surface and the tool face is almost nonexistent. This results in rapid heat transfer into the tool promoting chemical interaction between the tool and the chip accelerating tool wear.

Titanium chips generally show lower deformation than other metals and are consequently thinner. In accordance with cutting kinematics, a thin chip flows over the rake face of the tool faster than does a thick chip, for the same cutting speed, which will trigger higher temperatures at the tool-chip interface. Temperatures at the cutting edge are further elevated due to low thermal conductivity of titanium. Thin chips mean that tool-chip contact area is small thereby concentrating the heat generated over a small region and raising contact stress near the cutting edge. In addition, localization of shear bands causes cyclic variation of cutting forces imposing fatigue on the cutting tool and may result in tool chipping. The catastrophic thermoplastic shear mechanism of chip formation also creates a clean, hot surface repeatedly enhancing welding, adhesion and diffusion of constituents between the tool and the workpiece material.

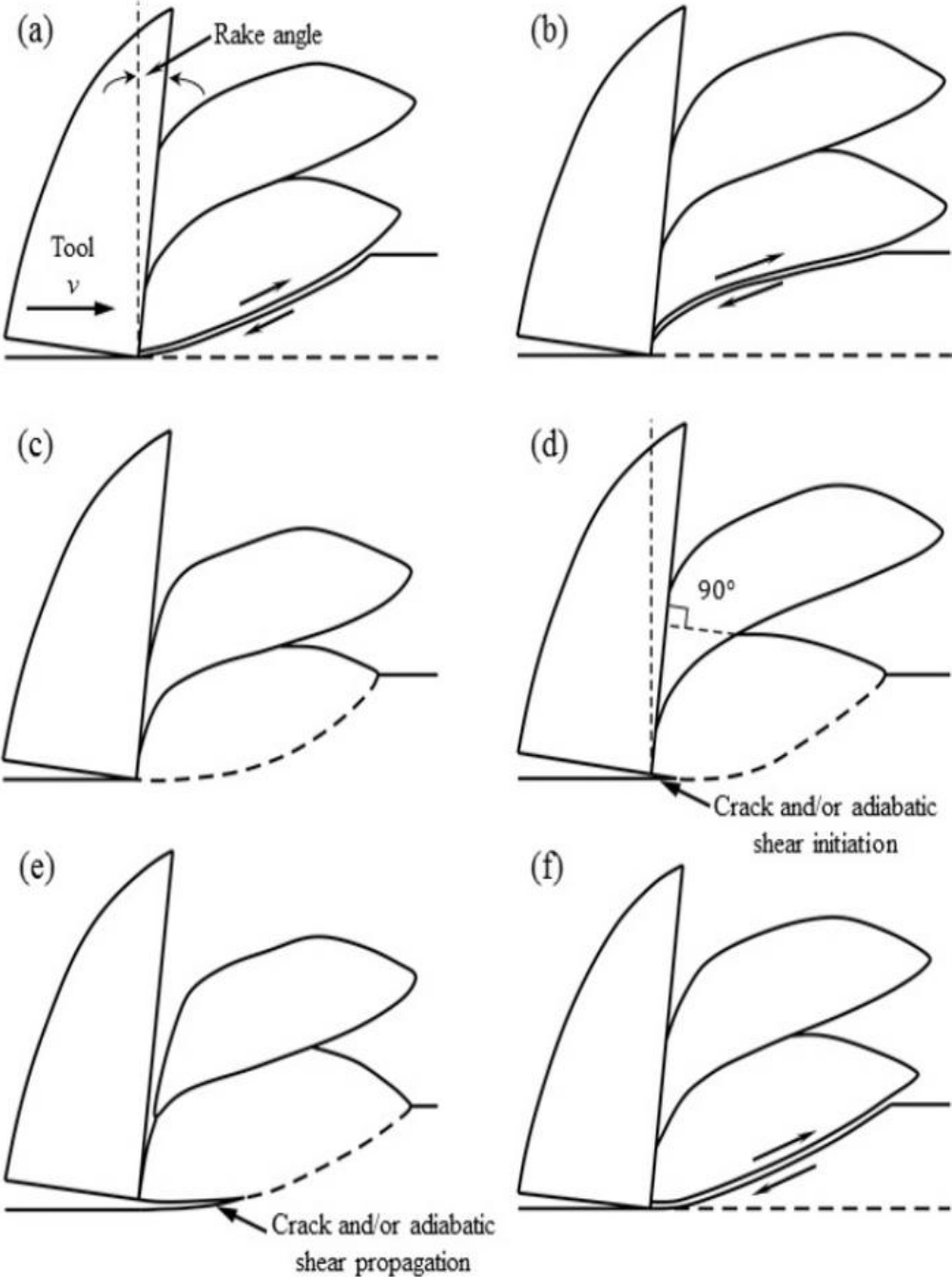


Figure 12: Sequential events illustrating serrated chip formation during titanium machining [reprinted from [26] with permission from Elsevier]

2.4.3 Cutting Tools and Substrate Material used in Titanium Machining

Over the years, different types of cutting tool materials have been applied in titanium machining in an attempt to obtain reasonable tool life [17], [19], [27]–[30]. Although new tool materials have led to significant advancements in productivity and tool life in the machining of steel, cast irons and high temperature alloys, these same tool materials have had little success in overcoming machinability problems of titanium. As mentioned before, high cutting zone temperatures are observed during titanium machining due to their poor thermal conductivity. At such high temperatures, the majority of the tool substrates cannot retain their hardness and face a reduction in strength of their inter-particle bonds which ultimately leads to accelerated wear and failure of the cutting tool [13], [30]. Table 1 shows the softening temperatures of some commercially available tool materials. Figure 13 shows typical hot hardness of common tool materials in relation to temperature.

Table 1: Softening temperatures of some tool materials [13], [31]

<u>Tool Material</u>	<u>Softening Point Temperature (°C)</u>
High-speed Steel (HSS)	600
Tungsten Carbide (WC)	1100
Aluminum Oxide (Al ₂ O ₃)	1400
Cubic Boron Nitride (CBN)	1500
Diamond	1500

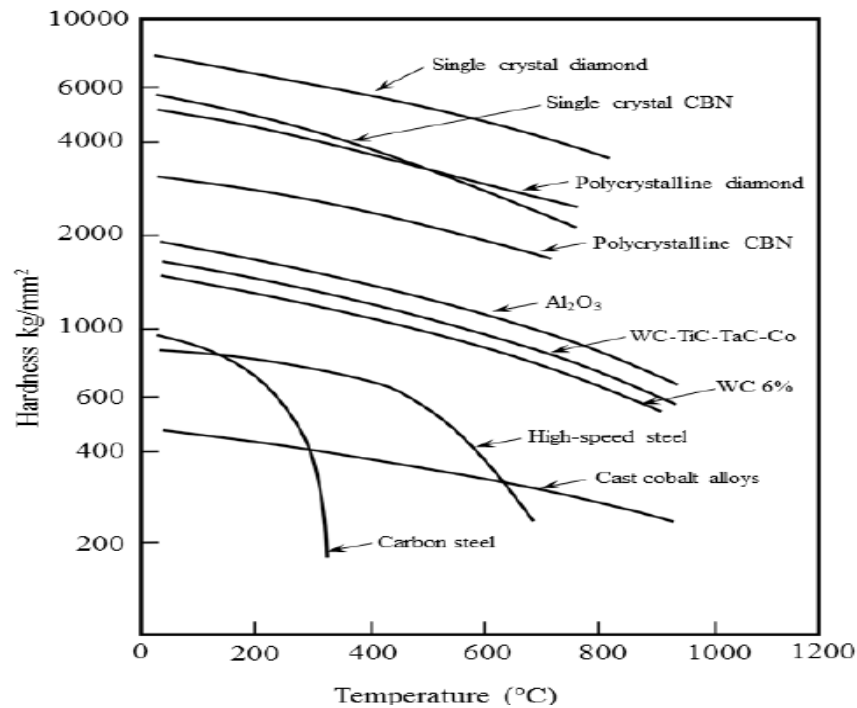


Figure 13: Characteristic hot hardness of some tool material [reprinted from [90] with permission]

For titanium alloy machining, a cutting tool must possess the following features [16], [19], [30]:

- Retain high hot hardness to withstand high stresses
- Good thermal conductivity to reduce thermal shock and thermal gradients at the cutting zone
- Chemical inertness to reduce tendency of reaction with titanium
- High tensile, compressive and shear strength
- Fatigue and toughness resistance to resist chip segmentation
- Chipping resistance due to chip segmentation

Different tool materials can be utilized to machine titanium; although each has its own limitations. Tool materials tested for titanium machining are high speed steels (HSS), cemented carbides (WC), cubic boron nitrides (CBN), polycrystalline cubic boron nitrides (PCBN), polycrystalline diamond (PCD) and ceramic. However, the behaviour and wear pattern varies and is unique to each tool material. The use of each type depends on the process requirements, tool cost and machining conditions [16], [30].

PCD tools are the most effective commercially available tool in machining titanium and its alloys [32]. Several researchers [17], [22], [32]–[35] have confirmed that PCD outperforms CBN, PCBN, uncoated and coated carbide tools for titanium machining, yielding the lowest wear rate and best workpiece surface finish. According to [33], PCD inserts can be used at cutting speeds three times higher than uncoated carbide inserts and can remove about twice the amount of material prior to reaching the failure criterion. The low tool wear rate of PCD tools can be related to the formation of a TiC protective barrier due to the diffusion of materials between the tool and the workpiece. However, their relatively high cost prevents their widespread use in industry [27], [36].

CBN tools have the highest hardness next to diamond tools. They sustain their high hardness characteristics even at elevated temperatures. They also remain oxidation resistant up to 2000°C. CBN features a very small crystal size (1-50µm). PCBN tools are formed by sintering CBN grains with a binder under high temperature and pressure [17], [37]. Researchers [17], [38], [39] have found that CBN and PCBN tools are able to sustain high cutting speeds when machining titanium alloys, up to 150 m/min for Ti6Al4V and 180-220 m/min for other $\alpha+\beta$ titanium alloys. However, their high hardness

and corresponding low toughness makes them susceptible to chipping and fracture especially if larger depths of cuts are used. This restricts their application to finishing operations during titanium machining. Furthermore, they are approximately 10-20 times more expensive than carbide tools making them economically infeasible [17], [30].

Ceramic tools are hard cutting tool materials and have high hot hardness, good oxidation resistance, chemical inertness and high compressive strength. Their high melting point prevents thermal softening from taking place under extreme machining conditions. However, they are brittle and have low fracture strength and toughness making them susceptible to thermal and mechanical shock during machining particularly milling [17], [30], [40]. Compared to cemented carbide tools, ceramic tools show higher flank and rake wear rates [41]. Generally, ceramic tools sustain notch and large groove wear during titanium machining [42]. Discontinuous serrated chips formed during titanium machining generate cyclic forces causing fracture which initiates notch wear. Thus ceramic tools are inappropriate for machining titanium and its alloys [17], [30].

HSS tools are extensively used for machining various materials. They have higher toughness compared to other materials. They are able to sustain intermittent or cyclic loading and unloading making them suitable for processes such as milling, drilling, reaming, tapping and broaching. HSS have a softening temperature of about 600°C. Hence, they are not suitable for machining at working temperatures over 500°C [13], [17], [19], [27], [30], [31]. At cutting speeds over 30 m/min, HSS tools are not at all suitable for titanium machining [43]–[45]. High temperatures generated during titanium machining soften the HSS tool material causing plastic deformation of the cutting edge or

the tool nose. Crater wear is also observed on the rake face. Both high temperatures and crater wear accelerate other wear mechanisms. Higher alloyed grades of HSS tool like T5, M40 etc. and some coated HSS tools are able to give better performance [17], [30], [45]. However, the loss of hardness at high temperatures, which is inevitable during titanium machining renders HSS tools incompatible for this application [17].

Carbide tools are the most accepted and widely used tools for titanium machining. In industry they are commonly referred to as cemented carbide, sintered carbide or hard metal. Commercially available cemented carbide tools fall under two categories: straight grade carbides and mixed grade carbides (also referred to as steel cutting grades). Chemical composition of straight grade carbides are as follows: 6 wt% Cobalt (Co) and 94 wt% tungsten-carbide (WC). The hard WC particles are bonded together in a cobalt matrix. The mixed grade carbides have additive elements in addition to the base composition of the straight grade cemented carbides. Common additive elements used to make mixed grade carbides are tantalum carbide (TaC), titanium carbide (TiC) and niobium carbide (NbC). The addition of TiC increases the hardness and wear resistance of the tools at the expense of fracture strength and toughness of the tool. TaC increases the capability of carbide tools to withstand high temperatures [17], [30]. Table 2 gives a summary of the effects of additive elements on carbide tools.

Table 2: Effects of additive elements on carbide tools [17]

<u>Additive Elements</u>	<u>Positive Effects</u>	<u>Negative Effects</u>
Cobalt (Co)	Increases toughness and shock resistance	Decreases hardness and wear resistance
Tungsten carbide (WC)	Increases hardness and wear resistance	Decreases toughness
Titanium carbide (TiC)	Increases wear resistance	Decreases toughness
Tantalum carbide (TaC)	Increases hot hardness and prevents plastic deformation	-

The wear resistance of carbide tools is affected by their grain sizes. Coarser grained carbides results in higher crater wear rates, since the coarse grains are more prone to being pulled out as the chips slide over the rake surface. However, reducing grain sizes to improve resistance against crater wear adversely affects flank wear. Cutting speeds over 60 m/min are not recommended for tungsten carbide tools due to the intense heat produced at higher cutting speeds often leading to plastic deformation of the tools. Cutting speeds less than 45 m/min reduces the possibility of thermal softening of the tools as well as the chemical interaction between the tool and the workpiece [17], [30], [42], [46].

Researchers [17], [30], [47], [19] have found that straight tungsten grade carbide tools are superior over mixed grade carbide tools. They give better performance irrespective of whichever wear mechanism is taking place [47]. Attrition wear is more prominent in mixed carbide grade tools. Diffusion wear is also higher in these tools due to the preferential dissolution of the mixed carbides [47].

Coated carbide tools have also been used for titanium machining. However, most coated tools perform worse in comparison to the straight grade carbides due to the reactivity of titanium with the coating materials. Therefore, uncoated straight grade cemented carbides are still the preferred choice for titanium machining [17], [30].

In the present research, straight grade WC/Co tools were used due to their above mentioned characteristics and wide usage in industry, with the intent of identifying and characterizing coatings that would further improve their tool life during titanium machining.

2.4.4 Wear Mechanisms of Cemented Carbide Tools in Titanium Machining

Cemented carbide tools encounter rapid tool wear during titanium machining due to the high temperatures generated, high chemical affinity of titanium, high cutting stresses and short chip-tool contact length [19]. Typically, both crater wear and flank wear are observed, as is a substantial built up edge formation extending over both rake and flank faces. Surface damage and failure by chipping at the tool nose are also commonly reported. A surface speed of about 45 m/min is typically adopted in industry, with attempts at higher cutting speeds typically resulting in plastic deformation of the cutting edge due to the intense heat generated [17], [41].

Tool wear in cemented carbide tools during titanium machining is dictated mainly by two wear mechanisms: Dissolution-diffusion and attrition. Dissolution-diffusion

normally produces smooth worn surfaces whereas attrition results in irregular worn surfaces [32], [41]. Both types of wear are prevalent on rake and flank faces of the tool.

Dearnley et al. [41] found that adhesion or attrition played a significant role in flank wear. Due to high chemical reactivity and adhesive characteristics of titanium, significant material transfer from the workpiece to the tool is observed in both flank and rake surfaces [17], [25], [41]. This adhered material builds up forming a layer referred to as a built up edge. Attrition wear results from the adhered particles breaking off on reaching a critical size tearing away fragments of tool material. Ikuta et al. [48] investigated the relationship between the adhesion area and the cutting speed of titanium alloys. They found that especially for Ti6Al4V, the adhesion area increases with cutting speed. Figure 14 shows the relationship between adhesion area and cutting speed for titanium machining for a K10 tool. Hartung and Kramer [49] suggested that adhesion may reduce tool wear as it prevents relative sliding at the tool-chip interface. They observed that while machining Ti6Al4V at low cutting speeds a stable built up layer forms which is able to reduce tool wear whereas the built up layer vanishes at higher cutting speed increasing tool wear. However, according to Rabinovich and Kovalev [11], the stability of built up layers under attrition wear conditions for cemented carbide tools are very low. Due to the cyclical stress applied at the adhesion point, microcracks are generated causing carbide grains to separate from the tool surface. Thus the formation of a built up layer with low stability further aggravates tool wear and results in chipping of the cutting edge.

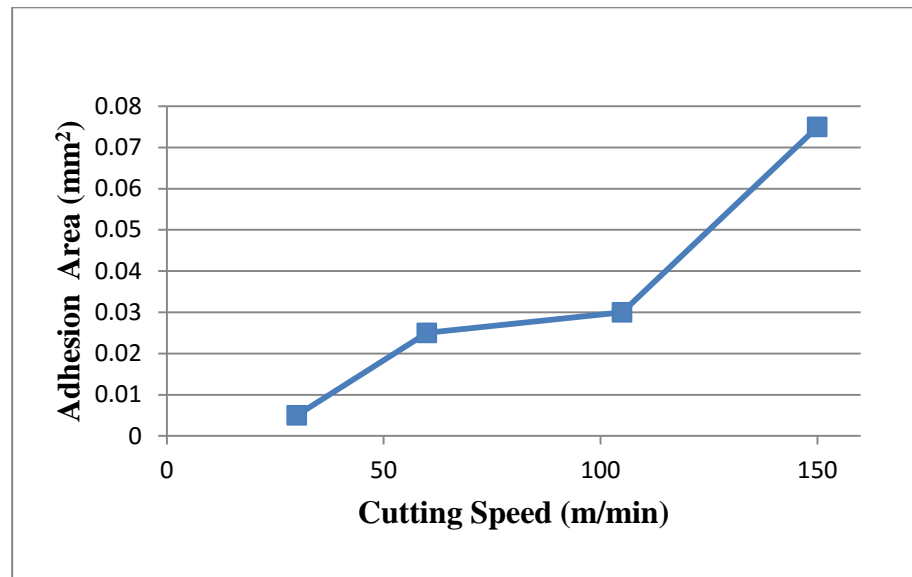


Figure 14: Relationship between adhesion area and cutting speed during dry milling of Ti6Al4V machining at feed: 0.1mm/tooth and depth of cut: 0.5 mm using K10 tool [Based on [48]]

Freeman [47] conducted tool life investigations of straight WC/Co grades and mixed or steel cutting grades (containing other additive carbides in addition to the base composition of straight grade carbides) of cemented carbides. The study showed that attrition wear was more prominent on mixed grade cemented carbides (containing γ -phase) in comparison to straight grade carbides. For cemented carbides having γ -phase, the γ -phase dissolves preferentially enhancing attrition wear. Diffusion wear is also higher in mixed grade carbides due to the preferential dissolution of the mixed carbides [47]. Lower attrition wear of straight grade carbides can be related to the increased toughness of the WC/Co alloys. Amongst the straight grade carbides, those having a grain size of $\leq 0.8 \mu\text{m}$ were most resistant to attrition wear. For straight grade carbides, dissolution-diffusion mechanisms dictated the rate of the main flank wear [41].

Due to titanium's low thermal conductivity, the heat generated during machining gets trapped into the cutting zone. In addition to this, high ductility of titanium which results in significant heat-producing shearing of chips and small tool-chip contact area elevates the temperature further. Temperatures at the tool-chip interface can reach about 1100°C. At temperatures above 500°C, titanium becomes very chemically reactive [50]. Such cutting conditions thereby provide an ideal environment for the dissolution-diffusion wear mechanism to take place. It has been reported [41] that the dissolution-diffusion wear mechanism dictates tool wear on the rake surface of uncoated cemented carbides. Freeman [47] observed crater wear formed as a result of shearing of the rake surface. Trent and fellow researchers [51], [52] investigated the commonly observed crater wear on the rake face of cemented carbide tools when machining titanium. Based on their observations they suggested that crater wear occurred due to tool material diffusing into the workpiece material which passes over the tool surface and not by mechanical fracture of tool fragments. This diffusion however may alter the tool structure thereby weakening the tool cutting edge and causing possible mechanical removal of the tool fragments by the moving chips [48], [49]. Diffusion of tool constituents into the workpiece or vice versa is observed and reported in the literature [53], [54]. Loss of cobalt binder from the tool surface due to diffusion allows for carbide grains to be detached from the surface thereby accelerating wear by mechanical action [55]. According to many researchers [13], [17], [41], [48], [49], during this diffusion wear stage, titanium atoms from the workpiece material migrate into the tool material and react chemically with the carbon present to form titanium carbide (TiC). This interlayer of TiC

formed is hard and it bonds with both the tool and the workpiece forming a seizure zone which reduces further diffusion. According to [41], straight grade carbides with large WC grain size (1.4 μm) gives better crater wear resistance but at the cost of decreased resistance to plastic deformation and attrition wear.

Chipping of tool edges are often observed during titanium machining and is prominent in milling processes. This can be attributed to the adhesion characteristics of titanium alloys at high temperatures and high thermal, mechanical and cyclical stresses associated with titanium machining [56], [57]. While milling titanium alloys with carbide tools, chipping has been a major failure mode [58]. The interrupted cutting nature of the milling process results in repeated mechanical and thermal shocks on the cutting edges causing cracks that lead to micro-chipping. The magnitudes of the thermal shocks in milling are severe because of the high cutting temperature generated as well as due to the huge temperature differential along the cutting edge. Higher cutting speeds and feeds increase tooth load and radial depth of cut which produce thicker chips generating high cutting forces. These forces are concentrated over a small area of the cutting edge exerting high stresses causing eventual chipping [59]. Ezugwu and Machado [58] observed normal flank wear before chipping initiated and suggested that flank wear enhances the conditions required for chipping. Wang and co-workers [55], [60] suggested that the redistribution of carbon in the tool due to diffusion wear results in tool surface weakening thereby encouraging tool chipping.

Plastic deformation of tools occurs at higher cutting speeds during titanium machining. Higher cutting speeds during machining generates very high temperatures and

gives rise to high compressive stresses near the cutting edge resulting in plastic deformation at the cutting edge or/and at the tool nose consequently leading to tool failure [16], [32], [61]. It has been reported in [19], [56] that plastic deformation and cracks developed due to thermal shock dictates tool wear mechanisms for cemented carbides at high speeds. During machining titanium and its alloys with straight grade carbides the cutting speed is limited to 60 m/min due to plastic deformation. A cutting speed less than 45m/min reduces thermal softening and the probability of chemical interaction between the tool and the workpiece [17], [41]. Straight grade carbides having a cobalt content of 6 wt-% tends to promote plastic deformation. Finer grain size of WC [0.8 μm] gives greater hardness and thereby provides better resistance to plastic deformation, however, at the cost of reduced crater wear resistance. Negative rake angle tools were reported to give better protection to plastic deformation at the tool nose as compared to inserts with a positive rake angle [41].

Dearnley et al. [41] observed notch wear at a relatively high cutting speed of 75 m/min. However, notch wear appeared only for the hardest uncoated mixed carbides containing high amounts of γ -phase and only in a few cases. Such depth of cut notching occurred as a result of localized fracture of the tools. They also suggested that straight grade carbides having cobalt content of less than 6wt-% promotes notch wear formation.

Some researchers have also reported abrasion wear mechanism during titanium machining [53], [62]–[65]. Pawar et al. [64] found that during machining of α titanium alloys the dominant tool wear mechanism is abrasion. They suggested that coatings on tools are not effective for machining such alloys as abrasion wear leads to faster coating

delamination. They also reported that $\alpha+\beta$ titanium alloys (e.g. Ti6Al4V) shows the presence of a built up edge, which encourages abrasion and diffusion wear mechanisms. Nouari et al. [62] investigated tool wear mechanisms for Ti55531 (a near β alloy) and Ti6Al4Valloys. They found that for Ti55531 abrasion wear dictates tool wear whereas for Ti6Al4V it was adhesion and diffusion. Jawaid et al. [53] reported that abrasion wear dominated tool wear mechanism at the flank and tool nose for Ti-6246 (a $\alpha+\beta$ alloy which is stronger than Ti6Al4V).

Coated carbide tools have also been applied to machine titanium alloys. A coating normally reduces friction at the tool-chip interface thus lowering cutting forces and cutting temperature. Furthermore, the coating layer protects the tool from thermal shock by acting as a shield. However, coated tools wear out rapidly as soon as the tool substrate is directly exposed due to coating delamination. During titanium machining, the coating layers on tools are often very quickly removed by the fast flowing chip and by the chemical interaction between the tool and workpiece material [13], [17].

2.4.5 Application of Coated Carbide Tools in Titanium Machining

Almost 80% of all tools used in industries for machining are coated tools. Performances of cutting tools are enhanced significantly due to the application of coatings. Coatings, being hard materials, offer better resistance to abrasion. They provide superior high temperature characteristics such as high hot hardness, increased resistance to oxidation wear and diffusion wear. They are able to reduce friction between the tool-chip or tool-workpiece interfaces because of their high lubricating abilities thereby

minimizing cutting temperature. They also reduce cutting forces during machining in comparison to uncoated tools. Increased cutting speeds are achievable with coated tools during the machining of aero-engine alloys [66]. Much research has been carried out to obtain suitable coatings for carbide tools during titanium machining. However, due to the complexity of titanium machining it is still an area that requires significant attention.

Although coated carbide tools have had significant success in machining cast irons, steels and many super alloys, they are yet to achieve the same level of success when it comes to titanium machining. In many cases, coated tools perform worse than straight grade cemented carbides thereby making straight grade carbides the preferable choice yet for titanium machining [36]. Many researchers [16], [41], [49], [67] have found that coatings such as TiN, TiC, TiCN, TiN-TiC, TiN-Ti(C,N)-TiC, Al₂O₃/TiC, Al₂O₃,HfN, and TiB₂ show higher tool wear rates than straight grade WC/Co cemented carbides.

Dearnley et al. [41] studied the effects of TiN, TiC, Al₂O₃, and HfN CVD coated inserts while machining Ti6Al4V. They reported that in most scenarios, the wear mechanism was attrition through the removing of fragments of the coatings. However, at lower feed rates e.g. 0.16 mm/rev diffusion wear characterized by smooth wear was observed in both flank and rake face. All the coated tools wore out more rapidly on both flank and rake compared to uncoated WC-Co tools. They also tested TiB₂ coated carbide inserts during machining of pure commercial titanium and found that it is more wear resistant in comparison to the other coatings.

Settineri and Faga [68] demonstrated improved tool life of AlSiTiN and TiCN WC/Co coated tools over uncoated tools in machining annealed and as-rolled TA48 in the range of 50-130 m/min, under wet and MQL coolant conditions. The authors claimed that the multilayer architecture of the nano crystalline structure in addition to better adhesion properties and superior abrasion resistance of AlSiTiN explained its better performance over TiCN coated tools. Bhattacharyya et al. [57] found that TiN/TiC/TiN coated tools wear out rapidly in comparison to fine grain WC/Co cemented carbides especially at high cutting speeds. This was due to the chemical interactions taking place between the coating and the workpiece material.

Jawaid et al. [69] investigated the wear mechanism and performance of PVD-TiN and CVD-TiCN + Al₂O₃ coated carbide tools for face milling operation under various operating conditions. They found that CVD-coated inserts performed better than PVD-coated inserts in most cases which can be attributed to the greater coating thickness, its better wear resistance and greater adhesion strength of the coating onto the substrate for the CVD coated tools. The only exception to this trend was at $f = 0.1$ mm/tooth and $V_c = 55$ m/min. Their study revealed that coating delamination and adhesion promoted the initial wear mechanism for the coated tools. Attrition and diffusion wear dictated wear on the flank and rake face of both tools. At higher cutting speeds, rapid tool wear occurred resulting in chipping of the cutting edge. Plastic deformations were also observed for both tools especially at higher cutting speeds.

Ezugwu and co-workers [70], [71] observed PVD coated tools outperform straight WC fine-grain carbide inserts. They found that single layer PVD TiN coated tools gave

higher flank wear compared to the multilayer PVD TiN/TiCN/TiN coated tool at low feed rates (0.13mm/rev) whereas the phenomenon is exactly opposite at higher feed rates (0.25 mm/rev) for turning operations.

Ozel and co-workers [72] compared the performance of uncoated and three coated tungsten carbide inserts during turning of Ti6Al4V in terms of wear rate and cutting forces. The coatings employed were single layer TiAlN, single layer CBN and multi-layer CBN + TiAlN. Finite element method (FEM) simulations were done to study tool wear development and cutting forces. They found that the TiAlN coating slightly outperforms uncoated WC/Co tools in terms of cutting forces and tool wear rate.

Cherukuri et al. [73] studied the effect of an ultra-hard AlMgB₁₄-20%TiB₂ composite coating, deposited by a pulsed laser technique on WC/6%CO carbide inserts, on dry turning of heat-treated Ti6Al4V. The hardness of the coating was twice that of the tool substrate. The composite coated tool showed similar tool wear to commercially available TiAlN coated tools and performed about two times better than uncoated tools. This is due to the formation of a strong, stable adherent layer at the tool-chip interface minimizing diffusion wear. They claim that boride coated tools performance are superior compared to typical coated tools such as TiAlN, TiN, TiC, Al₂O₃, and HfN, and are comparable to CBN and PCD tools.

Che Haron et al. [74] compared the tool life between uncoated alloyed carbide tools and CVD coated (TiC/TiN/Ti(C/N)) alloyed carbide tools for ball end milling of Ti-6242S. Based on their developed tool life equations, it can be said that multi-coated tools

perform better at higher depth of cut when matched with high cutting velocity and feed rate. At less aggressive cutting conditions, uncoated tools outperform coated tools.

Beake et al. [75] conducted tool life experiments with PVD $Ti_{1-x}Al_xN$ ($x=0.5$ and 0.67) coated tungsten carbide inserts for face milling of AISI 1040 steel and end milling of hardened 4340 steel and Ti6Al4V alloy. Experimental results showed that tool life for the AlTiN coated tool outperforms the uncoated tool significantly. TiAlN coated tools also perform slightly better than the uncoated tool. Lower tool life of the uncoated milling cutters can be related to the intensive interaction of the workpiece with the tool causing chipping of the cutting edge.

Corduan et al. [35] recommended TiB_2 coated carbide tools for high speed machining of Ti6Al4V at cutting speeds lower than 100 m/min. The wear pattern of the coated tool progressed in two stages: coating delamination followed by substrate damage. They suggested further research into refining the deposition techniques of the TiB_2 coatings as well as research into coatings which exhibit better thermal fatigue resistance. However, they did not conduct any tool life studies and no comparison with other coated or uncoated carbide tools. Their study also lacks explanation regarding why TiB_2 coated carbide tools have wear progression in the manner as they reported. Their investigation also revealed that PCD inserts shows better performance than CBN and coated tools and that CBN tools are better suited for finishing operations.

Prengel et al. [76] studied the performance of several coated carbide tools for the wet turning of Inconel 718 and A390 aluminium alloy. A multilayer TiAlN coated tool showed some improvement in tool life compared to a monolayer TiAlN coated tool for

Inconel 718 turning. This can be related to higher hardness of the multilayer coating. In machining A390 aluminium alloy, a harder PVD TiB_2 coated tool provided better abrasion resistance as compared to the TiN and TiAlN coated tools.

Rao et al. [77] showed that some multilayer coatings based on TiB_2 can address the issue of inherent brittleness of a monolayer TiB_2 coating. They demonstrated that by adding diamond like carbon (DLC) to TiB_2 , forming a multilayer DLC TiB_2 coating, the hardness of the TiB_2 coating can be reduced and thus provide the added advantage of lubricity of the DLC layers. They have also illustrated that by engineering a reactive PVD process for TiAlN- TiB_2 a multilayer coating can be created where the tool wear rates can be significantly reduced.

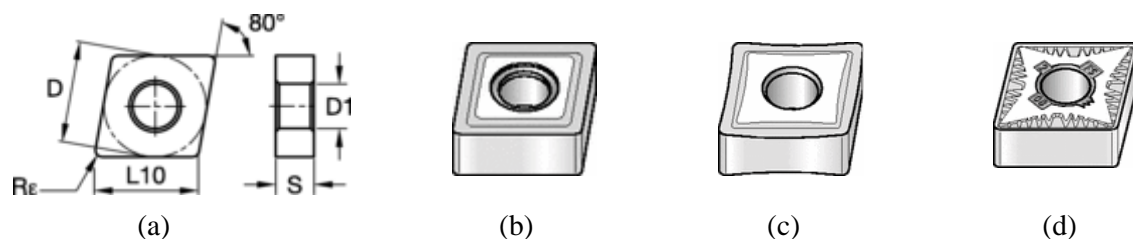
Chapter 3: Experimental Details

3.1 Introduction

The primary idea behind the present research endeavour was to study the effect of different tool coatings during titanium machining in order to obtain the best coating and understand its characteristics that allows it to best address the machinability issues associated with titanium and provides better tool life for cemented carbide tools. Tool life studies were conducted to identify the coatings that showed significant tool life improvement and detailed analyses were performed subsequently to better understand the behaviour and functionality of the successful coatings.

3.2 Cutting Tool and Workpiece Properties

In this study, experiments were conducted for turning and end milling processes. Both roughing and finishing operations were considered for turning operations. Kennametal CNMG432, CNMP432, CNMG432FS inserts were used for turning operations. CNMG432 and CNMP432 are roughing inserts and have similar geometry with different chip breaker profiles, while CNGG432FS is a finishing insert. The following tables and figures illustrate the geometry and property of the turning tools used in this study.



— Figure 15: Turning inserts used: (a) Geometry of the insert (b) CNMG432 roughing insert (c) CNMP432 roughing insert (d) CNGG432FS finishing insert — e



Figure 16: Chip Breaker profile: (a) CNMG432 (b) CNMP432

Table 3: Specifications of the Kennametal turning inserts

ANSI Catalog No.	Type	Grade	Clearance Angle	Rake Angle	D (mm)	L10 (mm)	S (mm)	R ϵ (mm)	D1 (mm)
CNMG432	Roughing	K313	0	12	10.7	12.9	4.76	0.8	5.16
CNMP432									
CNGG432FS	Finishing								

Kennametal K313 is a low binder content, hard, unalloyed WC/Co fine grain grade. It has excellent edge wear resistance in addition to very high strength making it suitable for machining titanium, austenitic stainless steels, cast irons, non-metals, non-ferrous metals, and most high temperature alloys. It has superior depth-of-cut notch wear and thermal deformation resistance. The grain structure has minimal pits and flaws ensuring long and reliable service life.

For end milling operations, Fullerton 3200 Series 4 Flute Square end mills were used. Figure 17 and Table 4 provide details of the end mill tools used in this study.



Figure 17: 4 Flute Fullerton Square End Mill

Table 4: Specifications of the Fullerton end mill

Series	3200
Type	4 Flute Square end mill
EDP No.	32152
Cutting Diameter (mm)	12.70
Tool Length Style	Stub
Cutting Length (mm)	19.05
Shank Diameter (mm)	12.70
Overall Length (mm)	76.2
Helix Angle	30
Spiral	Right Hand
Structure	Dura Carb (Micrograin)

ASTM B265 Grade 5 titanium alloy Ti6Al4V, also known as Ti64 or IMI 318, was used as the workpiece for all cutting experiments. The chemical composition and physical and mechanical properties of the alloys are given in the tables below.

Table 5: Chemical composition of Ti6Al4V workpiece

Element	Al	V	N	C	H	Fe	O	Residuals, each/total
Weight, max %	6.75-5.5	4.5-3.5	0.05	0.08	0.015	0.40	0.20	<0.1/<0.4

Table 6: Physical and Mechanical properties of Ti6Al4V workpiece at room temperature

Density	4.43 g/cc
Tensile Strength	895 MPa
Yield Strength	828 MPa
Elongation %	10 %
Reduction of Area %	20 %
Thermal Conductivity	7.3 W/mK
Specific Heat Capacity	580 J/kgK
Modulus of Elasticity, tension	110 GPa
Hardness, Rockwell C	37 HRC

3.3 Experimental Setup for Cutting and Process Parameters

The turning experiments were performed on a Nakamura-Tome SC-450 CNC lathe center. The spindle can operate in the range 25 to 2500 RPM. A MCLN-5° Kennametal tool holder (right hand tool) was used to setup the tools. Figure 18 shows the tool holder used for the turning operation. The tool offsets were properly calculated to provide a consistent uncut chip thickness for all testing. Figure 19 shows the experimental setup for the turning operation.

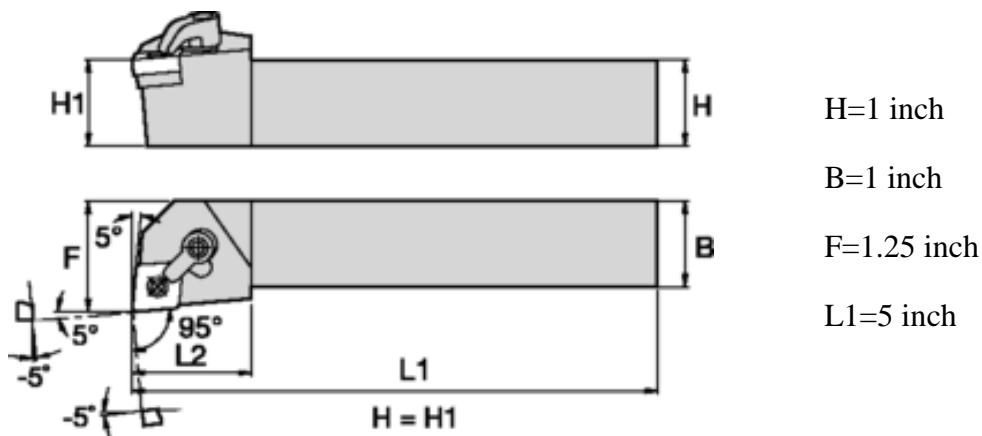


Figure 18: MCLN-5° Kennametal Kenloc™ Tool Holder

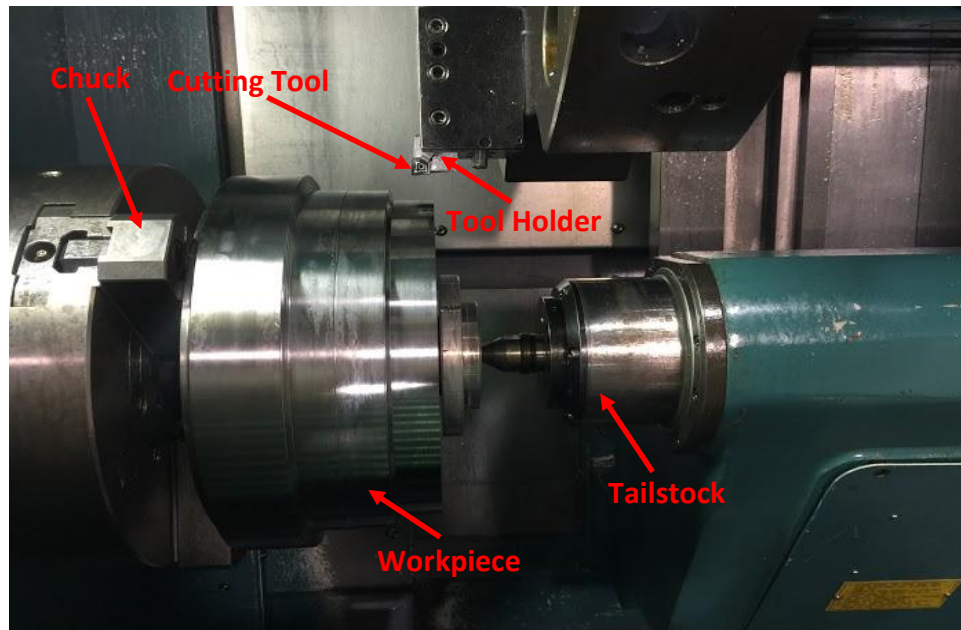


Figure 19: Experimental setup for turning operation

The cutting parameters used for rough turning and finish turning operations are given in Table 7 below. The cutting parameters chosen for rough turning were based on industrial recommendations and literature review. For finish turning, the cutting speed chosen was higher than the industrial recommendation to ensure that the formation of tribofilms on the tool surface takes place. Flood coolant was applied during all tests.

Table 7: Cutting parameters for turning operation

Cutting Parameters	Rough Turning	Finish Turning
Cutting Speed (m/min)	45	150
Feed rate (mm/rev)	0.15	0.1225
Depth of cut (mm)	2	0.25
Coolant	COMMCOOL™ 8800	

Cutting forces for select turning operations were measured using a Kistler 9121 Tool Dynamometer. The force signals were amplified using a Kistler 5010 charge amplifier. The analog signal was converted to digital signals using a National Instruments Data Acquisition Card which was then stored using a customized LABVIEW program. The cutting force information was also extracted by the LABVIEW software. Figure 20 shows the dynamometer setup used to collect force readings for turning operations.

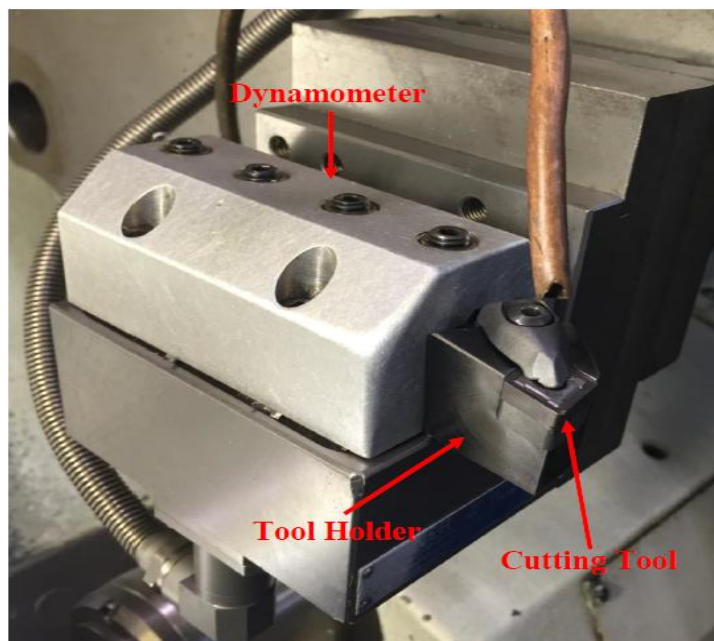


Figure 20: Dynamometer setup for collecting force readings during turning

The wet milling tests were performed on a five axis Makino MC56 milling center, using a down milling configuration. The machine has a maximum spindle speed of 15,000 RPM. It is equipped with HSK 100A tool holders. To ensure that tool deflection and vibrations do not affect the results, the tool overhang length was kept to a minimum. A highly sensitive dial gauge was used to check the run out of the tool to make sure that

the load on all flutes was even. The tool cutting path was straight with zero tilt angle.

Figure 21 shows the experimental setup for the milling operation.

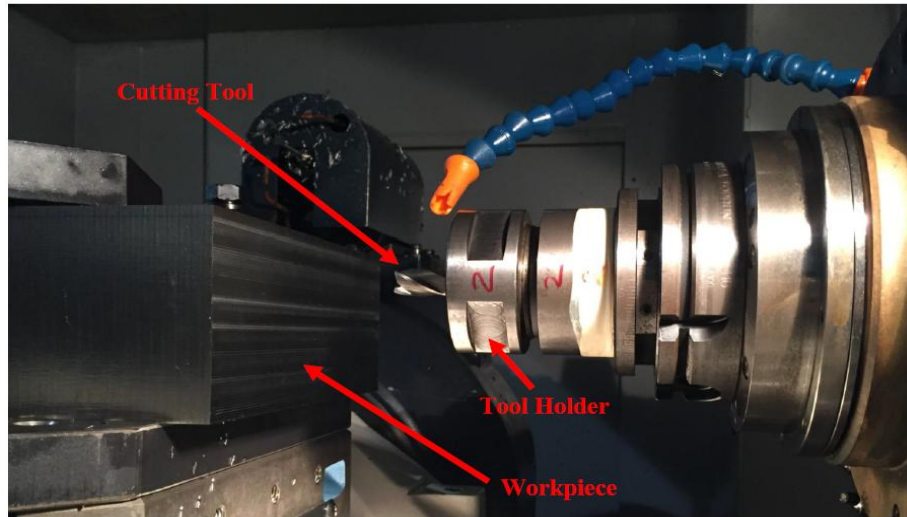


Figure 21: Experimental setup for milling operation

The cutting parameters used for the wet milling tests are given in Table 8. The cutting parameters were chosen based on the literature review and industrial recommendations.

Table 8: Cutting parameters for end milling operation

Cutting Parameters	Values
Cutting Speed (m/min)	100
Feed per tooth (mm)	0.05
Axial depth of cut (mm)	5
Radial depth of cut (mm)	1
Coolant Conditions	Castrol Hysol MB 50

3.4 Experimental Methodology

The following steps were followed in this research:

- ❖ A tool life study was conducted for rough turning operations with recommended industrial coated (TiAlN) and uncoated straight grade cemented carbide tools to determine the benchmark tool.
- ❖ Tool life studies of several PVD coated rough and finish turning inserts were carried out against the benchmark tool. Coatings that extended tool life of the carbide tools compared to the benchmark were identified.
- ❖ Since detailed analyses of coatings are expensive and time consuming, analyses were done only on coatings that significantly outperformed the benchmark tool to better understand the behaviour of the coating and how it affects tool life. Focus was given to the best coating that gave the highest improvement in tool life.
- ❖ The effects of chip breaker profiles of turning inserts were then studied for both the benchmark tool and the best coating. Tool life studies and chip analyses were conducted. Comparisons of cutting forces were also made.
- ❖ Different variants of the best coating obtained from different tool coating companies were tested to illustrate how deposition parameters affect coating properties like hardness and consequently affect tool performance.
- ❖ Milling tests were then carried out with the coatings that showed significantly better performance compared to the benchmark in turning operations. This was done to observe how the coatings behave in milling processes.

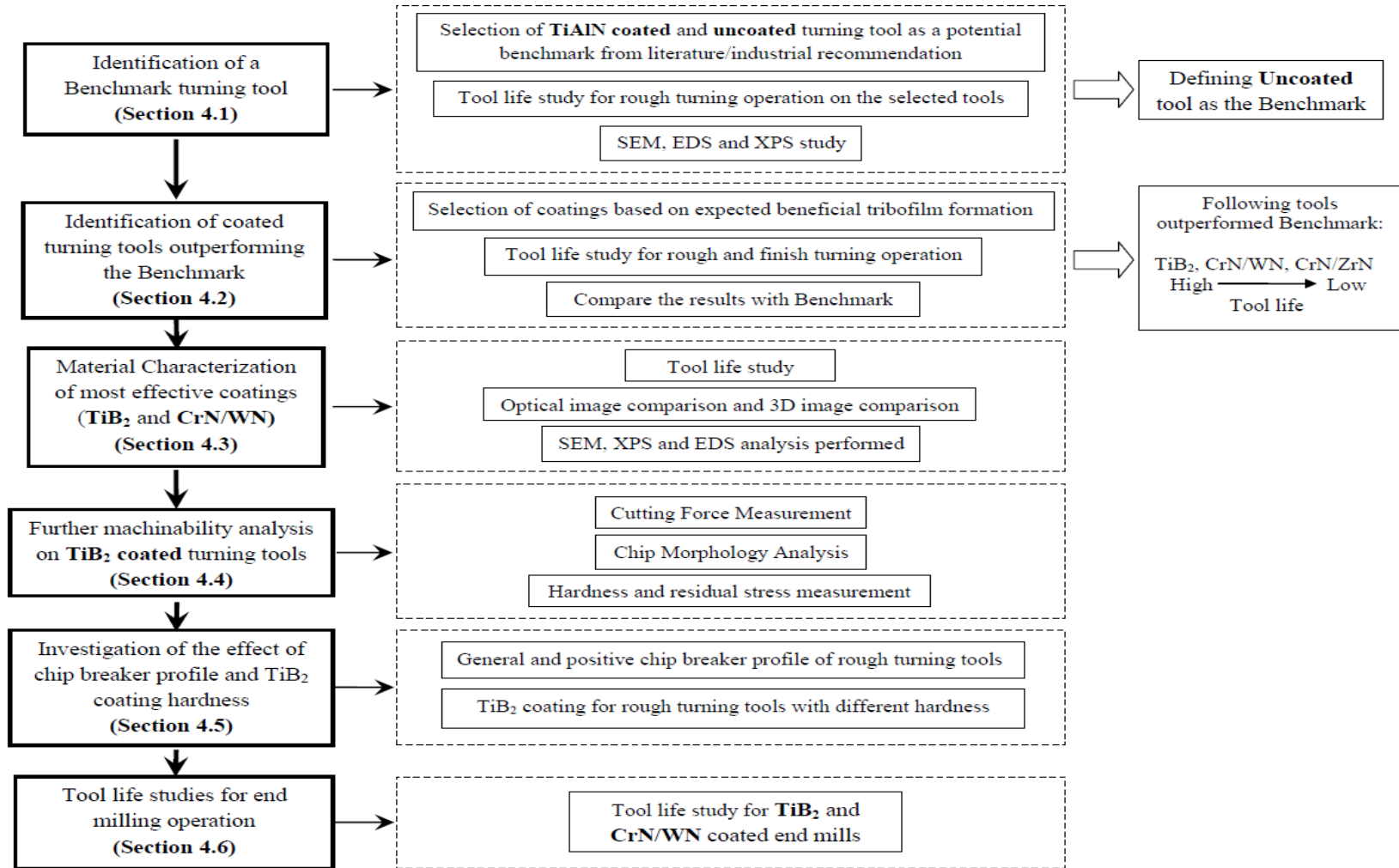


Figure 22: Experimental Flow Chart

3.5 Tool Life Study

Tool life studies were conducted for all tool coatings used in this research and were used to identify effective coatings for Titanium machining. All tool life studies were performed initially for turning operations. First, a tool life study was conducted between recommended industrial coated and uncoated cemented carbide tools to identify the benchmark tool. Then tool life studies for all other coatings were carried out and compared with the benchmark tool. Tool life studies in a milling operation were only done with selected coatings once the coatings had shown improvement of tool life in turning operations.

During the turning tool life test, the tool flank wear was measured after each pass using an optical toolmaker microscope (Mitutoyo TM). According to ISO 3685:1993 and ISO 8688-2:1989, the tool life criterion was set to be 0.3 mm of flank wear. Chips were collected after the first pass for all tools. After each pass, images of the rake face, flank face and nose of the turning insert were taken with a multipurpose zoom microscope system (Nikon AZ100), to keep a visual record of the progressive tool wear. The AZ100 Multizoom microscope combines the characteristics of both a stereomicroscope and a compound high magnification microscope. It has 1x and 4x objective lens with a built-in 8x zoom optic that provides 1x to 8x magnification. NIS-Elements Microscope Imaging Software was used to capture and record the images. 3D images of tools were taken with a Keyence VHX-5000 digital microscope. Some 3D images were also provided by Kobe Steel Ltd.

During tool life tests for milling, the end mills were periodically examined with the Mitutoyo tool maker's microscope to measure flank wear, rake wear and chipping. The tool life criterion was taken as 0.3 mm of flank wear, as with turning experiments. Figure 23 shows the microscopes used for the tool wear studies in this research.

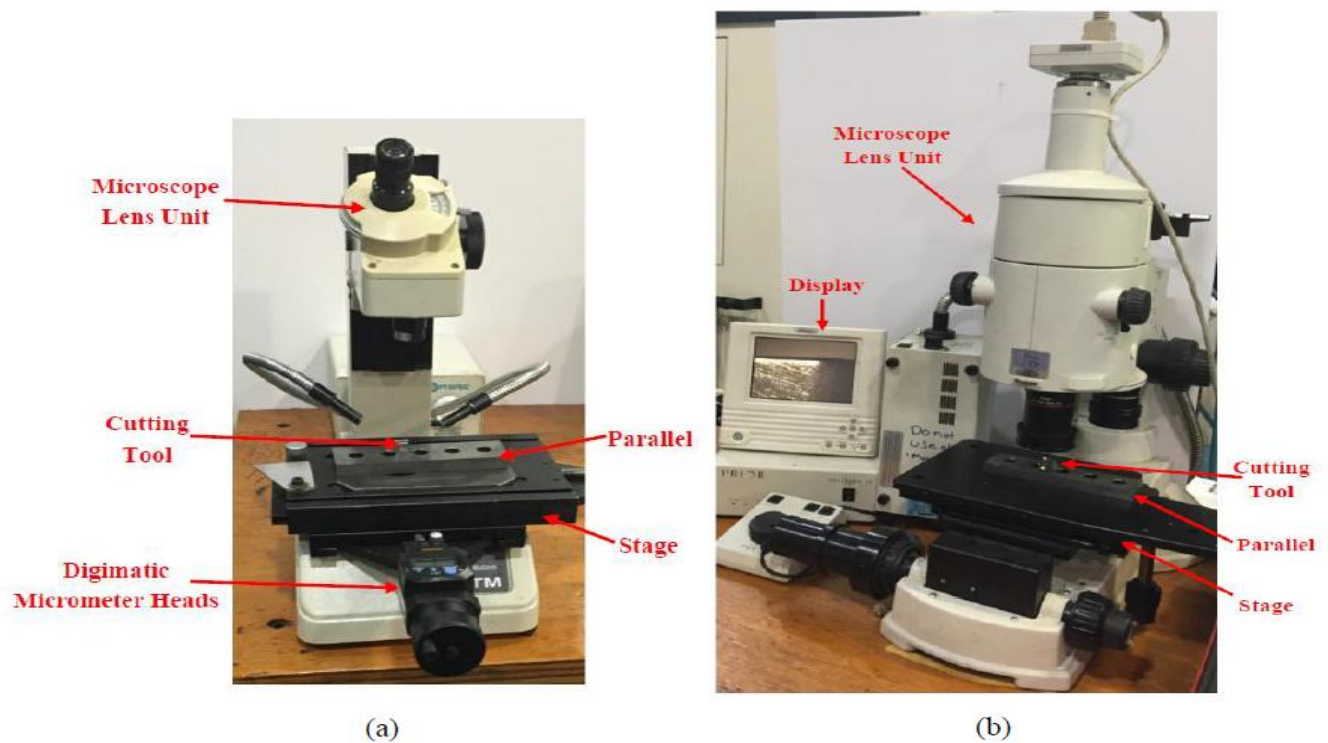


Figure 23: Microscopes used for tool wear studies (a) Mitutoyo Toolmaker Microscope (b) Nikon AZ100 Multizoom Microscope

3.6 Tool Coatings

3.6.1 Coating Details

The coatings investigated in the current research were deposited using the PVD processes. All the coatings, however, were not deposited with the same type of PVD process. The focus of the present investigation was not on how the coatings were deposited or how the deposition parameters of the PVD processes were varied. The aim was to study the effect of the coatings at resisting tool wear during Ti6Al4V machining and to study their self-adaptability through tribofilm formation. All the coatings, except TiB₂, were selected and developed in conjunction with Materials Research Laboratory, Kobe Steel Ltd., Japan.

The coatings studied were chosen based on the expectations of in-situ formation of self-lubricating tribo-oxide layers with low shear strength and thermal conductivity, which should result in lower friction between the contacting surfaces thereby reducing tool wear. However, it is worth mentioning that such lubricious tribo-oxides formation is a very complicated process due to the complexity of the mechanics of the cutting operations. Hence, the actual formation of the tribo-oxides and their effectiveness in addressing tool wear is hard to predict. Thus, the effectiveness of the coatings can be judged only through actual tool life experiments. The table below discusses the coatings chosen for investigation in this research based on the expected tribo-oxides formations.

Table 9: List of coatings investigated and expected tribo-oxides formation

<u>Coating</u>	<u>Expectations</u>
TiAlN	Monolayer, hard coating used in industry for Ti machining. Expected formation of Al ₂ O ₃ which gives improved wear resistance and enhanced chemical stability.
TiAlN/WN	Multilayer coating. Expected formation of Al ₂ O ₃ which gives improved wear resistance and enhanced chemical stability. Possible formation of self-lubricating solid W-O tribo-oxides.
TiB ₂	Monolayer, self-lubricating coating. Expected formation liquid B ₂ O ₃ tribo-oxides.
CrN/ZrN	Multilayer, self-lubricating nitride coating. Possible formation of lubricating/self-protective solid Cr-O tribo-oxides and self-protecting solid Zr-O tribo-oxides.
CrN/WN	Multilayer, self-lubricating nitride coating. Possible formation of self-lubricating solid Cr-O and W-O tribo-oxides.
TiCrAlBN	Hard, monolayer nitride coating. Expected formation of solid Cr-O tribo-oxides and liquid B ₂ O ₃ tribo-oxides.
CrWN	Monolayer nitride coating. Possible formation of self-lubricating solid Cr-O and W-O tribo-oxides.
CrWN/WN	Multilayer nitride coating. Possible formation of self-lubricating solid Cr-O and W-O tribo-oxides.
CrN/WN-WC	Multilayer coating. Possibly harder coating with formation of self-lubricating solid Cr-O and W-O tribo-oxides.
CrC/WC	Multilayer coating. Possibly harder coating with formation of self-lubricating solid Cr-O and W-O tribo-oxides.
CrWC/CrWN	Multilayer coating. Possibly harder coating with formation of self-lubricating solid Cr-O and W-O tribo-oxides.

3.6.2 Techniques for Coating Investigation

Various techniques were utilized to investigate the tool performance, study the effects of the coatings and characterize their properties. The techniques are listed as follows:

➤ Scanning Electron Microscopy (SEM) and Energy Dispersive Spectroscopy (EDS): SEM analysis was done to study the surface morphology of the worn tool. Chip shape and chip under-surface morphology was also studied using a SEM. Elemental analysis was also performed on worn tools to study the tribo-oxide formation on tool surface. SEM images were collected using a TESCAN VEGA\\LSU SEM at 20kV electron beam energy. For EDS analysis, the same device was used. INCA Software from Oxford Instruments was utilised for processing and analysis of EDS spectre.

➤ X-Ray Photoelectron Spectroscopy (XPS): Phase analysis was mainly performed with XPS to identify the tribo-oxides formed during the cutting process. XPS spectra were collected using a Physical Electronics (PHI) Quantera II spectrometer. The device uses an Aluminium anode source for X-Ray generation and a quartz crystal monochromator for focusing the generated X-Rays. The monochromatic Al K- α X-ray (1486.7 eV) source was operated at 50W and 15kV. The maximum system base pressure and operating pressure was 1.0×10^{-9} Torr and 2.0×10^{-8} Torr respectively. Survey spectra were obtained with 280eV pass energy whereas high resolution scans were performed with 55eV pass energy. All spectra were collected at take-off angles of 45° and a dual beam charge compensation system was utilized for neutralization of all samples.

The spot size of the beam was 200 μm . Calibration of the device was done with a sputter-cleaned piece of Silver (Ag) where the Ag $3d_{5/2}$ peak had a binding energy and full width half maximum (FWHM) of 368.0 ± 0.1 eV and 0.52 eV (at least) respectively. For data manipulation, PHI MultiPak Version 9.4.0.7 software was used.

➤ X-Ray Diffraction (XRD): XRD is a non-destructive, versatile technique and was used to measure the residual stress formation in the coating. A Bruker D8 DISCOVER with DAVINCI.DESIGN diffractometer equipped with a cobalt sealed tube source was utilized to examine the samples. The device has a Laser-Video sample alignment, parallel focus Goebel mirror, and a Vantec 500 MikroGap area detector. Data collection was done with the generator at 35 kV and 45 mA. Three scans at ϕ angles of 0° , 90° and 225° were collected. Each scan had 4 still frames collected at ψ angles of 10° , 30° , 50° , and 70° . DIFFRAC Measurement Centre Version 4.0 software and Leptos Version 7 was used to collect the 2D frames and perform residual stress calculations respectively.

➤ Nano-indentation: The micro-mechanical characteristics of the coatings were measured on WC-Co using a Micro Materials Nano Test system. Nano-indentation has been performed in the load controlled mode with a Berkovich diamond indenter calibrated for load, displacement, frame compliance and indenter shape according to an ISO14577-4 procedure. The area function for the indenter was determined by indentations under loads in the range of 0.5–500 mN into a fused silica reference sample. For nano-indentations into the coatings, the peak load of 20 mN was selected and 40 indentations were performed per coating. This load was chosen to

minimize any influence of surface roughness on the data whilst ensuring that the indentation contact depth is under 1/10 of the film thickness, so that coating-only (load-invariant) hardness can be measured in combination with coating-dominated elastic modulus. Nano-indentations were performed at room temperature with a 60 seconds post indentation thermal drift correction and dwell period of 5 seconds at maximum load.

3.7 Chip Analysis

Chip analysis was done for select tools to study and compare the effect of tool workpiece tribology of the cutting process. Chips were analyzed by SEM to study their shapes and under-surface morphology. The cross-sections of the chips were also measured to determine the chip thickness ratio and the shear plane angle. The cross-sections of the chips were first prepared by cold mounting using epoxy resin and hardener. The samples were then ground with SiC paper and polished. For SEM analysis, the chips were mounted on stubs with carbon tapes and then sputter coated with gold (36nm).



Figure 24: Mounted chips

Chapter 4: Results and Discussion

4.1 Identification of a Benchmark Tool for Turning Operations

As mentioned in earlier sections, researchers have found that uncoated straight grade cemented carbides are still the ideal choice for titanium machining. However, some researchers and tool industries recommend a TiAlN coating on tools for titanium machining. TiAlN has been reported to have strong chemical stability, low thermal conductivity, high oxidation wear resistance at 900°C and excellent crater wear resistance [62], [78]. The Al component of TiAlN coatings forms Al_2O_3 on the surface of the tool during machining which is the reason behind its improved wear resistance and enhanced chemical stability [79], [80].

Therefore, in the current study a tool life comparison was first made for rough turning operation for uncoated and TiAlN straight grade cemented carbide tools. The tool which showed better tool life was used as the benchmark tool and all other coatings tested in the current research were compared against this tool. Both the uncoated and TiAlN coated tool were of Kennametal CNMG432 type. Figure 25 shows the tool life comparison between the TiAlN coated and uncoated tool. Figure 26 shows 3D images of the worn uncoated and TiAlN coated roughing insert after a 1000 m cut.

Tool Wear Curve for Rough Turning Operation

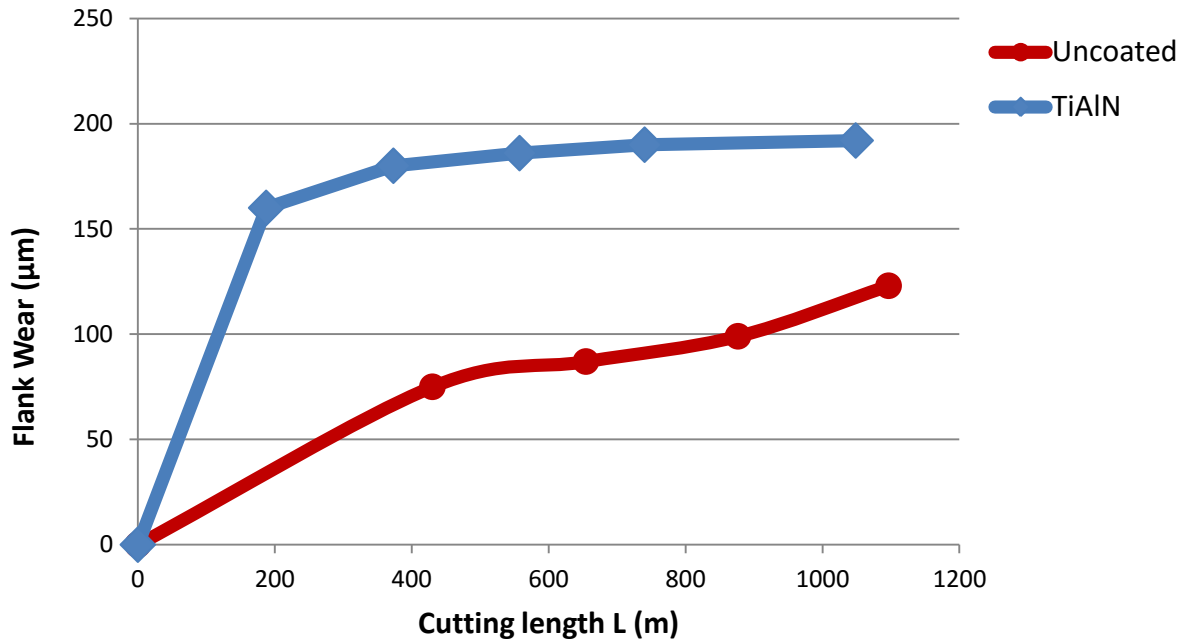


Figure 25: Tool wear curve for rough turning of uncoated and TiAlN coated tools

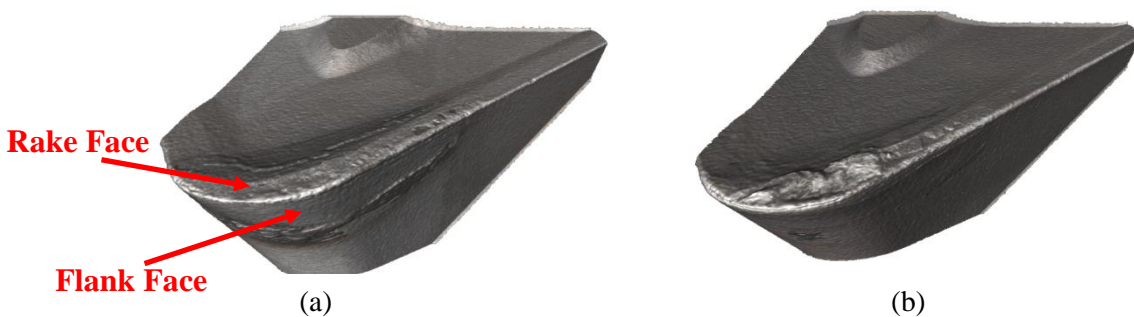


Figure 26: 3D images of worn tool after 1000 m cut: (a) uncoated insert (b) TiAlN coated insert [Provided by Kobe Steel Ltd.]

As can be seen from Figure 25, WC/Co tool outperforms TiAlN for rough turning operations in terms of tool life. From Figure 26, it is evident that wear is significantly higher on both the rake and flank face of the TiAlN coated tool compared to the uncoated tool. Intensive adhesion of the workpiece material is seen on the rake face of the coated tool. Crater wear is also prominent on the coated tool. SEM elemental mapping of both the uncoated and TiAlN coated tool shows the formation of more W-O lubricious tribofilm on the uncoated tool as compared to TiAlN coated tool (Figure 27 and Figure 28). XPS studies performed on the uncoated tool compliments the EDS results.

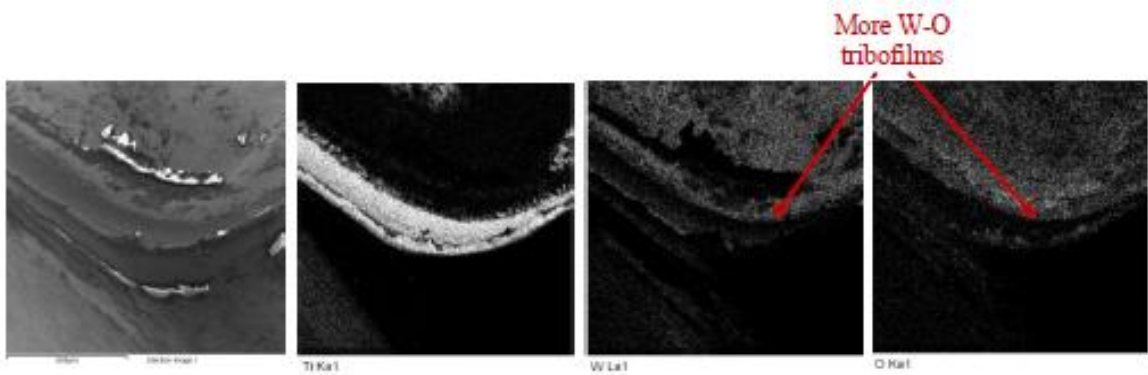


Figure 27: SEM image and EDS elemental maps of the worn rake surface of uncoated tool

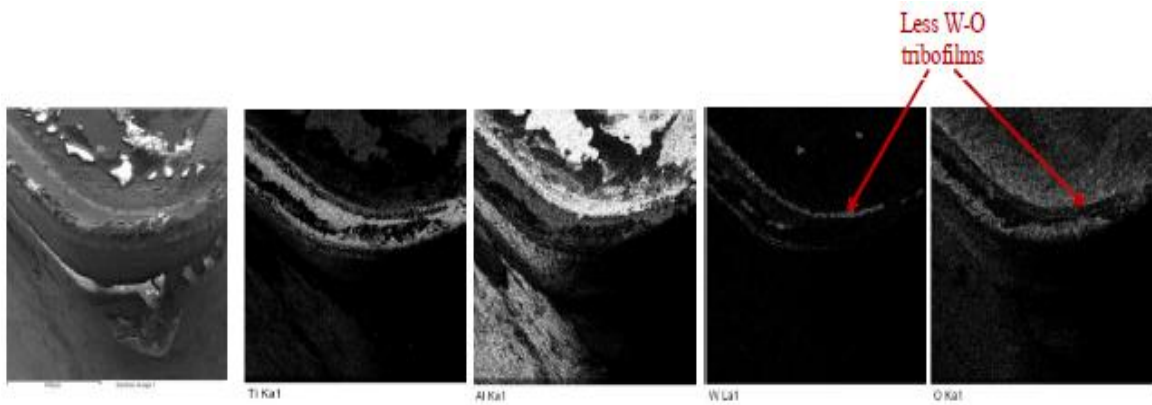


Figure 28: SEM image and EDS elemental maps of the worn rake surface of TiAlN coated tool

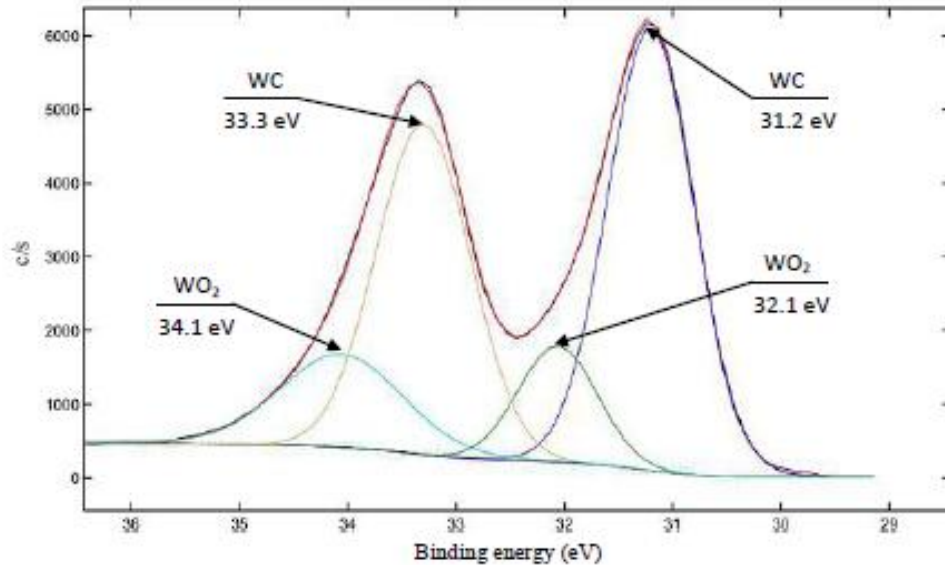


Figure 29: XPS of rake surface of uncoated tool

Figure 29 shows the data obtained from XPS of the uncoated tool based on intensity peaks at W4f. From XPS analysis, evidence of some tribo-oxidation formation is found. W-O tribo-films are very good high temperature solid lubricants. Thus W-O solid lubricant serves to lubricate the tool surface leading to a reduction of the adhesive interaction at the chip/tool interface and thereby results in better tool life for the uncoated tool.

Thus from the experimental results it is clearly evident that the uncoated tool outperforms the TiAlN tool. Elemental mapping and XPS results suggest that formation of a lubricious WO₂ tribofilm contributes to the better performance of the uncoated tools. It's worth mentioning that the WO₂ tribofilm layer is less probable to form on the coated tool as the coating on the oxidized tool surface shields the underlying tungsten-based substrate and diminishes the development of W-O tribo-oxides.

Therefore, based on the aforementioned experimental results and analysis, the uncoated straight grade cemented carbide tool was taken as the benchmark tool. Tool performances of all the different coated tools tested in the present research were compared with the benchmark (uncoated) tool.

4.2 Identification of Coated Turning Tools Outperforming Benchmark

As mentioned before (Table 9), based on the expected generation of beneficial tribofilms, a series of coatings were selected for machining of Ti6Al4V. Rough turning and finish turning tests were performed with coated tools and their tool life was compared with that obtained for the pre-defined benchmark (uncoated) tool. The machining results are presented in this section. The tool wear curves for all the selected tools for roughing and finishing operations are provided in Figure 30 and Figure 31 respectively. The roughing operations for all tools were conducted for a cutting length of 1000 m first. Tool life studies were continued for much longer lengths of cut only for the uncoated tool (benchmark) and coated tools that outperformed the uncoated tool up to this initial cutting length.

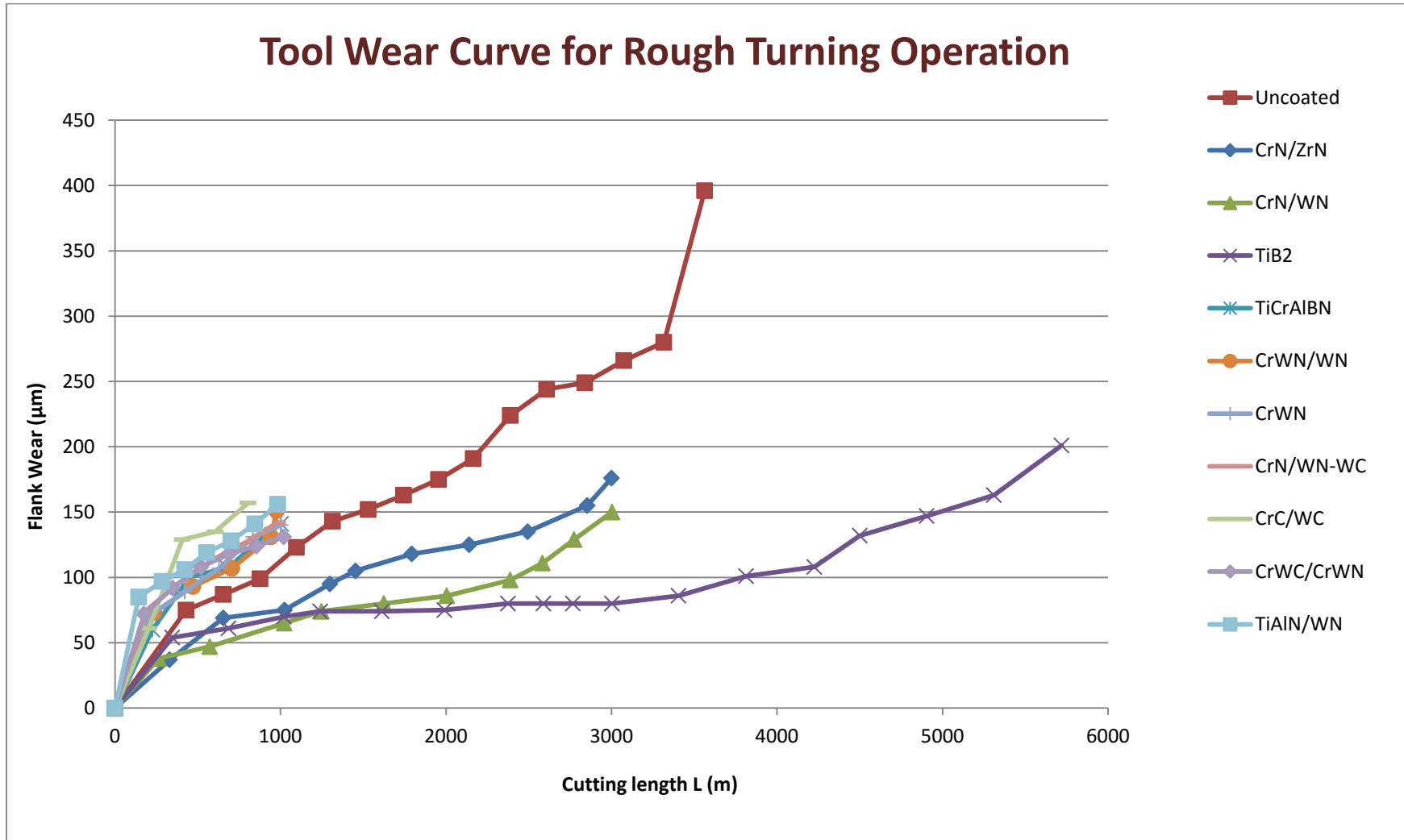


Figure 30: Tool wear curve of uncoated and several coated tools for rough turning operation

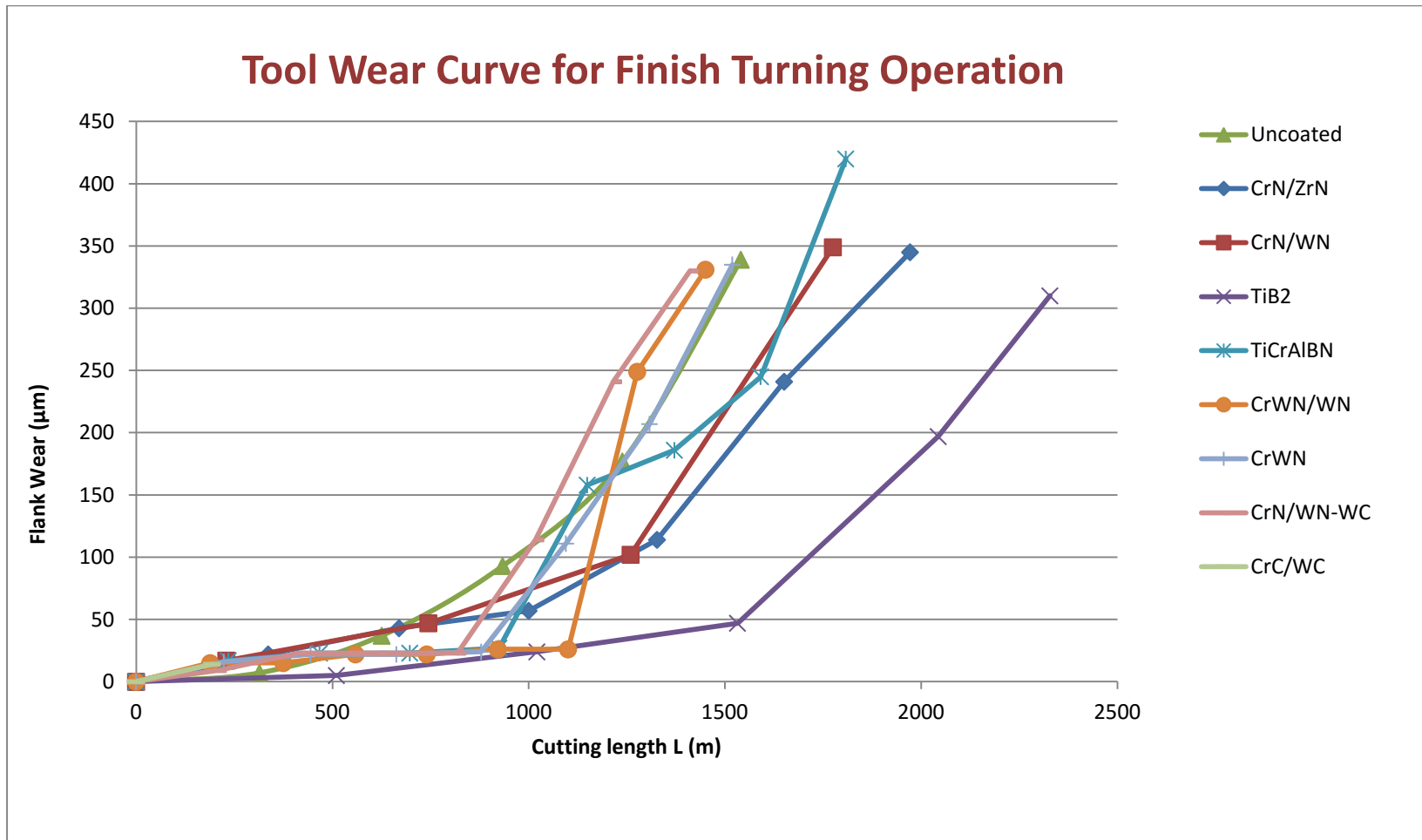


Figure 31: Tool wear curve of uncoated and several coated tools for finish turning operation

Based on tool life studies for both roughing and finishing operations (as seen in Figure 30 and Figure 31), it was found that TiB_2 had the best performance. It demonstrated the most improvement in tool life compared with the benchmark tool, followed by CrN/WN and CrN/ZrN coated tools respectively. The remaining TiAlN/WN, TiCrAlBN, CrWN/WN, CrWN, CrN/WN-WC, CrC/WC and CrWC/CrWN coated tools did not perform well and showed worse tool life than the uncoated tool.

Possible reasons behind the failure of these coatings may be due to the shortcomings of the solid lubricants they were able to generate. Solid lubricants often under high temperature and oxidative environments undergo irreversible chemical structural change that reduces their lubricity and forms non-lubricious, abrasive by-products. Their coefficients of friction fluctuate based on contact conditions and the replenishment of the lubricants over time is also very limited [81]. However, the exact reason for the poor performance of the other coatings is not understood completely nor was it investigated.

4.3 Material Characterization of Most Effective Coatings

As mentioned before (Section 4.2), the TiB_2 , CrN/WN and CrN/ZrN coated tool outperformed the benchmark tool. However, the improvement with the CrN/ZrN coated tool was lower as compared to the TiB_2 and CrN/WN coated tool. Hence, material characterization has been performed for only TiB_2 and CrN/WN coated tools in order to assess the tribofilm formation on the tool surfaces. This section gives a detailed account of the material characterization studies along with other relevant studies performed.

4.3.1 TiB₂ Coated Tool

Out of all the coatings tested, TiB₂ showed the best performance. Figure 32 shows the 3D images of the worn uncoated and TiB₂ coated roughing insert after 1000 m cut. Figure 33 and Figure 34 show the tool wear curve for both uncoated and TiB₂ coated tool for rough turning and finish turning operation respectively. From the tool wear curves, it is clear that the TiB₂ coating increases tool life significantly. Table 10 and Table 12 show the optical images of the flank surface of both the uncoated and TiB₂ coated roughing and finishing tools taken with the multipurpose zoom microscope system. The images give an account of how flank wear progressed over time and also gives confirmation of less progressive flank wear and built up edge formation on the TiB₂ coated tools compared to the uncoated tools. Table 11 and Table 13 show the optical images comparing the rake surface of the uncoated and TiB₂ coated tools for roughing and finishing for different lengths of cut.

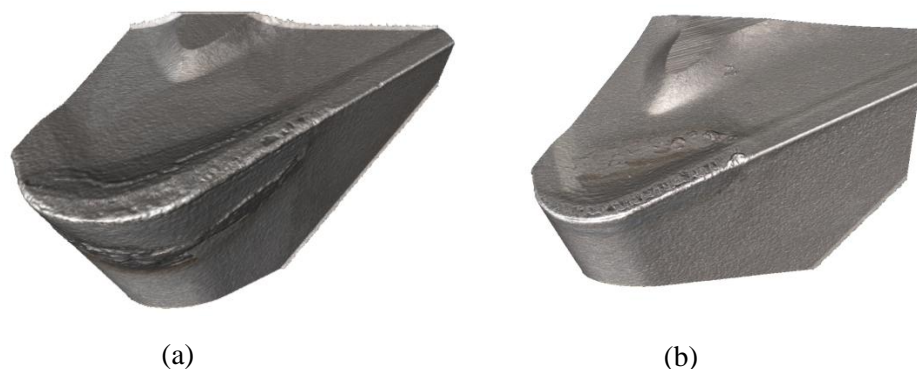


Figure 32: 3D images of worn tool after 1000 m cut: (a) uncoated insert
(b) TiB₂ coated insert [Provided by Kobe Steel Ltd.]

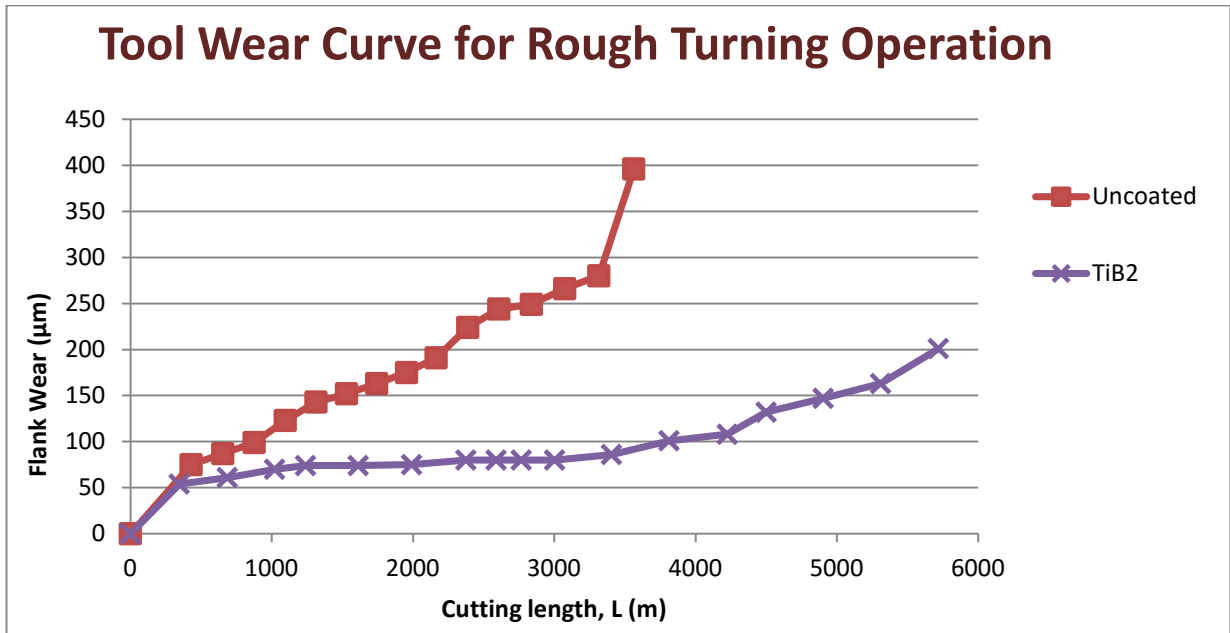


Figure 33: Tool wear curve for uncoated and TiB₂ coated tool for roughing operation

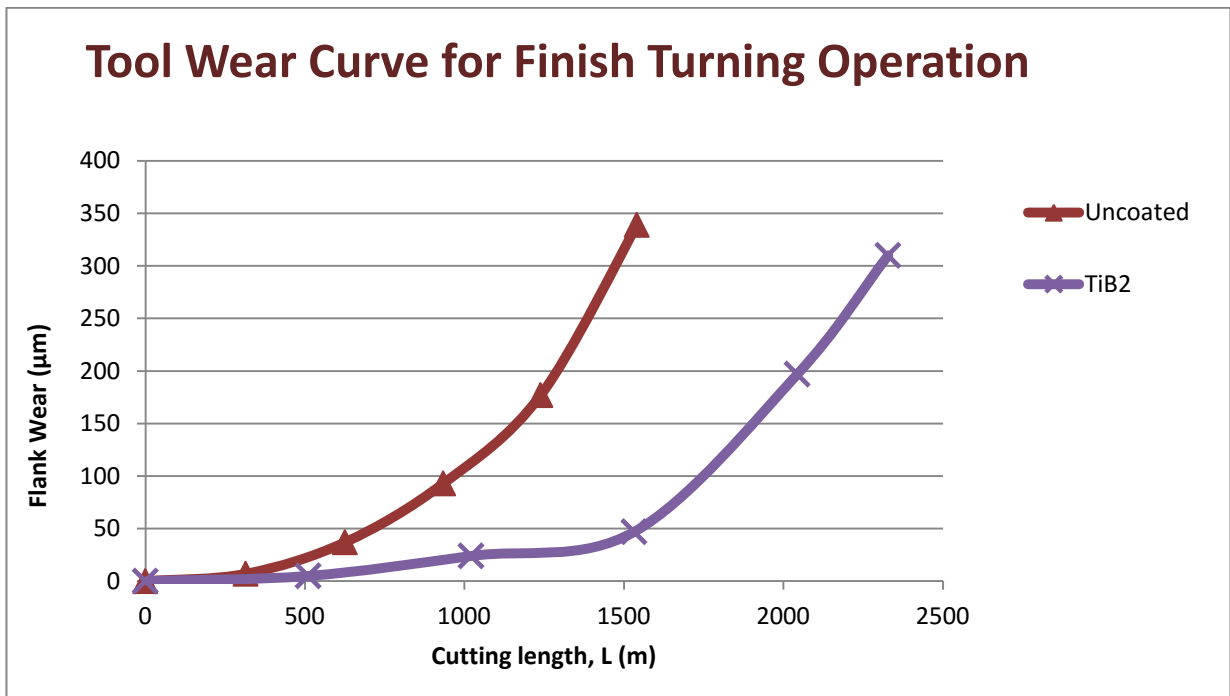


Figure 34: Tool wear curve for uncoated and TiB₂ coated tool for finishing operation

Table 10: Optical images of Flank Wear vs. Length of Cut for uncoated and TiB₂ coated worn roughing inserts

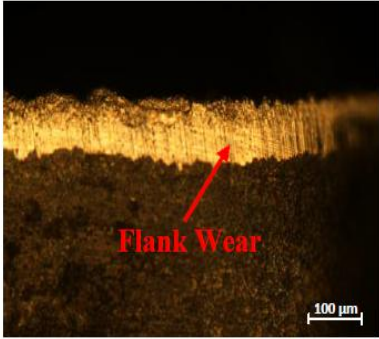
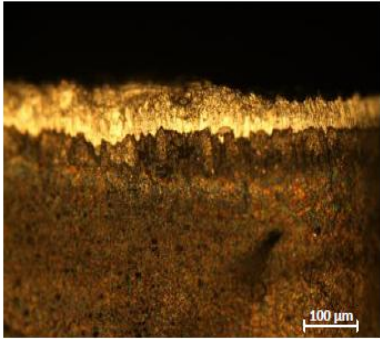
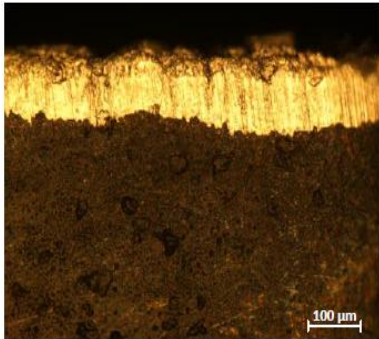
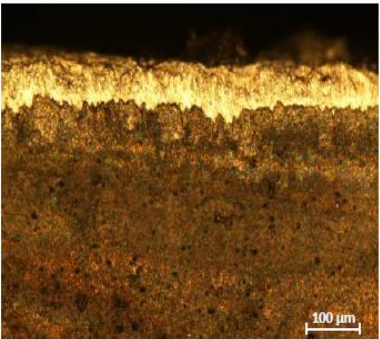
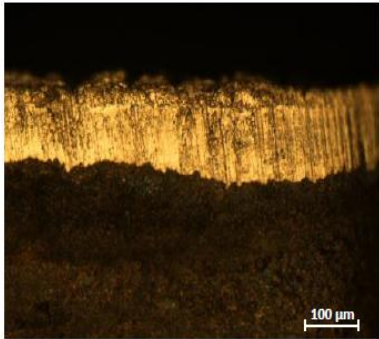
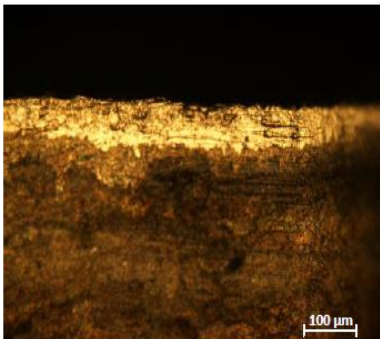
<u>Uncoated</u>		<u>TiB₂</u>	
<u>Length of cut (m)</u>	<u>Image of Flank Surface</u>	<u>Length of cut (m)</u>	<u>Image of Flank Surface</u>
654.5		686.21	
1096.6		1021.31	
1955.43		1991.07	

Table 10: Optical images of Flank Wear vs. Length of Cut for uncoated and TiB₂ coated worn roughing inserts (continued)

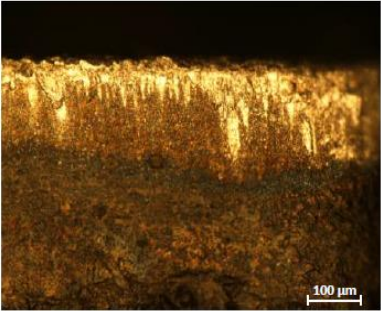
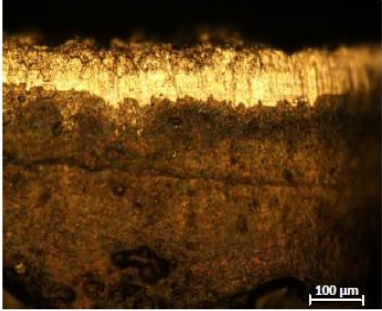
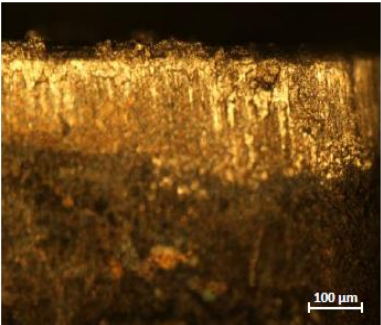
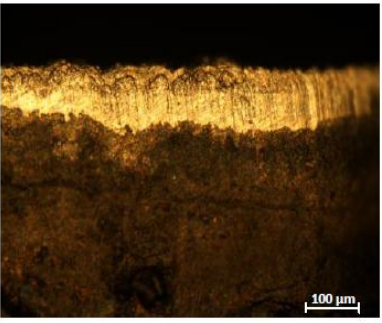
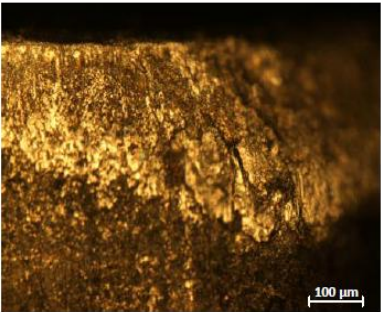
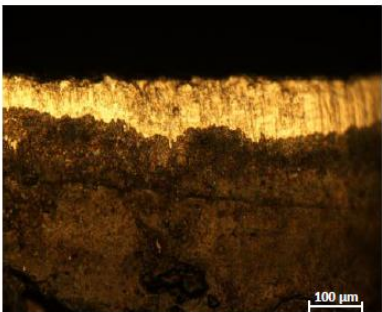
<u>Uncoated</u>		<u>TiB₂</u>	
<u>Length of cut (m)</u>	<u>Image of Flank Surface</u>	<u>Length of cut (m)</u>	<u>Image of Flank Surface</u>
2838.95		2767.02	
3074.95		3003.13	
3563		3405.67	

Table 11: Optical images of Rake Wear vs. Length of Cut for uncoated and TiB₂ coated worn roughing inserts

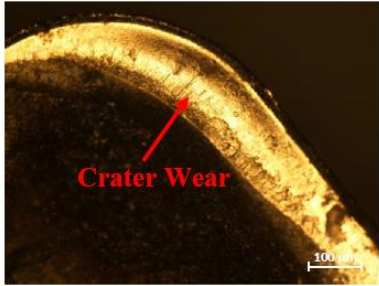
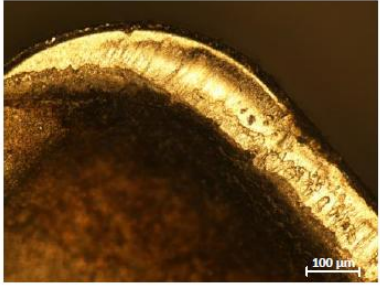
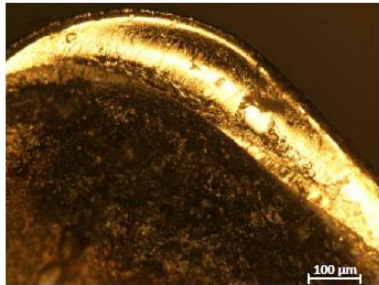
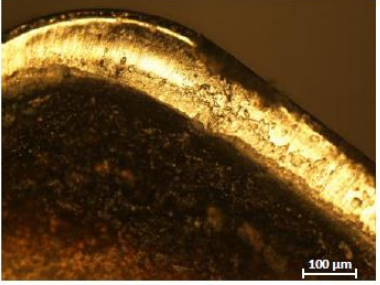
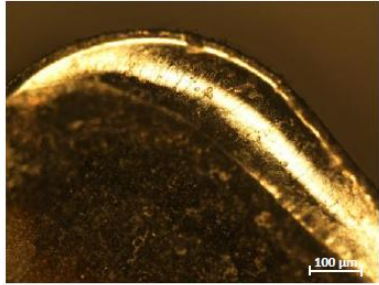
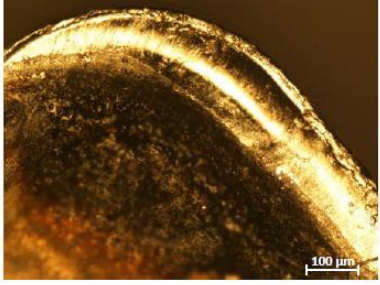
<u>Uncoated</u>		<u>TiB₂</u>	
<u>Length of cut (m)</u>	<u>Image of Rake Surface</u>	<u>Length of cut (m)</u>	<u>Image of Rake Surface</u>
654.5		686.21	
1096.6		1021.31	
1955.43		1991.07	

Table 11: Optical images of Rake Wear vs. Length of Cut for uncoated and TiB₂ coated worn roughing inserts (continued)

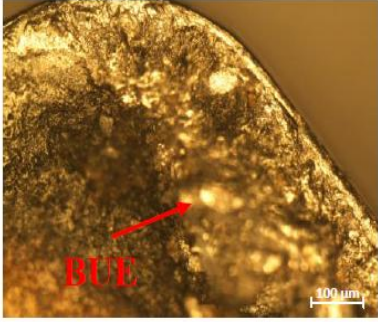
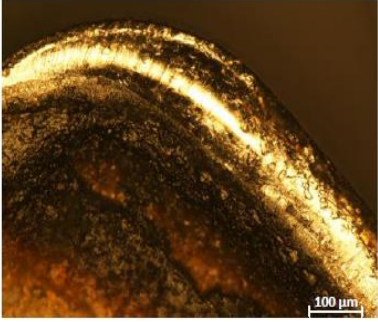
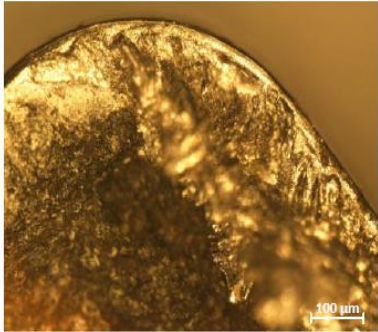
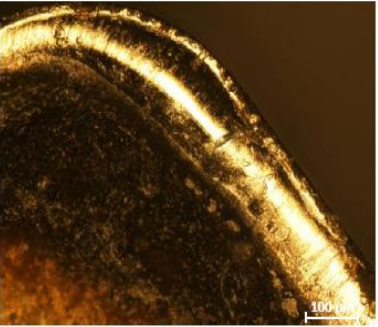
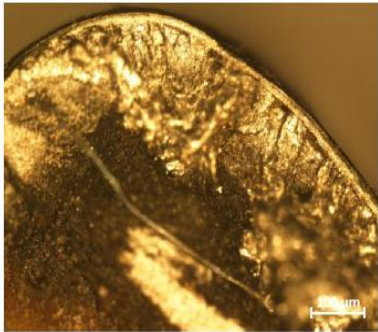
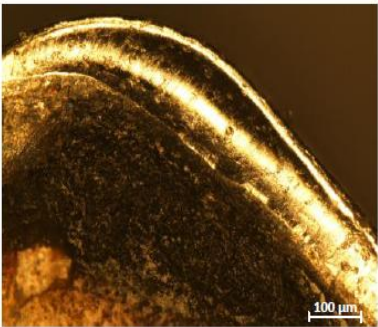
<u>Uncoated</u>		<u>TiB₂</u>	
<u>Length of cut (m)</u>	<u>Image of Rake Surface</u>	<u>Length of cut (m)</u>	<u>Image of Rake Surface</u>
2838.95		2767.02	
3074.95		3003.13	
3563		3405.67	

Table 12: Optical images of Flank Wear vs. Length of Cut for uncoated and TiB₂ coated worn finishing inserts

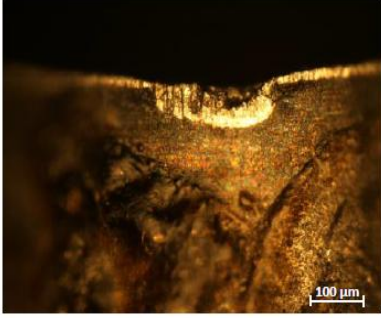
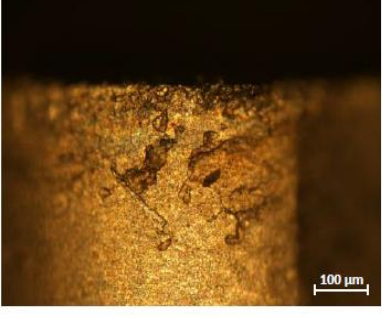
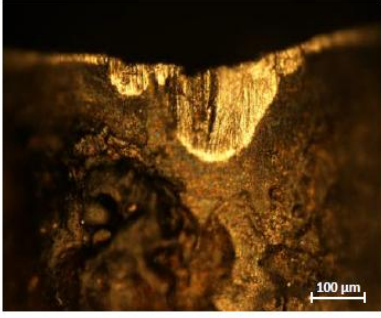
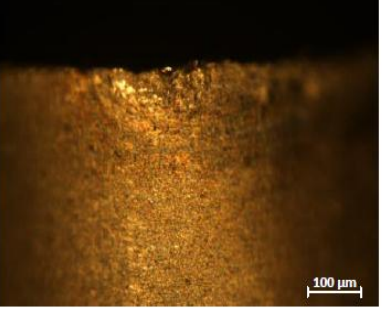
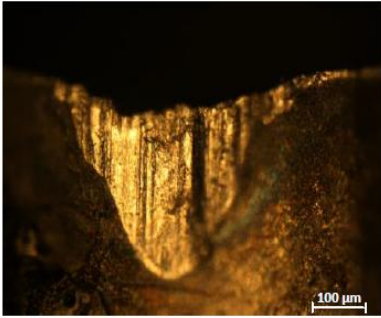
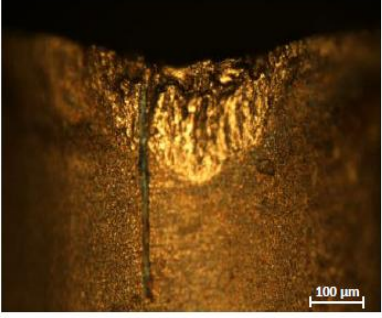
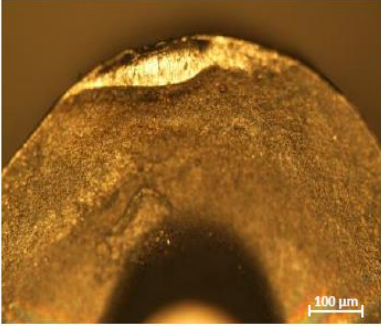
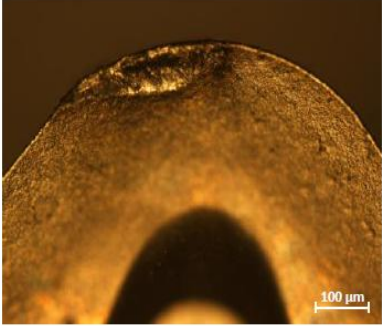
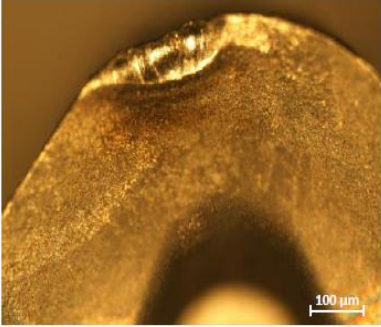
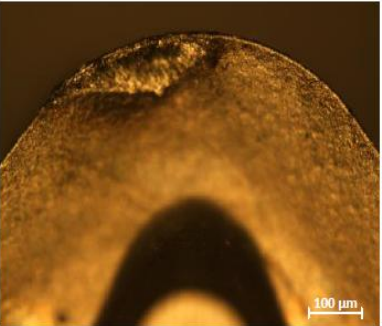
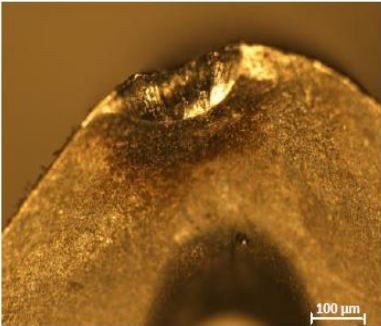
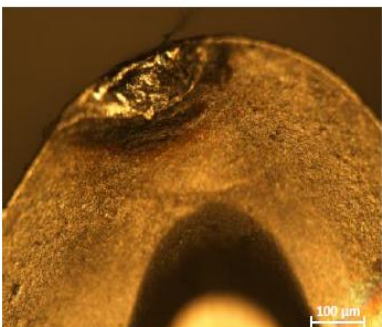
<u>Uncoated</u>		<u>TiB₂</u>	
<u>Length of cut (m)</u>	<u>Image of Flank Surface</u>	<u>Length of cut (m)</u>	<u>Image of Flank Surface</u>
933.87		1021.17	
1238.89		1532.24	
1540.79		2043.64	

Table 13: Optical images of Rake Wear vs. Length of Cut for uncoated and TiB₂ coated worn finishing inserts

<u>Uncoated</u>		<u>TiB₂</u>	
<u>Length of cut (m)</u>	<u>Image of Rake Surface</u>	<u>Length of cut (m)</u>	<u>Image of Rake Surface</u>
933.87		1021.17	
1238.89		1532.24	
1540.79		2043.64	

As can be seen from the optical images of the rake surfaces of roughing and finishing uncoated and TiB_2 coated tools (Table 11 and Table 13), crater wear progression is less on TiB_2 coated tools compared to uncoated tools. Built up edge (BUE) is quite significant on the uncoated tools while negligible on the TiB_2 coated tools. Similar trend is seen for flank wear (Table 10 and Table 12). Figure 35 shows SEM images of rake surfaces of uncoated and TiB_2 coated worn tools after roughing cut of 3000 m.

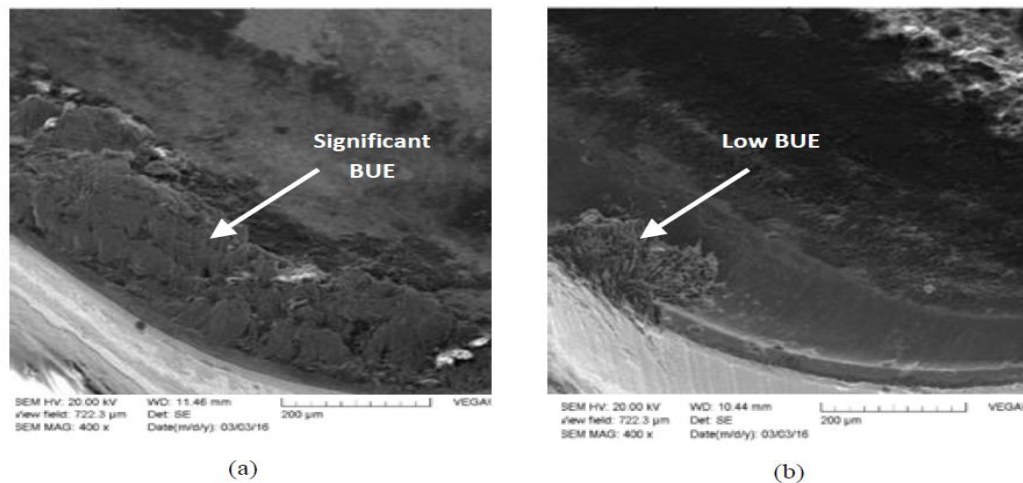


Figure 35: SEM images of rake surfaces of worn inserts after 3000 m cut:
(a) Uncoated tool (b) TiB_2 coated tool

From the optical and SEM images, it is apparent that uncoated tools suffer from significant built up edge formation. XPS spectra were collected to compare the built up material on uncoated and TiB_2 coated roughing tools after different Ar etching time (3 and 8 min). The XPS spectre was collected based on the intensity of the peaks at locations Ti 2P, W 4f, Al 2p and O 1s. The following figures and tables give the high resolution XPS spectra and the relative percentages of the phases present in the built up material for the uncoated and TiB_2 coated tool after 3000 m cut.

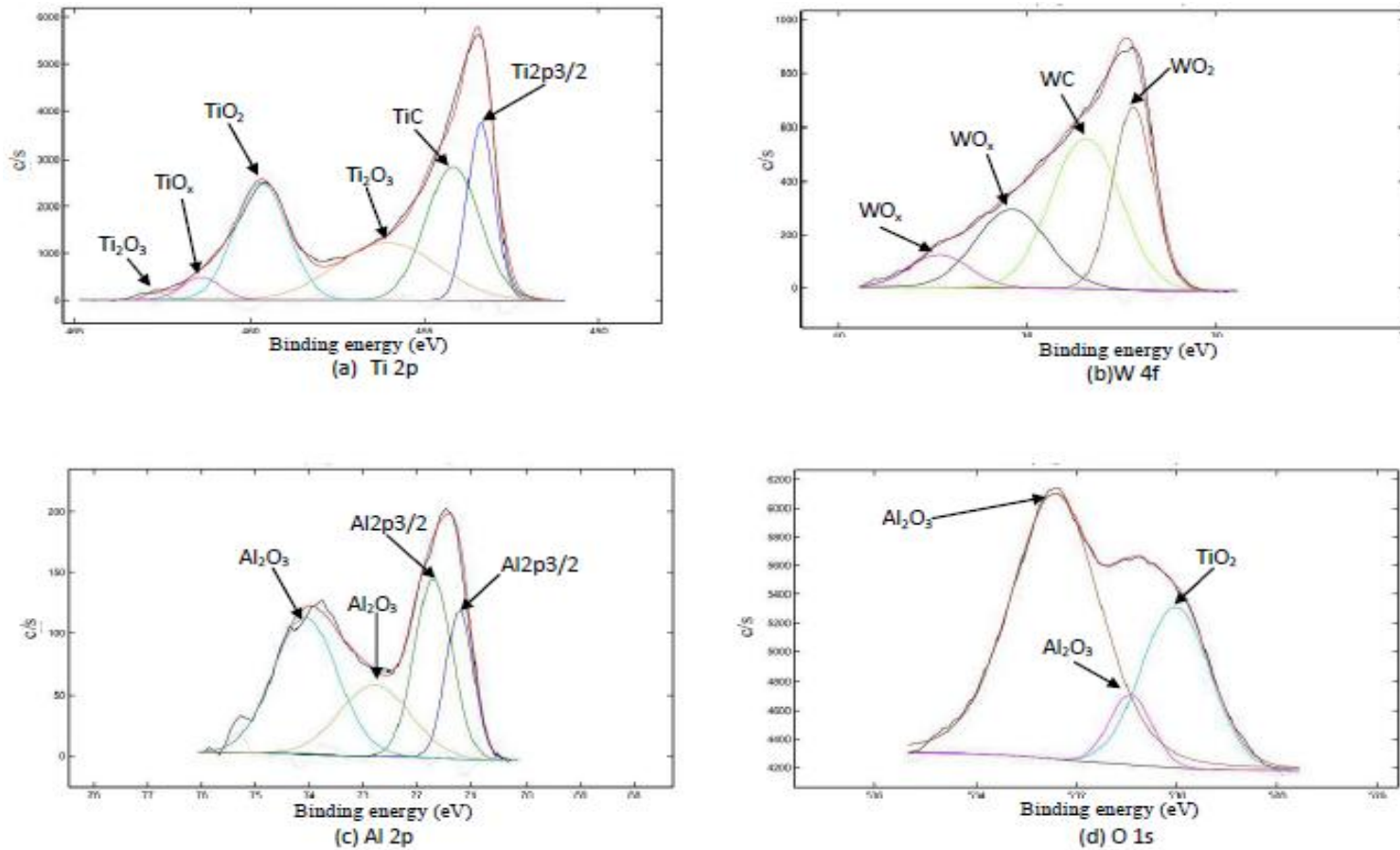


Figure 36: High Resolution XPS after 3 min Ar etching time on the built up of rake surface of uncoated tool after 3000 m cut

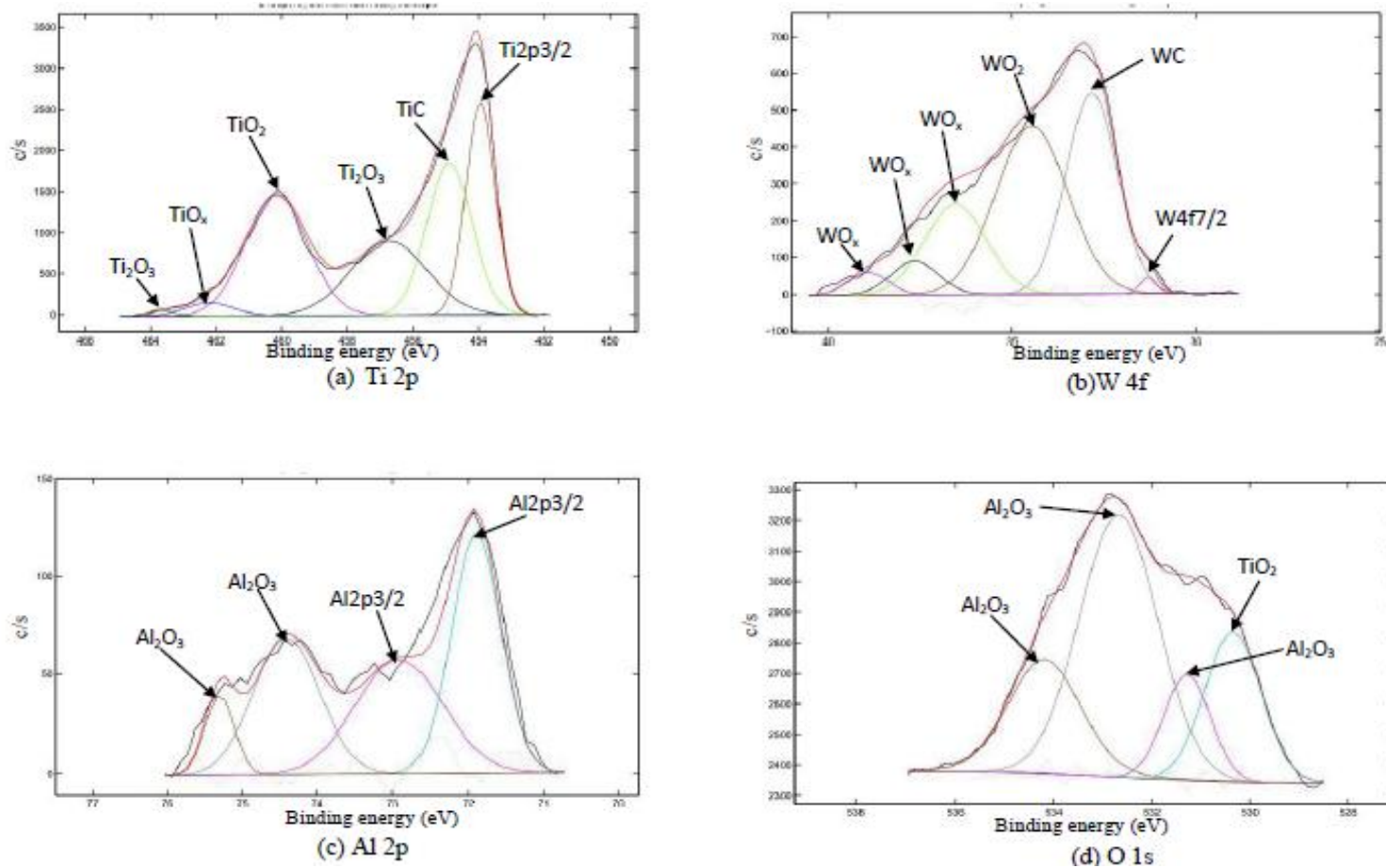


Figure 37: High Resolution XPS after 3 min Ar etching time on the built up of rake surface of TiB_2 coated tool after 3000 m cut

Table 14: Relative percentages of the phases present on the built up of the rake surface of uncoated tool after 3000 m cut obtained from High Resolution XPS after 3 min Ar etching time

Peak (eV)	Present Phases	Percentage (%)
453.4	Ti2p3/2	19.2%
454.2	TiC	28.7%
456.1	Ti ₂ O ₃	23.2%
459.7	TiO ₂	24.6%
461.4	TiO _x	3.6%
462.7	Ti ₂ O ₃	0.7%

(a) Ti 2p

Peak (eV)	Present Phases	Percentage (%)
32.2	WO ₂	29.3%
33.4	WC	40.7%
35.4	WO _x	22.3%
37.3	WO _x	7.8%

(b)W 4f

Peak (eV)	Present Phases	Percentage (%)
71.2	Al2p3/2	16.7%
71.9	Al2p3/2	27.3%
72.8	Al ₂ O ₃	20.5%
74.1	Al ₂ O ₃	35.4%

(c) Al 2p

Peak (eV)	Present Phases	Percentage (%)
530.0	TiO ₂	27.4%
530.9	Al ₂ O ₃	7.4%
532.4	Al ₂ O ₃	65.1%

(d) O 1s

Table 15: Relative percentages of the phases present on the built up of the rake surface of TiB₂ coated tool after 3000 m cut obtained from High Resolution XPS after 3 min Ar etching time

Peak (eV)	Present Phases	Percentage (%)
453.9	Ti2p 3/2	23.1%
454.9	TiC	25.5%
456.7	Ti ₂ O ₃	20.9%
460.2	TiO ₂	27.7%
462.2	TiO _x	2.3%
463.7	Ti ₂ O ₃	0.5%

(a) Ti 2p

Peak (eV)	Present Phases	Percentage (%)
31.3	W4f _{7/2}	0.9%
32.8	WC	33.6%
34.5	WO ₂	39.4%
36.5	WO _x	18.2%
37.6	WO _x	5.1%
38.9	WO _x	2.9%

(b) W 4f

Peak (eV)	Present Phases	Percentage (%)
71.9	Al2p3/2	35.8%
72.9	Al2p3/2	29.6%
74.4	Al ₂ O ₃	27.5%
75.3	Al ₂ O ₃	7.1%

(c) Al 2p

Peak (eV)	Present Phases	Percentage (%)
530.4	TiO ₂	19.8%
531.3	Al ₂ O ₃	11.6%
532.7	Al ₂ O ₃	48.4%
534.2	Al ₂ O ₃	20.3%

(d) O 1s

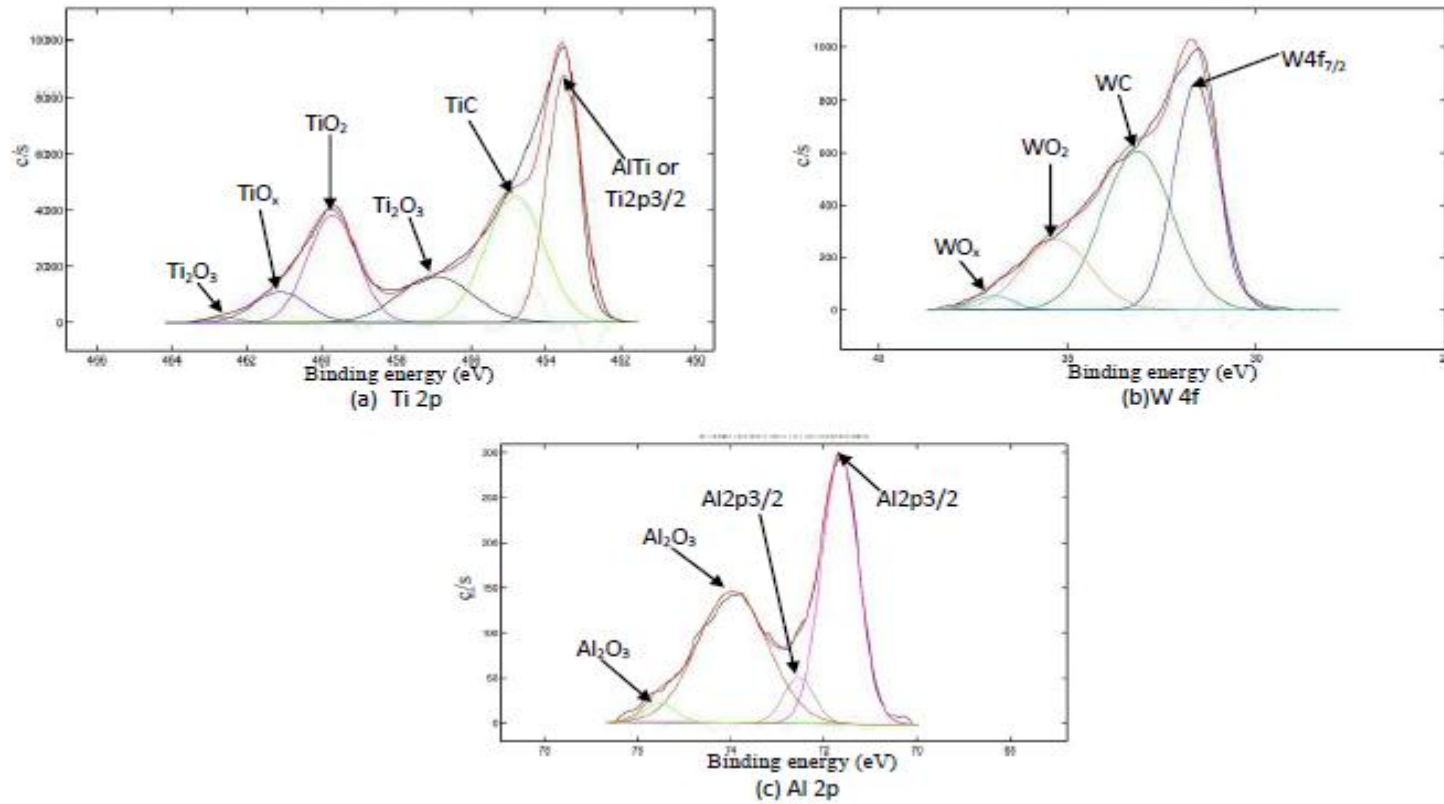


Figure 38: High Resolution XPS after 8 min Ar etching time on the built up of rake surface of uncoated tool after 3000 m cut

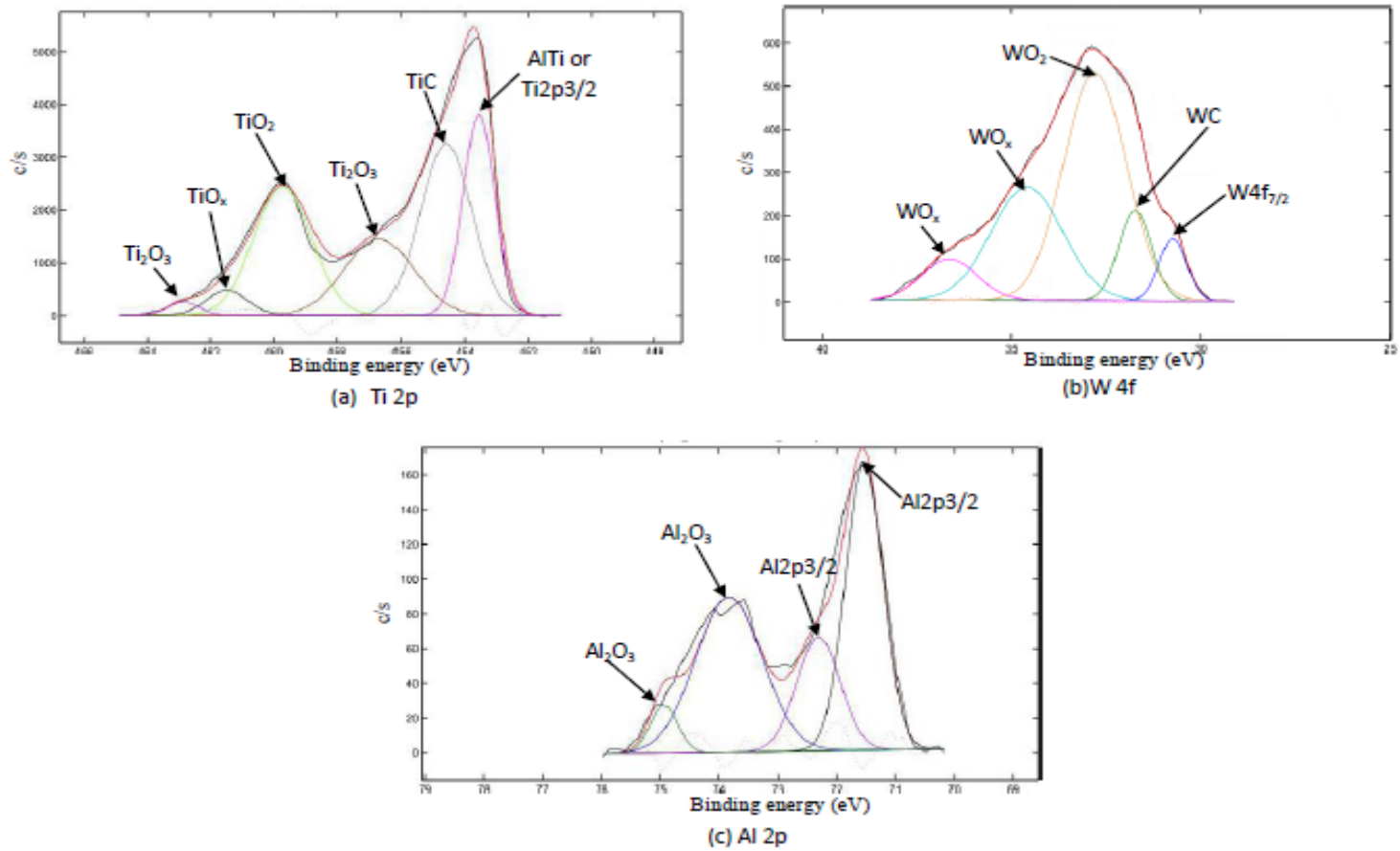


Figure 39: High Resolution XPS after 8 min Ar etching time on the built up of rake surface of TiB₂ coated tool after 3000 m cut

Table 16: Relative percentages of the phases present on the built up of the rake surface of uncoated tool after 3000 m cut obtained from High Resolution XPS after 8 min Ar etching time

Peak (eV)	Present Phases	Percentage (%)
453.5	AlTi or Ti2p3/2	31.9%
454.8	TiC	27.9%
457.0	Ti ₂ O ₃	12.9%
459.7	TiO ₂	20.3%
461.1	TiO _x	6.3%

(a) Ti 2p

Peak (eV)	Present Phases	Percentage (%)
31.6	W4f _{7/2}	38.0%
33.2	WC	42.3%
35.3	WO ₂	17.9%
37.0	WO _x	1.9%

(b)W 4f

Peak (eV)	Present Phases	Percentage (%)
71.7	Al2p3/2	47.3%
72.5	Al2p3/2	6.6%
74.0	Al ₂ O ₃	43.4%
75.5	Al ₂ O ₃	2.7%

(c) Al 2p

Table 17: Relative percentages of the phases present on the built up of rake surface of TiB₂ coated tool after 3000 m cut obtained from High Resolution XPS after 8 min Ar etching time

Peak (eV)	Present Phases	Percentage (%)
453.6	AlTi or Ti2p3/2	21.9%
454.6	TiC	30.2%
456.7	Ti ₂ O ₃	17.7%
459.7	TiO ₂	25.4%
461.5	TiO _x	3.4%
462.9	Ti ₂ O ₃	1.4%

(a) Ti 2p

Peak (eV)	Present Phases	Percentage (%)
30.7	W4f _{7/2}	5.9%
31.7	WO ₂	10.1%
32.8	WC	48.7%
34.6	WO _x	27.6%
36.6	WO _x	7.7%

(b)W 4f

Peak (eV)	Present Phases	Percentage (%)
71.5	Al2p3/2	39.6%
72.3	Al2p3/2	18.0%
73.8	Al ₂ O ₃	37.7%
74.9	Al ₂ O ₃	4.7%

(c) Al 2p

Built up edge is a dynamic structure that forms on a tool surface during cutting. It forms as a result of mass transfer from the counter body (workpiece material) onto the tool surface with further interaction with environment as well as tribo-oxidation. Built up edge in this case is a ceramic-like composite layer consisting of a number of compounds. The XPS results show that there is no visible difference in composition of built up edge between TiB_2 coated and uncoated cutting tools. No substantial difference was found with increase of etching time. The presences of the following compounds were confirmed by XPS study during machining of Ti (rough turning):

- Ti-C phase, reduces diffusion rate of tool material into the contacting body
- Ti-O phases, different forms of non-protective phase
- W-O phases, different forms of solid lubricant
- Al-O phases, mostly alumina (ceramic phase)
- W-C phase

TiC formed is a hard interlayer and formulates a seizure zone reducing diffusion of tool constituents into the workpiece material [13], [17], [41], [48], [49]. Hartung and Kramer [49] suggested that a stable ceramic-like built up layer offers significant protection of the tool surface and reduces tool wear as it reduces the diffusion rate of tool components. However, the stability of build-up edge is very low under adhesive/attrition wear conditions [11] and eventually results in deep surface damage and massive fracture of the cutting edge.

To confirm and study the mechanism of formation of tribofilms, XPS and EDS analyses of the worn tool surfaces were carried out. Figure 40 shows the EDS

spectroscopy of the rake surface of TiB_2 coated tool. Figure 42 and Figure 43 show the photoelectron spectra of the flank and rake surface of the TiB_2 coated worn roughing insert. The XPS spectra was interpreted based on the changes in the intensity that occurred at the positions of $\text{Ti}2p$ and $\text{B}1s$ lines for the coating after wear. Intensive tribo-oxidation was found to have occurred on the surface of the coating after wear took place. Due to high temperatures generated during friction, metallic elements of the coating oxidized to form corresponding oxides such as Ti-O and B-O . Table 18 and Table 19 illustrate the relative percentages of the phases present obtained by XPS of the worn TiB_2 coated tool.

Both EDS and XPS studies show that TiB_2 coating tribo-oxidises with the formation of lubricious B_2O_3 phase. Boron oxide is a very good lubricant with a low coefficient of friction [83]. Figure 41 compares the average frictional coefficients of various oxides. As mentioned earlier (in section 2.3.2 and 2.3.4), the temperature on the rake surface during titanium machining reaches above 1000°C . This is significantly above the melting point of B_2O_3 (melting point of B_2O_3 is 450°C). Hence, the tribo-oxide acts as a liquid lubricant and thus reduces friction between the tool-chip and tool-workpiece interfaces resulting in less BUE formation. Consequently, TiB_2 coated tools show a substantial tool life improvement as compared to the uncoated carbide tool and other coatings studied during continuous cutting operations.

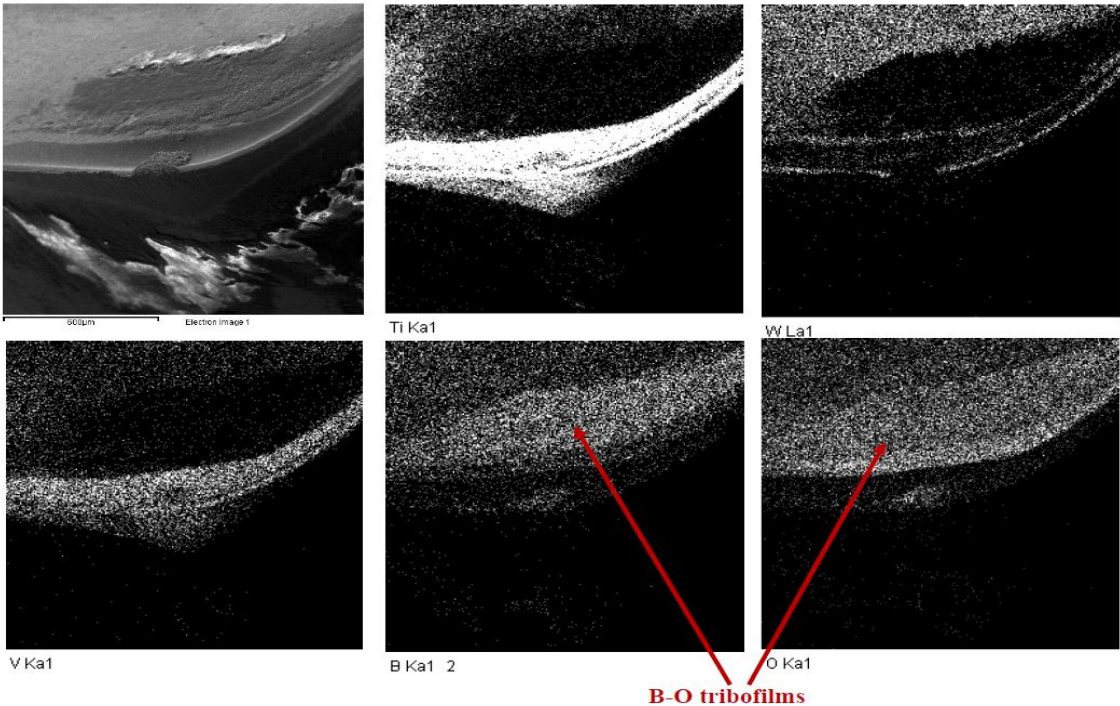


Figure 40: SEM image and EDS elemental maps of the worn rake surface of TiB₂ tool

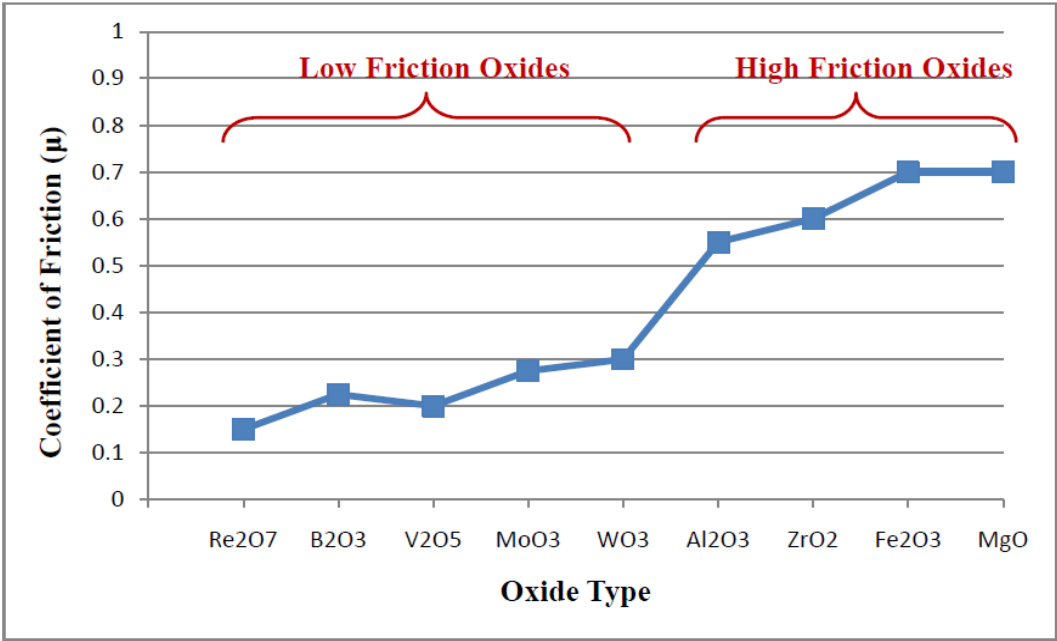


Figure 41: Average friction coefficients of various oxides [Based on [83]]

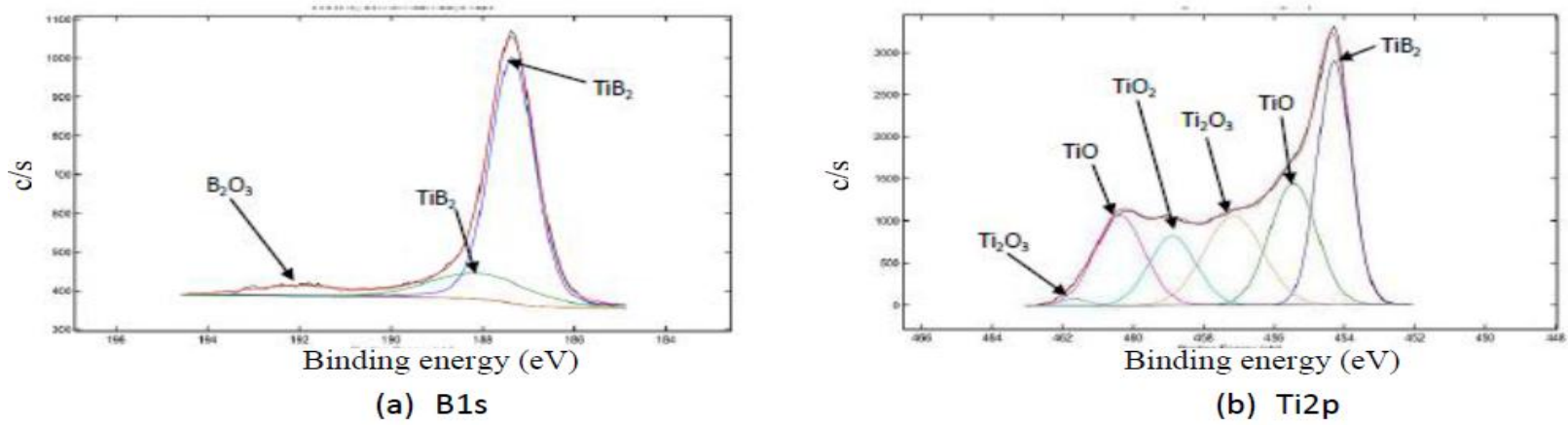


Figure 42: High Resolution XPS after 3 min Ar etching time on flank surface of TiB₂ coated tool after 1000 m cut

Table 18: Relative percentages of the phases present on the flank surface of TiB₂ coated tool after 1000 m cut obtained from High Resolution XPS after 3 min Ar etching time

Peak (eV)	Present Phases	Percentage (%)
187.3	TiB ₂	76.7%
188.0	TiB ₂	16.8%
192.0	B ₂ O ₃	6.5%

(a) B 1s

Peak (eV)	Present Phases	Percentage (%)
454.3	TiB ₂	30.6%
455.5	TiO	21.0%
457.2	Ti ₂ O ₃	19.2%
458.9	TiO ₂	11.9%
460.4	TiO	16.6%
461.7	Ti ₂ O ₃	0.7%

(b) Ti 2p

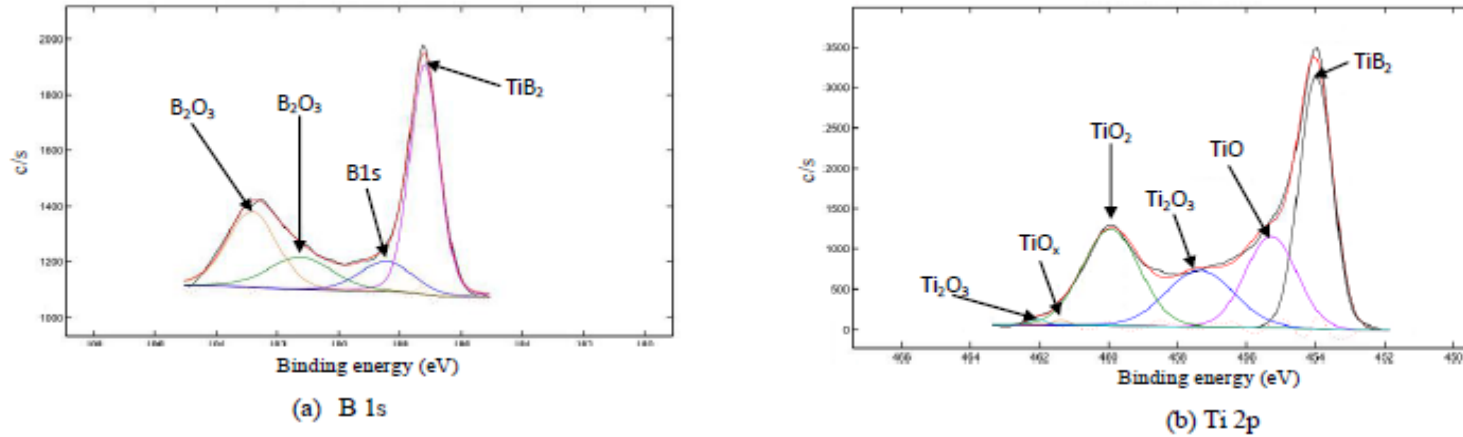


Figure 43: High Resolution XPS after 3 min Ar etching time on rake surface of TiB₂ coated tool after 1000 m cut

Table 19: Relative percentages of the phases present on the rake surface of TiB₂ coated tool after 1000 m cut obtained from High Resolution XPS after 3 min Ar etching time

Peak (eV)	Present Phases	Percentage (%)
187.2	TiB ₂	47.2%
188.4	B1s	11.5%
191.2	B ₂ O ₃	14.6%
192.8	B ₂ O ₃	26.7%

(a) B 1s

Peak (eV)	Present Phases	Percentage (%)
454.0	TiB ₂	37.6
455.3	TiO	20.7
457.4	Ti ₂ O ₃	16.8
459.9	TiO ₂	24.3
461.4	TiO _x	0.3
462.1	Ti ₂ O ₃	0.4

(b) Ti 2p

It should be noted that the amount of lubricious tribo-oxides formed on the flank and rake surface of the TiB_2 coated tool are quite different. On the rake surface, 26.7% of the coating transforms to B_2O_3 tribo-phase. On the contrary, only 6.5% of the tribo-phase is forming on the flank surface. This phenomenon can be related to the temperature profile of the tool. The temperature generated at the rake surface is typically higher in relation to the flank surface of the tool [7]. As a consequence, the adaptive response of the coating is promoted more on the rake surface as compared to the flank surface resulting in 4.1 times higher lubricious B_2O_3 tribo-phase formations.

4.3.2 CrN/WN Coated Tool

After TiB_2 , CrN/WN coating showed the best performance. Figure 44 shows the 3D images of the worn uncoated and CrN/WN coated roughing insert after 3000 m length of cut. Figure 45 and Figure 46 illustrate the tool wear curves for both uncoated and CrN/WN coated tools for rough turning and finish turning, respectively. The tool life curves demonstrate that CrN/WN coated tools perform better than uncoated tools. The following tables show the optical images illustrating the flank and rake wear progression over time for the uncoated and CrN/WN coated roughing and finishing tools.



Figure 44: 3D images of worn tool after 3000 m cut:
(a) uncoated insert (b) CrN/WN coated insert

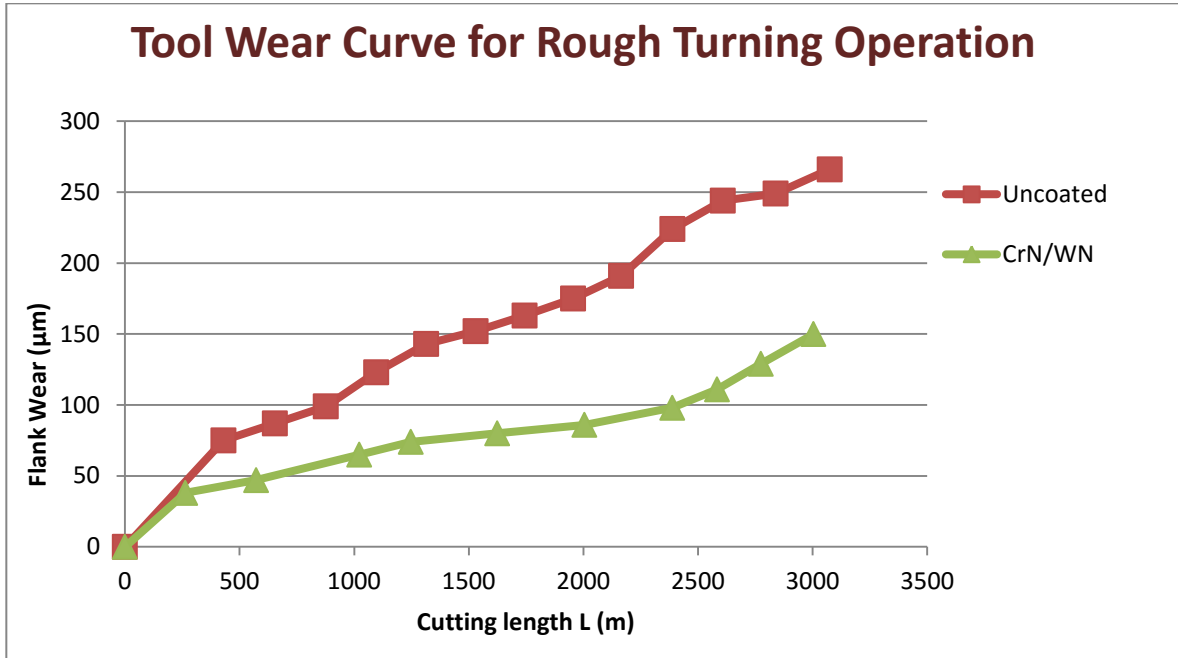


Figure 45: Tool wear curve for uncoated and CrN/WN coated tool for roughing operation

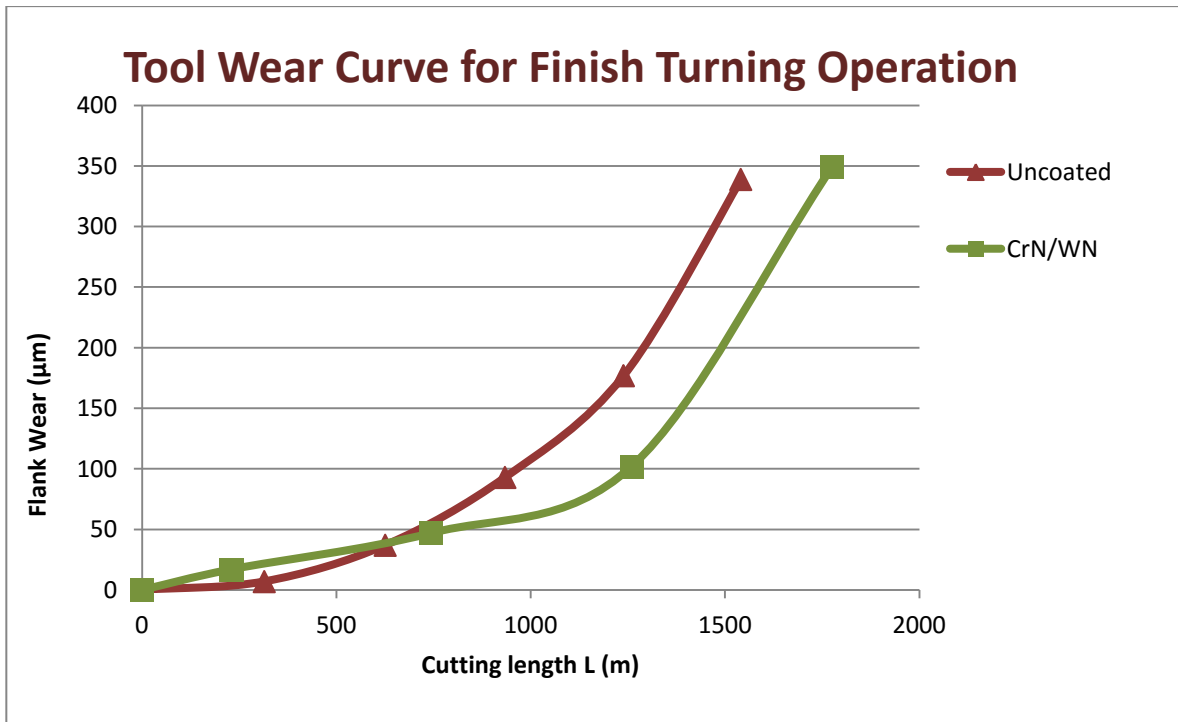


Figure 46: Tool wear curve for uncoated and CrN/WN coated tool for finishing operation

Table 20: Optical images of Flank Wear vs. Length of Cut for uncoated and CrN/WN coated worn roughing inserts

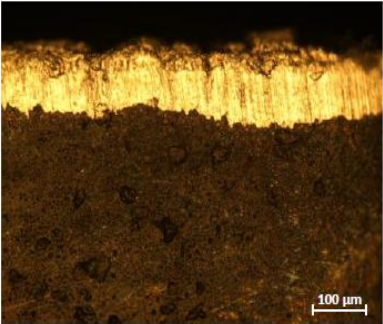
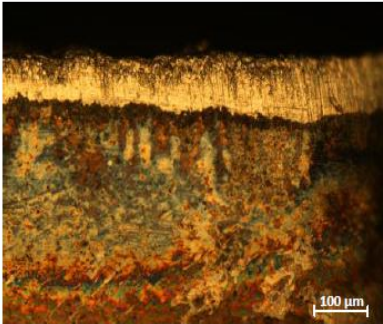
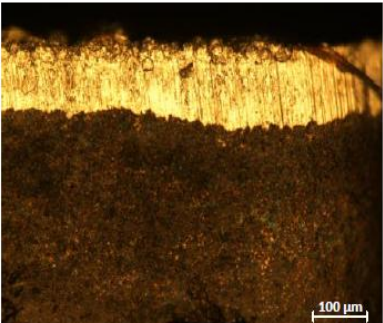
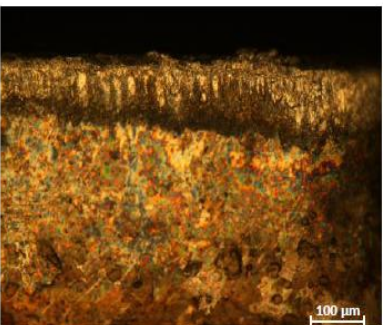
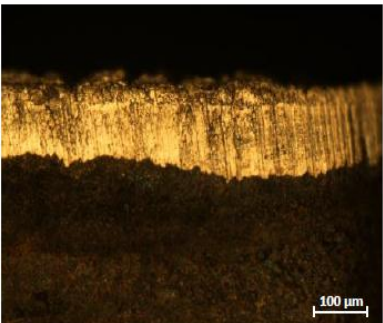
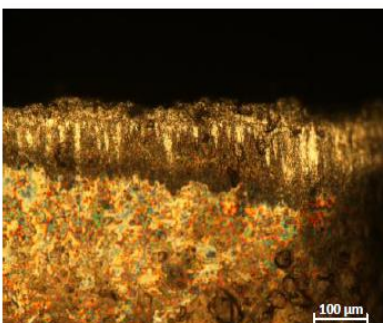
<u>Uncoated</u>		<u>CrN/WN</u>	
<u>Length of cut (m)</u>	<u>Image of Flank Surface</u>	<u>Length of cut (m)</u>	<u>Image of Flank Surface</u>
1096.6		1022.5	
1530.25		1624.39	
1955.43		2004.61	

Table 20: Optical images of Flank Wear vs. Length of Cut for uncoated and CrN/WN coated worn roughing inserts (continued)

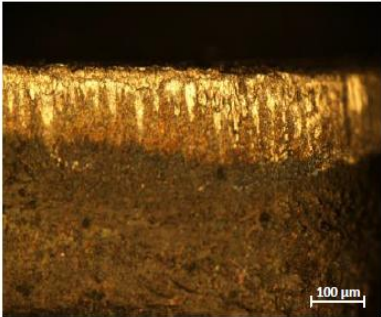
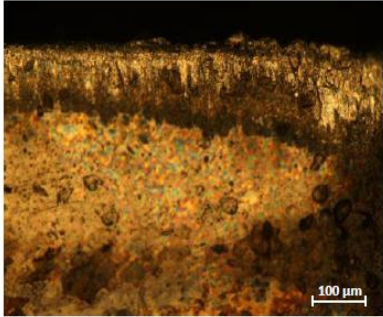
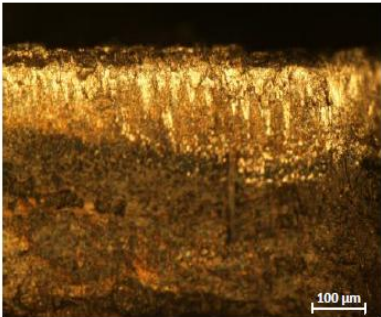
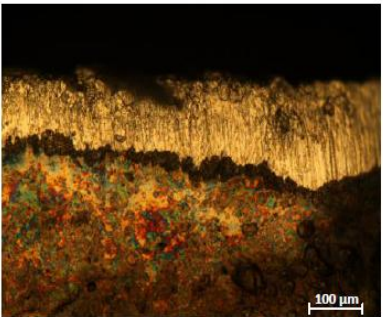
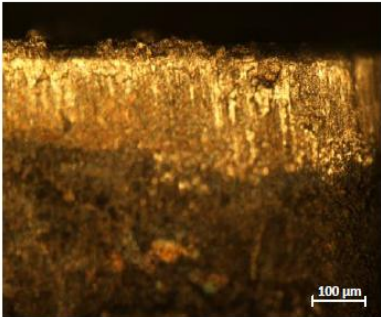
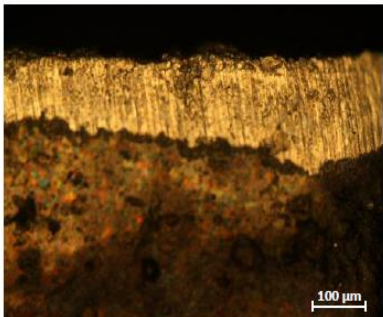
<u>Uncoated</u>		<u>CrN/WN</u>	
<u>Length of cut (m)</u>	<u>Image of Flank Surface</u>	<u>Length of cut (m)</u>	<u>Image of Flank Surface</u>
2388.75		2388.02	
2608.5		2583.21	
3074.95		3003.8	

Table 21: Optical images of Rake Wear vs. Length of Cut for uncoated and CrN/WN coated worn roughing inserts

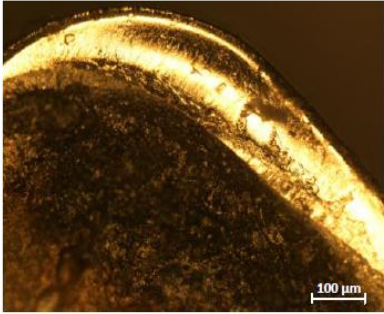
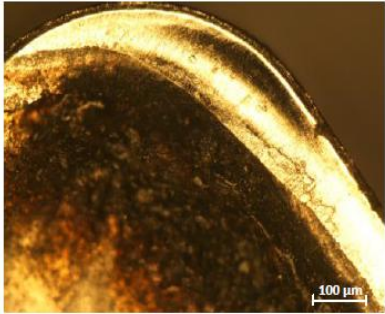
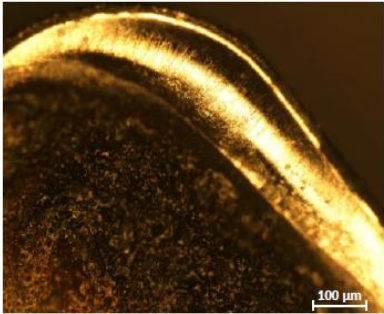
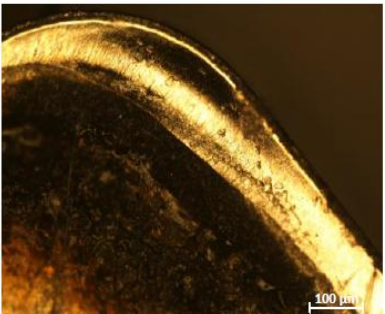
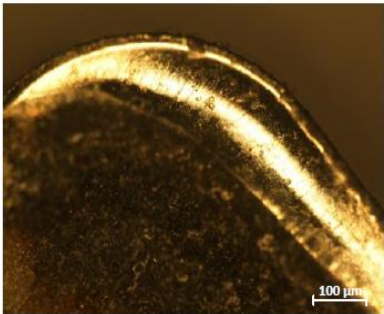
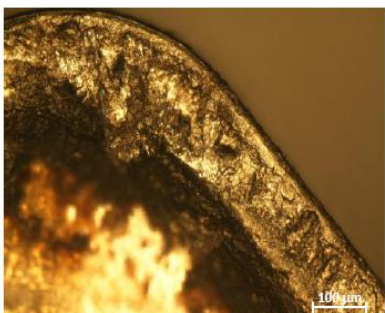
<u>Uncoated</u>		<u>CrN/WN</u>	
<u>Length of cut (m)</u>	<u>Image of Rake Surface</u>	<u>Length of cut (m)</u>	<u>Image of Rake Surface</u>
1096.6		1022.5	
1530.25		1624.39	
1955.43		2004.61	

Table 21: Optical images of Rake Wear vs. Length of Cut for uncoated and CrN/WN coated worn roughing inserts (continued)

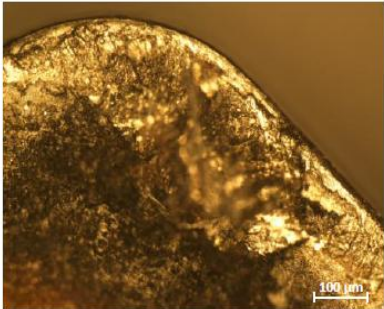
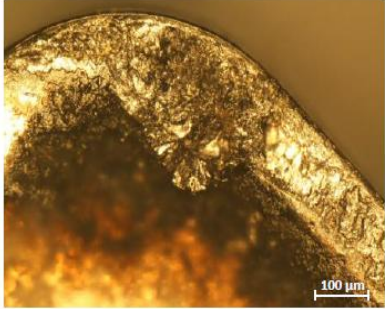
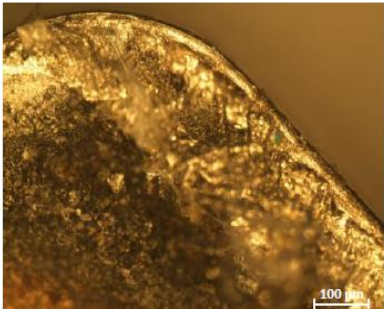
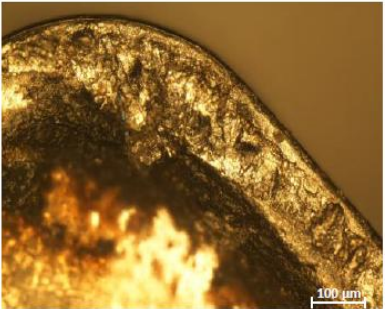
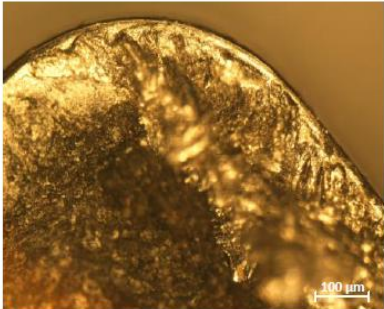
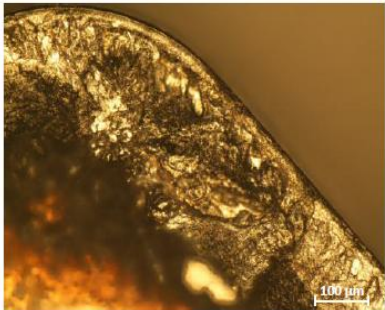
<u>Uncoated</u>		<u>CrN/WN</u>	
<u>Length of cut (m)</u>	<u>Image of Rake Surface</u>	<u>Length of cut (m)</u>	<u>Image of Rake Surface</u>
2388.75		2388.02	
2608.5		2583.21	
3074.95		3003.8	

Table 22: Optical images of Flank Wear vs. Length of Cut for uncoated and CrN/WN coated worn finishing inserts

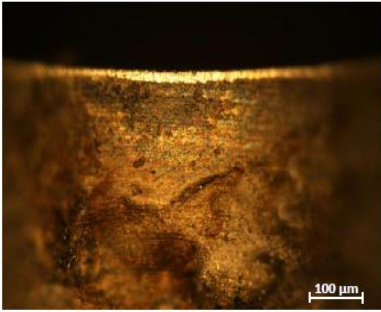
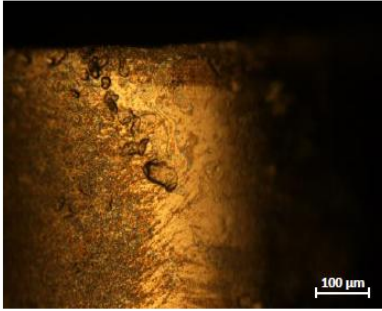
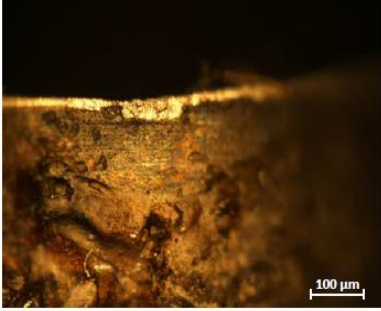
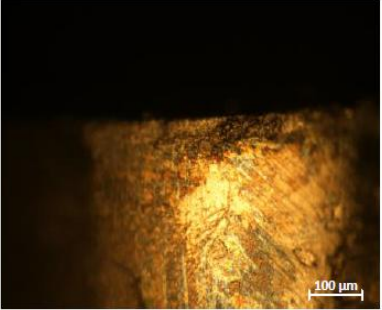
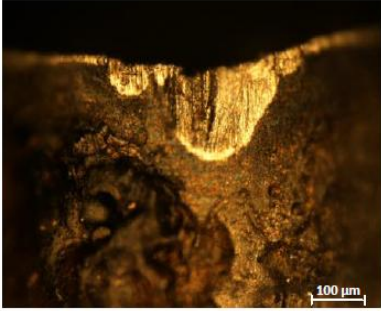
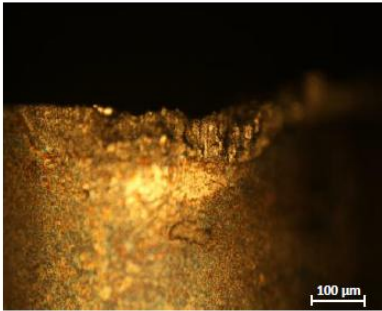
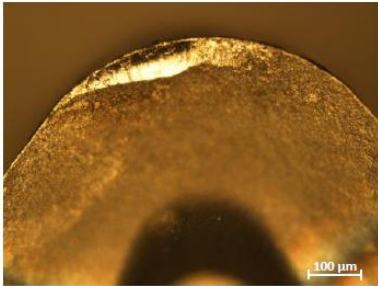
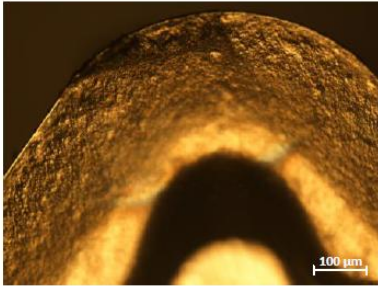
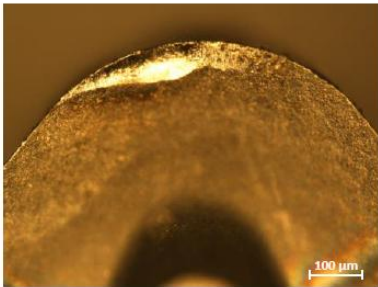
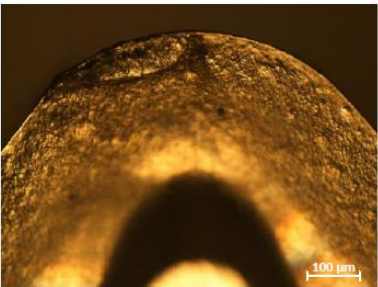
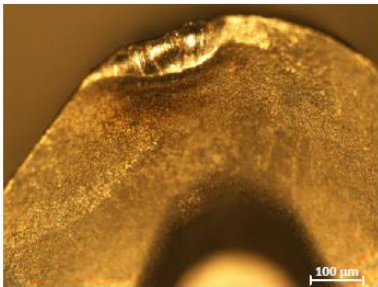
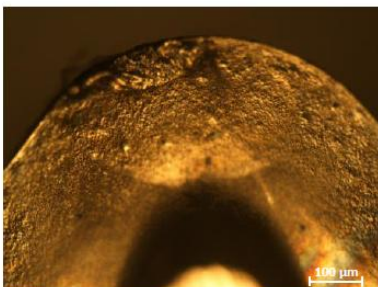
<u>Uncoated</u>		<u>CrN/WN</u>	
<u>Length of cut (m)</u>	<u>Image of Flank Surface</u>	<u>Length of cut (m)</u>	<u>Image of Flank Surface</u>
314.43		229.93	
625.72		744.78	
1238.89		1259.94	

Table 23: Optical images of Rake Wear vs. Length of Cut for uncoated and CrN/WN coated worn finishing inserts

<u>Uncoated</u>		<u>CrN/WN</u>	
<u>Length of cut (m)</u>	<u>Image of Rake Surface</u>	<u>Length of cut (m)</u>	<u>Image of Rake Surface</u>
314.43		229.93	
625.72		744.78	
1238.89		1259.94	

The 3D images and optical images of the flank and rake surfaces of the uncoated and CrN/WN coated tool compliment the tool wear studies. Lower BUE is seen on the CrN/WN coated tool as compared to the uncoated tool. Progression of flank wear and crater wear is higher for uncoated tool compared to CrN/WN coated tool.

To study the tribofilm formation high resolution XPS on the worn tool surfaces was performed. Figure 47 shows the XPS spectra of the rake surface of the CrN/WN coated worn roughing insert. The XPS spectra were obtained based on intensity peaks at the positions Cr 2p, W 4f and O 1s. Extensive tribo-oxidation is observed on the rake face of the worn tool. In addition to the W-O tribo-oxides formation, a significant amount of Cr-O tribo-oxides was also formed. Cr oxides have lubricating properties and thus play a significant role in reducing friction at the tool-chip interface thereby decreasing tool wear.

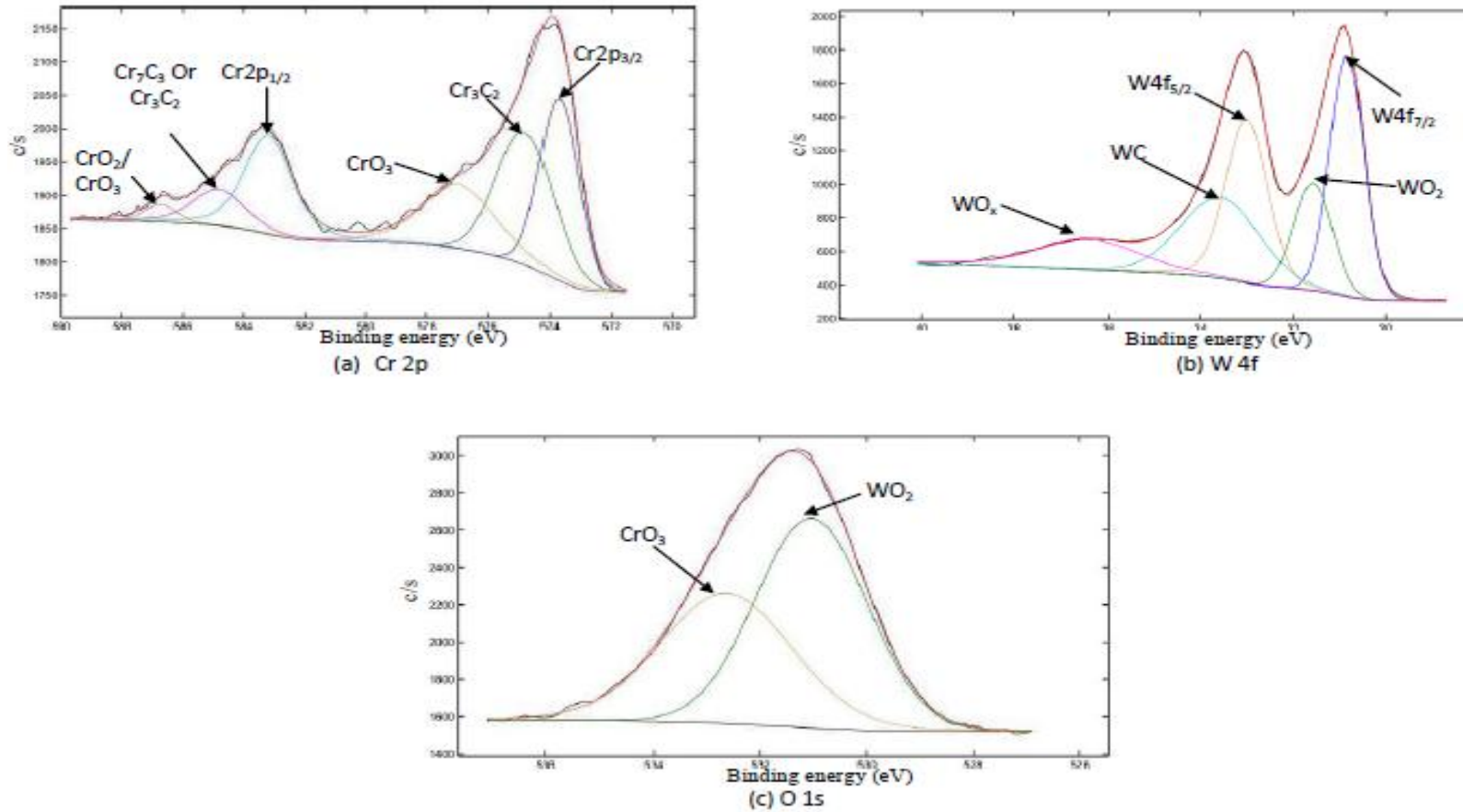


Figure 47: High Resolution XPS after 5 min Ar etching time on rake surface of CrN/WN coated tool after 1000 m cut

Table 24: Relative percentages of the phases present on the rake surface of CrN/WN tool after 1000 m cut obtained from High Resolution XPS after 5 min Ar etching time

Peak (eV)	Present Phases	Percentage (%)
573.7	Cr2p _{3/2}	24.3%
574.8	Cr ₃ C ₂	26.2%
576.9	CrO ₃	19.5%
583.2	Cr2p _{1/2}	19.7%
584.8	Cr ₇ C ₃ OR Cr ₃ C ₂	8.0%
586.7	CrO ₂ /CrO ₃	2.3%

(a) Ti 2p

Peak (eV)	Present Phases	Percentage (%)
30.8	W4f _{7/2}	27.8%
31.6	WO ₂	13.8%
33.0	W4f _{5/2}	24.6%
33.6	WC	22.3%
36.4	WO _x	11.5%

(b) W 4f

Peak (eV)	Present Phases	Percentage (%)
531.0	WO ₂	56.7%
532.6	CrO ₃	43.3%

(c) O 1s

4.4 Further Machinability Analysis of TiB₂ Coated Turning Tool

To better understand the effect of the TiB₂ coating in machining Ti6Al4V, further analyses on the chip morphology, chip cross-section, cutting forces, as well as residual stress and nano-hardness of the coating were carried out.

Cutting forces for both uncoated and TiB₂ coated tools were collected using a dynamometer for rough turning of 100 m length of cut. Table 25 compares the average cutting forces for an uncoated and a TiB₂ coated tool in the radial, feed and tangential direction. Figure 48 and Figure 49 illustrates the cutting forces obtained with the force dynamometer and LABVIEW data acquisition setup.

Table 25: Average cutting forces measured for 100 m cutting length

<u>Tool</u>	<u>Forces (N)</u>		
	<u>Radial</u>	<u>Feed</u>	<u>Tangential</u>
Uncoated	300.11 ± 1.0	654.90 ± 0.8	777.60 ± 3.9
TiB ₂ Coated	267.73 ± 1.0	565.84 ± 0.8	739.52 ± 3.9

As observed, the cutting forces in all directions are lower with the TiB₂ coated tool as compared to the uncoated tool. This can be explained in relation to the B₂O₃ tribofilm formation confirmed before with XPS and EDS analyses. As mentioned before, B₂O₃ is highly lubricious and at temperatures generated during Ti6Al4V machining, it acts as a liquid lubricant. Hence it is able to reduce the friction between the tool-chip and tool-workpiece interfaces and consequently lowers the cutting forces.

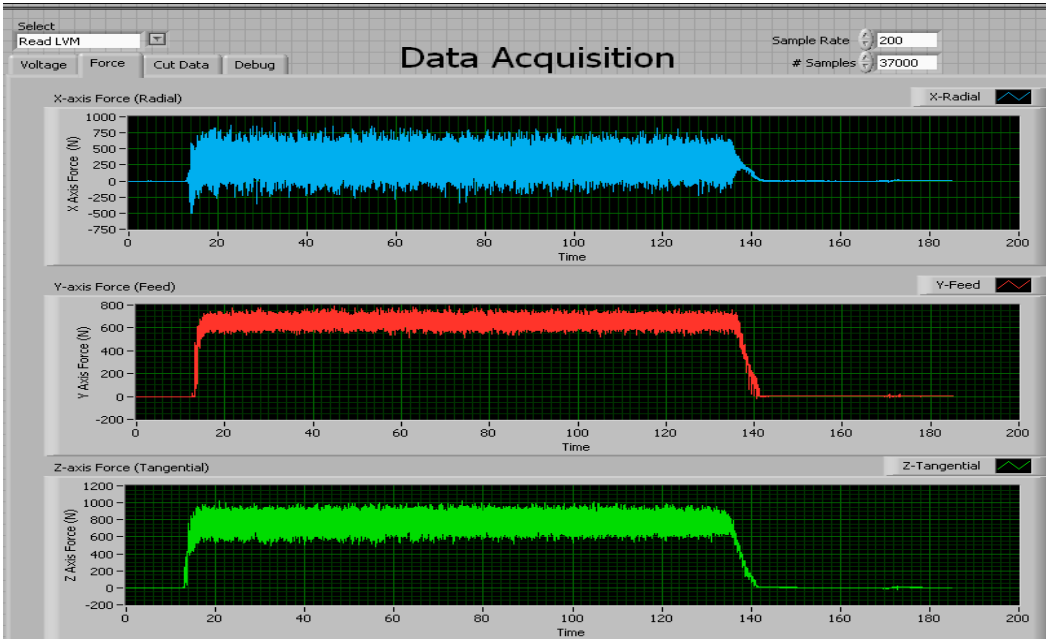


Figure 48: Cutting forces measured for 100 m cutting length with uncoated tool

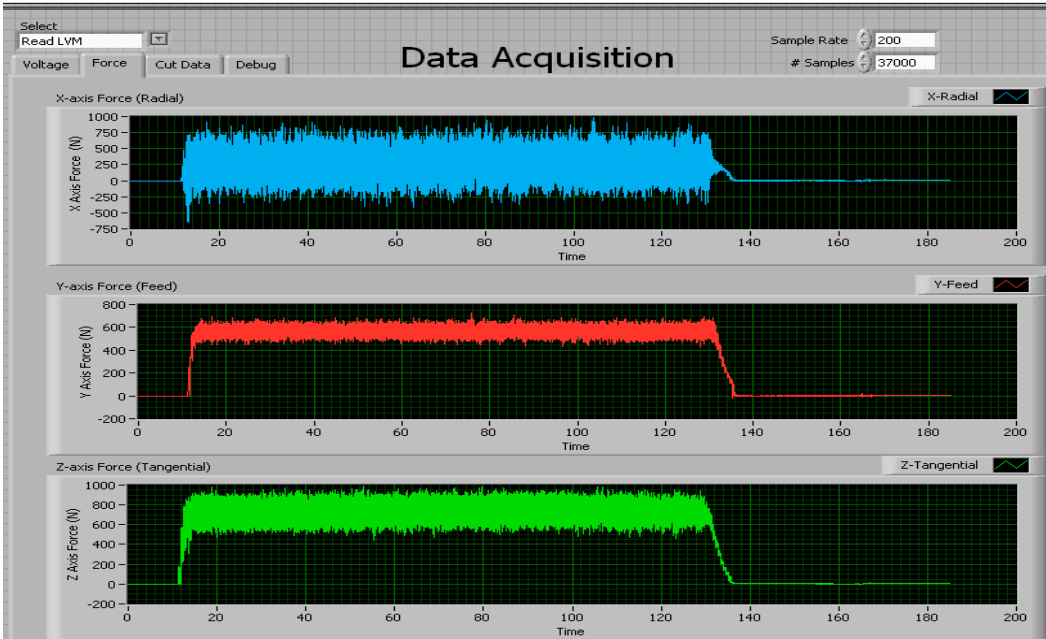


Figure 49: Cutting forces measured for 100 m cutting length with TiB₂coated tool

Chip type and chip under-surface morphology can be related to frictional conditions at the tool-chip interface. Analyses of the worn TiB_2 coated tool revealed better frictional characteristics at the contact interfaces due to less workpiece material adhesion on the coated tool in comparison to the uncoated tool. The chips formed during cutting supports this observation.

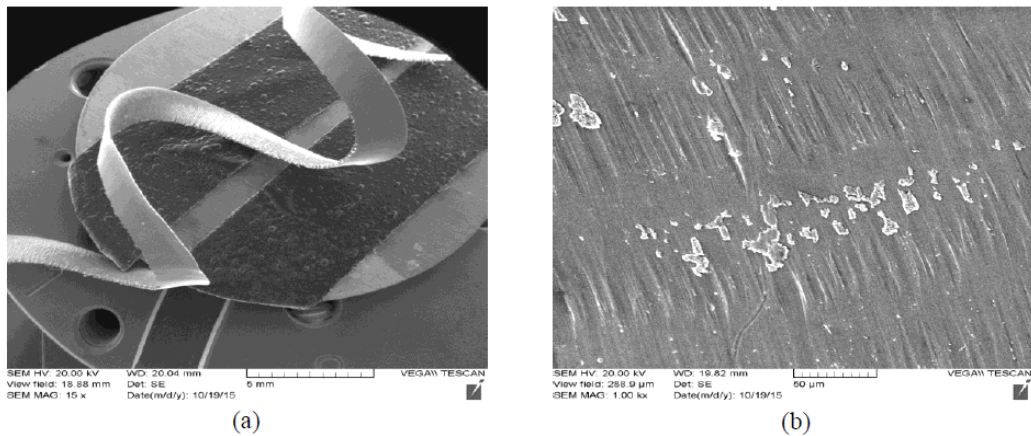


Figure 50: SEM image of chips during roughing with an uncoated tool: (a) chip shape and (b) chip under-surface morphology

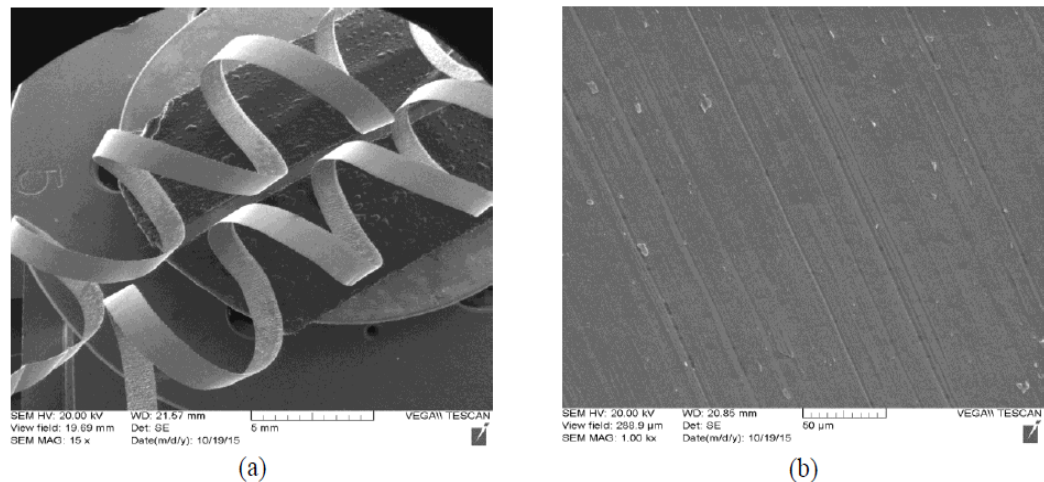


Figure 51: SEM image of chips during roughing with TiB_2 coated tool: (a) chip shape and (b) chip under-surface morphology

Generally, less friction and tool wear causes the chip to be curlier and the under-surface morphology of the chips to be smoother [84]. Chips were collected after a 100 m length of cut. Comparison of Figure 50 and Figure 51 reveals that the TiB₂ coated tool produces curlier chips and have almost negligible adhered material giving an even under-surface as compared to the uncoated tool. Thus it further illustrates the effectiveness of the TiB₂ coating at improving the frictional characteristics at tool-chip interface.

The chip cross-sections for roughing operations of both uncoated and TiB₂ coated tool were also studied to measure the chip thickness ratio. Cross-sections of the chips were first cold mounted and then the chip thicknesses were measured using the Nikon Eclipse LV100 polarizing microscope. Chip thickness ratio, r , is given by:

$$r = \frac{t}{t_c} \quad \begin{array}{l} \text{Where } t = \text{uncut chip thickness (feed)} \\ t_c = \text{chip thickness} \end{array}$$

The cut chip thickness (t_c) is always larger than the uncut chip thickness (t) due to the plastic shearing and subsequent stacking up of the chips. Hence, the chip thickness ratio is always less than 1 ($r < 1$). The chip thickness ratio is related to the shear plane angle through a geometric calculation. If the chip thickness ratio is high, it indicates that the shear plane angle is higher and vice versa. A higher shear plane angle means a smaller shear plane which indicates that lower shearing force is required to plastically deform the chips thus reducing the cutting energy. The friction between the tool-chip interface plays a critical role in this regard. The shear plane angle is given by:

$$\tan(\varphi) = \frac{r \cos(\alpha)}{1 - r \sin(\alpha)}$$

Where φ = shear plane angle
 r = chip thickness ratio
 α = tool rake angle

The ratio of radial force to tangential force, F_R/F_P , provides an indication about the frictional characteristics at the tool-chip interface. A higher ratio indicates higher friction at the tool chip interface.

Figure 52 shows the cross-section of the roughing chips for both uncoated and TiB₂ coated tools.

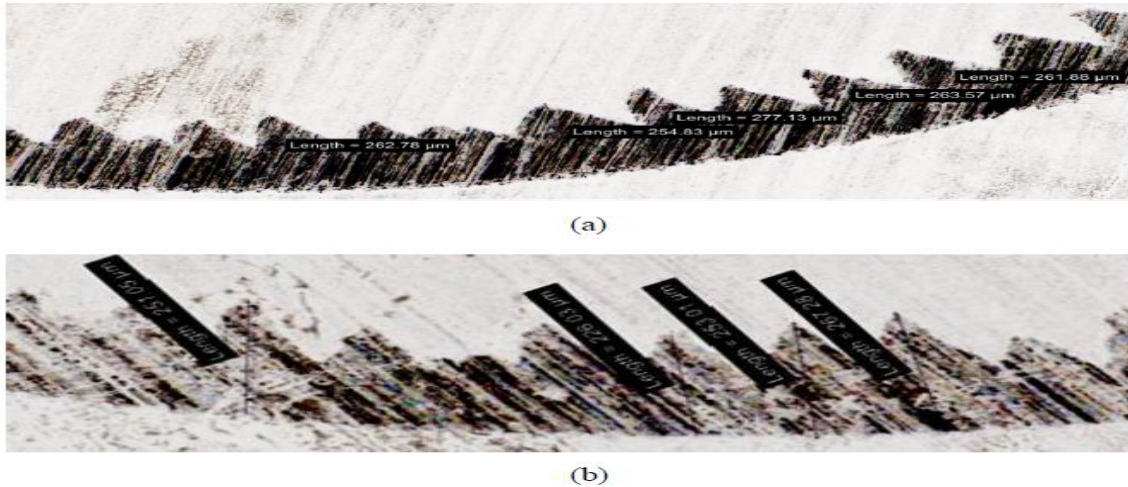


Figure 52: Chip cross-section for roughing tool: (a) Uncoated tool (b) TiB₂ coated tool

Table 26 provides the measured chip thicknesses and the calculated chip thickness ratio and shear plane angle.

Table 26: Calculated chip thickness ratio, shear plane angle and ratio of radial force to tangential force for uncoated and TiB₂ coated tool

<u>Tool</u>	<u>Uncut Chip Thickness, t (mm)</u>	<u>Average Chip Thickness, t_c (mm)</u>	<u>Chip Thickness Ratio, r</u>	<u>Tool Rake Angle, α (degrees)</u>	<u>Shear plane angle, φ (degrees)</u>	<u>F_R/F_P</u>
Uncoated	0.15	0.264	0.568	12	32.215	0.386
TiB ₂	0.15	0.249	0.602	12	33.923	0.362

As seen in Table 26, the chip thickness of the chips for the TiB₂ coated tool is lower than the uncoated tool giving a higher shear plane angle. Hence, it indicates that lower shearing forces are acting on the chips. The cutting force data obtained earlier also compliments this observation. The calculated ratio of radial force to tangential force is also lower confirming that TiB₂ coating is able to reduce the friction during cutting.

Table 27 shows the properties of the TiB₂ coating. TiB₂ coating has a lower hardness of 15.5_±4.3 GPa compared to the TiAlN coating that has a hardness of 30.1_±8.4 GPa. Low hardness coatings have low shear strength allowing them to shear more easily thereby reducing friction at contact interfaces. Coatings with high hardness are generally brittle and have lower adhesion to the tool substrate. In Ti6Al4V machining, lower hardness coating is better suited as it reduces friction at interfaces thereby decreasing built up edge formation. TiB₂ coating also has compressive residual stress. Compressive residual stress results in enhanced mechanical properties and prolongs tool life [4]. In general, compressive residual stresses reduce crack propagation and improve fatigue life, coating adhesion and durability of the coating during its service life [85].

Table 27: Properties of TiB₂ coating

<u>Coating</u>	<u>Architecture</u>	<u>Properties</u>			
		<u>Thickness</u> <u>(μm)</u>	<u>Hardness</u> <u>(GPa)</u>	<u>Reduced Elastic</u> <u>Modulus</u> <u>(GPa)</u>	<u>Residual</u> <u>Stresses</u> <u>(GPa)</u>
TiB ₂	Monolayer	1.79	15.5 _± 4.3	363.6 _± 76.4	-0.633 _± 0.08

4.5 Investigation of the Effect of Chip Breaker Profile and Coating Hardness on the Performance of TiB₂ Coated Tool

In the previous sections, analyses focused on the effect of different coatings on tool wear during Ti6Al4V machining and the self-lubricating characteristics of the coatings. It was established that due to self-adaptability of the coatings beneficial tribofilms were formed that resulted in lower tool wear. TiB₂ coated tool showed the highest reduction in tool wear with a subsequent reduction in cutting forces and analyses showed that this was due to the lubricious B₂O₃ tribo-oxide formation. However, in addition to tribofilm formation, other factors like deposition parameters of the PVD coating and tool geometry, amongst many others, also have considerable effect on tool performance. Deposition parameters effect the coating's hardness, residual stress, modulus of elasticity, etc., which in turn affects tool wear. A comparison was made between two different chip breaker profiles of the turning tool inserts in order to study their effect on tool wear. Investigation was also conducted with three TiB₂ coated tools with the same geometry but with different deposition parameters of the coating obtained from three different companies in order to see the effect of deposition parameters. However, it should be mentioned that defining the optimum deposition parameters was not the focus of this study and only their effects on tool wear were studied. The results of varying deposition parameters and chip breaker profiles are presented in this section.

4.5.1 Chip Breaker Profile

Chip breaker profile of the cutting inserts play a significant role in controlling the chip flow and chip breakability. With better chip flow and chip breakability, chips formed are more curly thereby reducing friction and cutting forces. Heat transferred to the tool is also reduced causing less tool wear and less material adhesion on the tool.

All the tools used to conduct the cutting tests so far were of CNMG432 type which had a general chip breaker profile. To investigate the effect of chip breaker profile on tool wear and cutting forces, tool wear studies were repeated with a more positive chip breaker profile for roughing operations of uncoated and TiB₂ coated tool. The positive chip breaker tools used were of CNMP432 type. Both of the tool types are similar in every other regard. Figure 16 (section 3.2) compares the chip breaker profile of the two insert types. Figure 53 compares the tool wear between uncoated and TiB₂ coated tools with both general and positive chip breaker profile. It is clearly evident from the tool wear curves that both uncoated and TiB₂ coated tool with positive chip breaker profile outperform their counterparts with general chip breaker profile. Table 28 and Table 29 illustrate the optical images comparing the tool wear progression over time for uncoated tools with the general chip breaker profile and a positive chip breaker profile for the roughing operation. Table 30 and Table 31 show the optical images of the flank and rake surfaces of TiB₂ with the general chip breaker profile and TiB₂ with the positive chip breaker profile tools for the roughing operation. Higher flank and crater wear progression as well as higher BUE formation are observed for tools with general chip breaker profile.

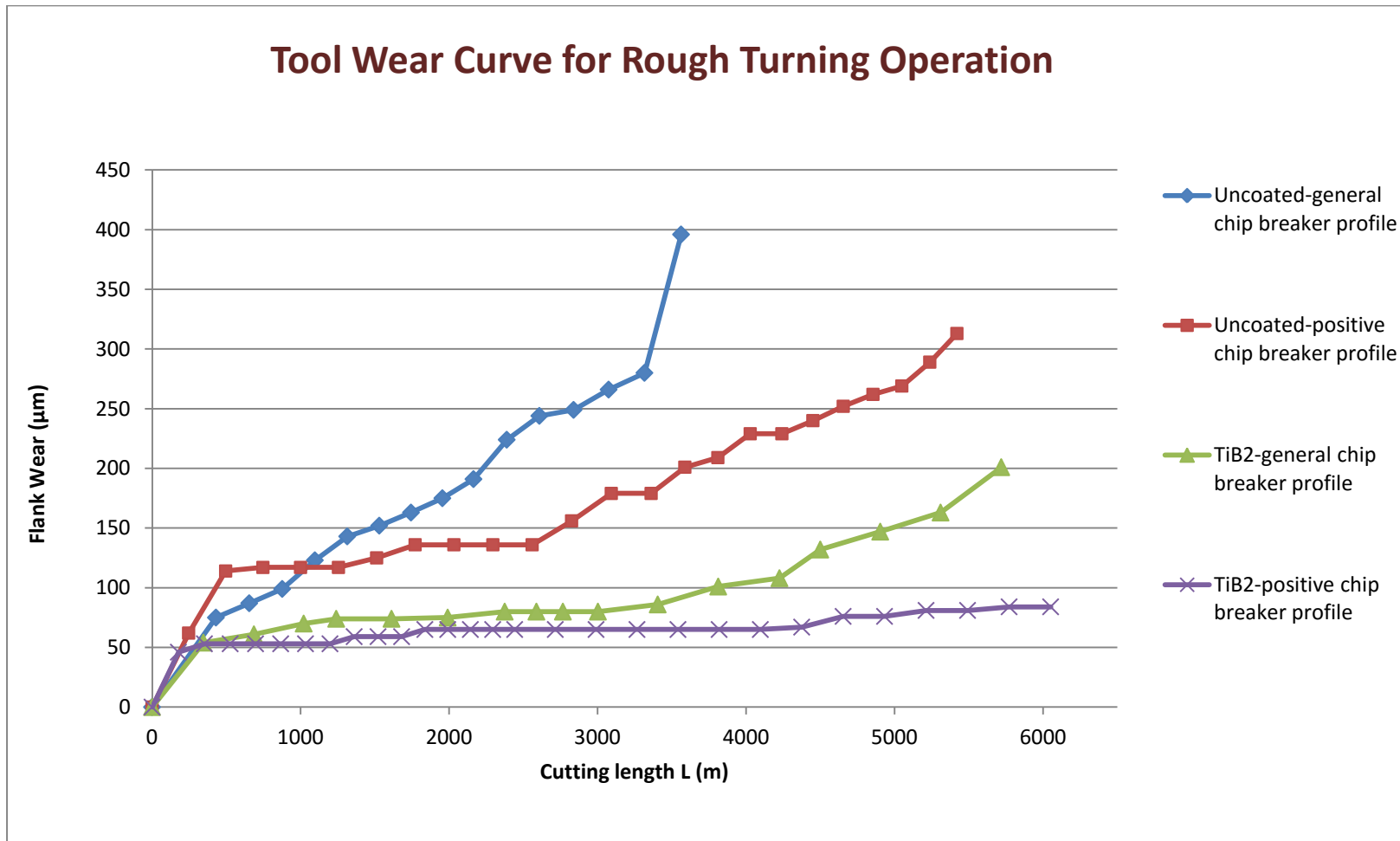


Figure 53: Tool wear curve for rough turning of uncoated and TiB₂ coated tools with general and positive chip breaker profile

Table 28: Optical images of Flank Wear vs. Length of Cut for uncoated tools with general and positive chip breaker profiles for worn roughing inserts

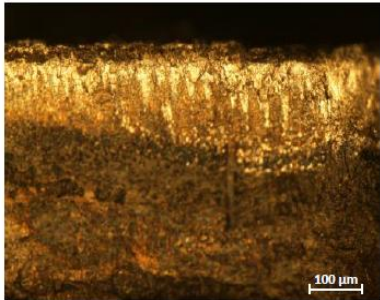
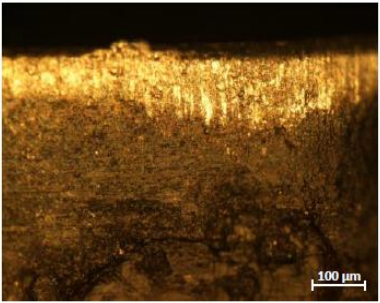
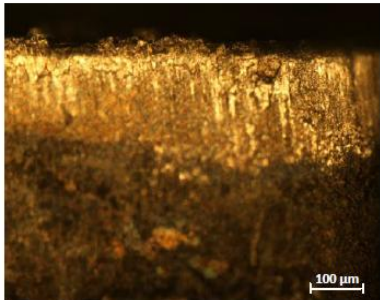
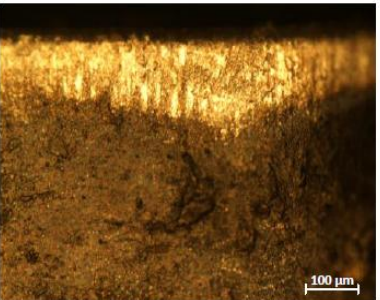
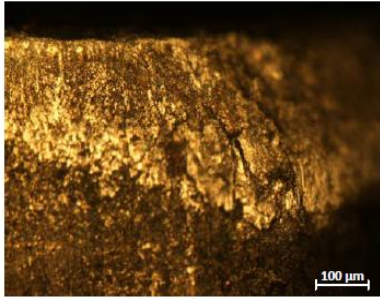
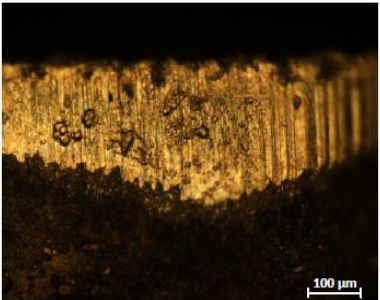
<u>Uncoated</u> General Chip Breaker Profile		<u>Uncoated</u> Positive Chip Breaker Profile	
<u>Length of cut (m)</u>	<u>Image of Flank Surface</u>	<u>Length of cut (m)</u>	<u>Image of Flank Surface</u>
2608.50		2825.76	
3074.95		3588.88	
3563		5049.78	

Table 29: Optical images of Rake Wear vs. Length of Cut for uncoated tools with general and positive chip breaker profiles for worn roughing inserts

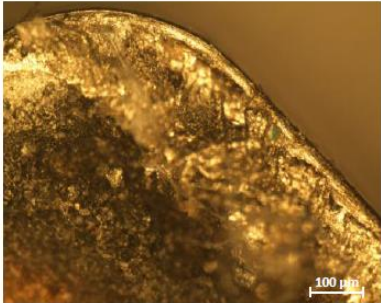
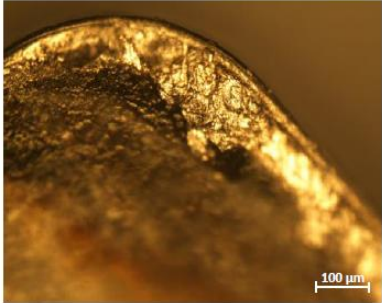
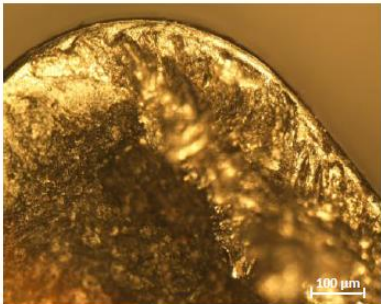
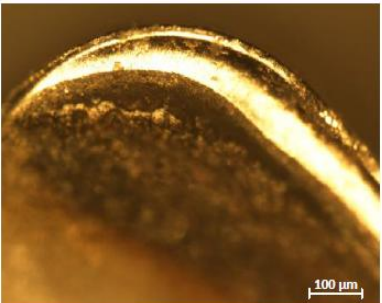
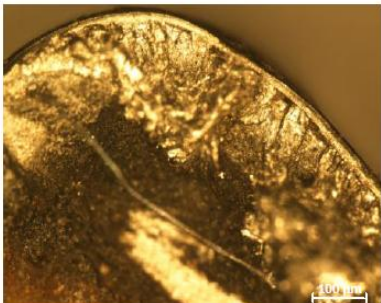
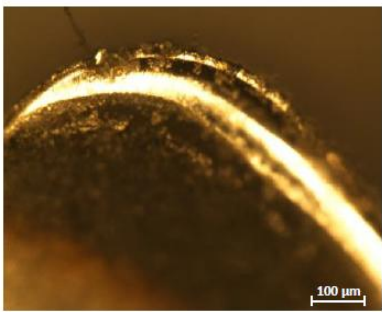
<u>Uncoated</u> <u>General Chip Breaker Profile</u>		<u>Uncoated</u> <u>Positive Chip Breaker Profile</u>	
<u>Length of cut (m)</u>	<u>Image of Rake Surface</u>	<u>Length of cut (m)</u>	<u>Image of Rake Surface</u>
2608.50		2825.76	
3074.95		3588.88	
3563		5049.78	

Table 30: Optical images of Flank Wear vs. Length of Cut for TiB₂ coated tools with general and positive chip breaker profiles for worn roughing inserts

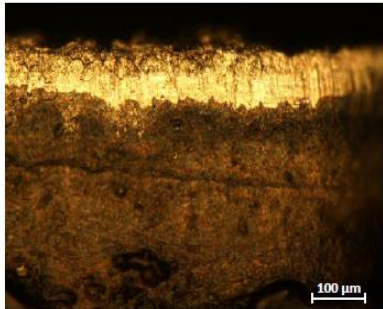
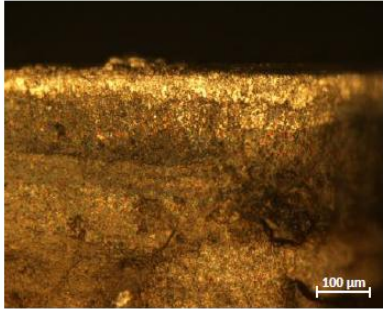
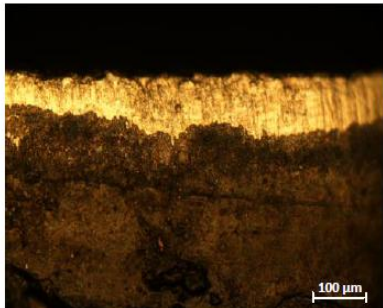
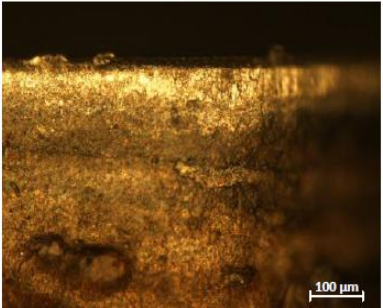
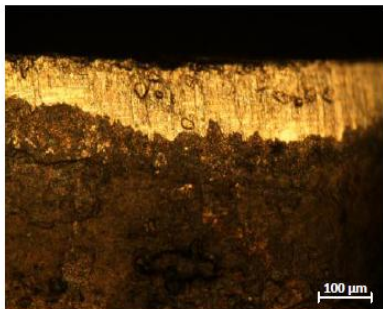
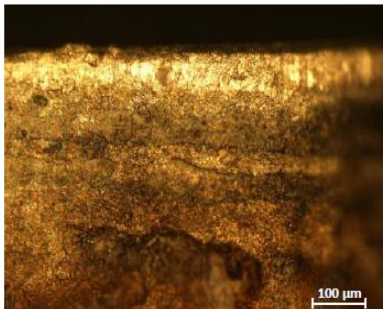
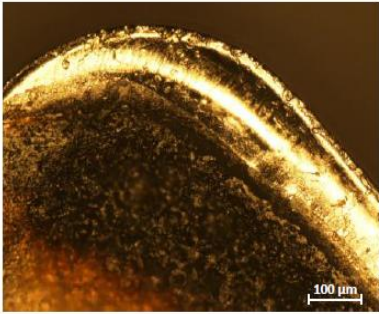
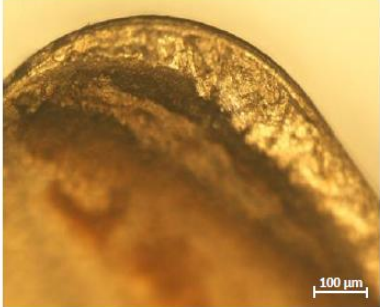
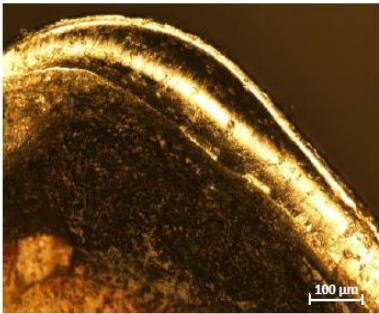
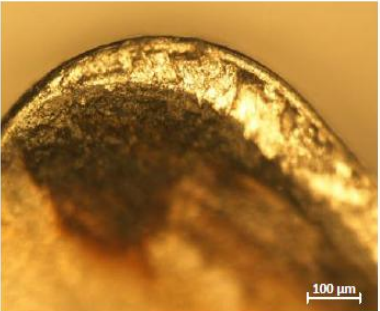
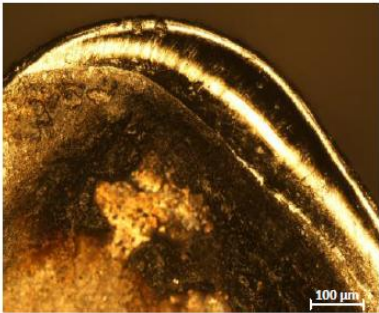
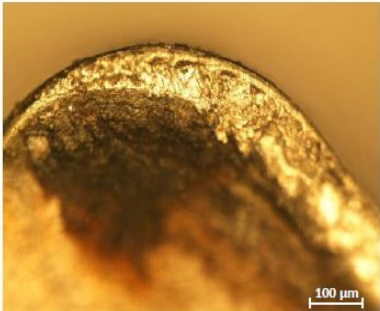
<u>TiB₂</u> General Chip Breaker Profile		<u>TiB₂</u> Positive Chip Breaker Profile	
<u>Length of cut (m)</u>	<u>Image of Flank Surface</u>	<u>Length of cut (m)</u>	<u>Image of Flank Surface</u>
2767.02		2990.43	
3405.67		4375.48	
4225.76		5213.06	

Table 31: Optical images of Rake Wear vs. Length of Cut for TiB₂ coated tools with general and positive chip breaker profiles for worn roughing inserts

<u>TiB₂</u> <u>General Chip Breaker Profile</u>		<u>TiB₂</u> <u>Positive Chip Breaker Profile</u>	
<u>Length of cut (m)</u>	<u>Image of Rake Surface</u>	<u>Length of cut (m)</u>	<u>Image of Rake Surface</u>
2767.02		2990.43	
3405.67		4375.48	
4225.76		5213.06	

Cutting forces for both uncoated and TiB₂ coated tools with positive chip breaker profile were collected using a dynamometer for 100 m cutting lengths. Table 32 compares the average cutting forces obtained from the uncoated and TiB₂ coated tools for both general and positive chip breaker profiles. Figure 54 and Figure 55 illustrate the cutting forces obtained with force dynamometer and LABVIEW data acquisition system for tools with positive chip breaker profile (see Figure 48 and Figure 49) for cutting forces for tools with general chip breaker profile. It can be seen that the tools with positive chip breaker profile reduce cutting forces significantly. This agrees with the tool wear studies shown before.

Table 32: Average cutting forces measured for 100 m cutting length for different chip breaker profiles

<u>Tool</u>	<u>Chip Breaker Profile</u>	<u>Forces (N)</u>		
		<u>Radial</u>	<u>Feed</u>	<u>Tangential</u>
Uncoated	General	300.11 ± 1.0	654.90 ± 0.8	777.60 ± 3.9
Uncoated	Positive	156.80 ± 1.0	445.48 ± 0.8	664.00 ± 3.9
TiB ₂	General	267.73 ± 1.0	565.84 ± 0.8	739.52 ± 3.9
TiB ₂	Positive	153.71 ± 1.0	431.59 ± 0.8	658.59 ± 3.9

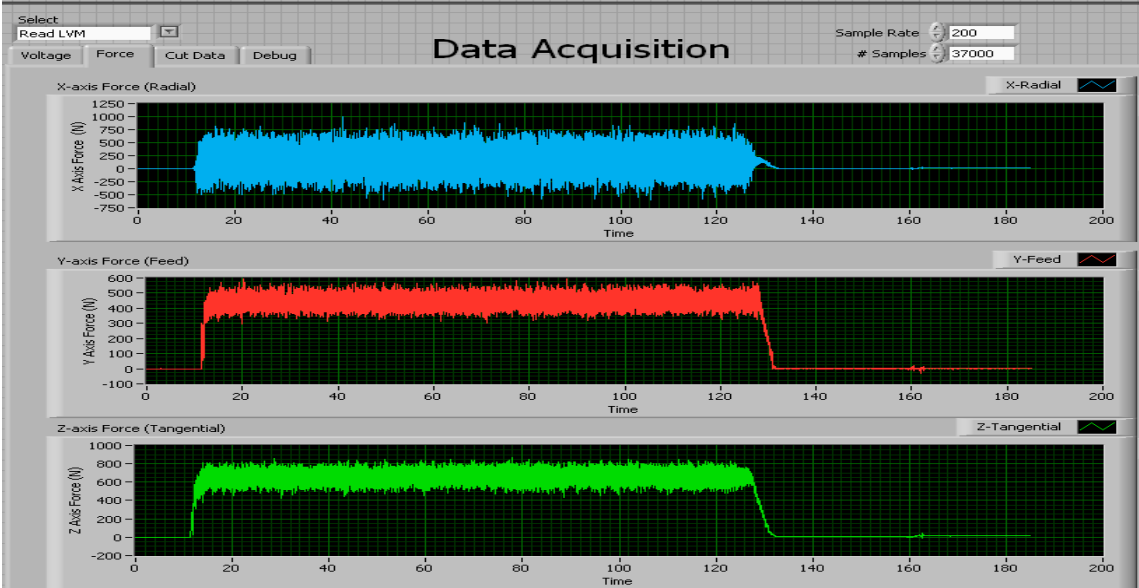


Figure 54: Cutting forces measured for 100 m cutting length for uncoated tool with positive chip breaker profile

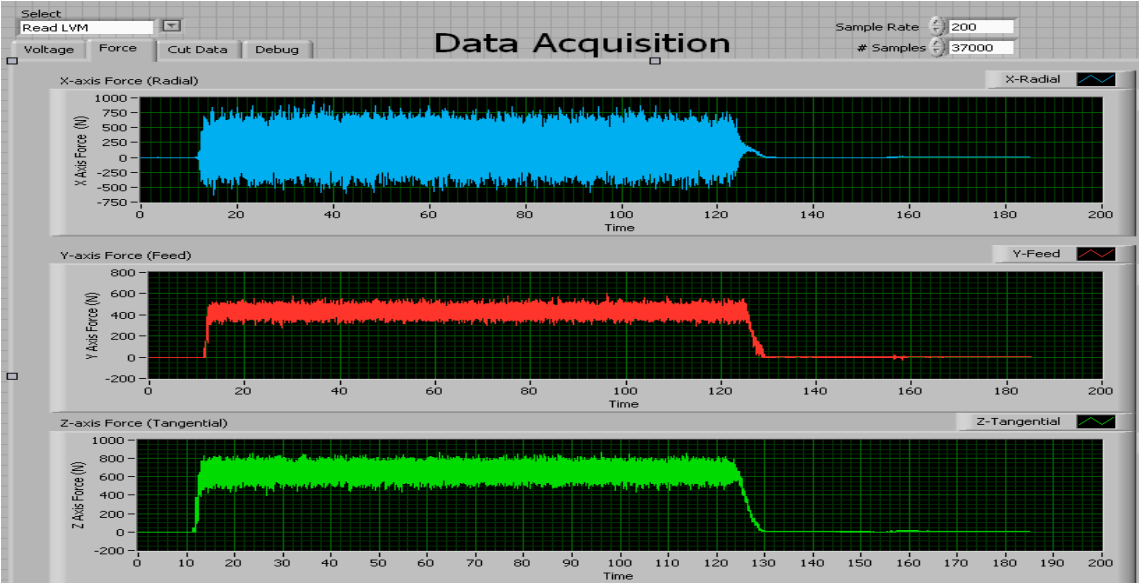


Figure 55: Cutting forces measured for 100 m cutting length for TiB₂ coated tool with positive chip breaker profile

Figure 56 shows the SEM images of chips for uncoated tools with general and positive chip breaker profiles. The chips for tools with positive chip breaker profile are much curlier and smaller. This can be related to lower cutting forces, tool wear and tool-chip contact length.

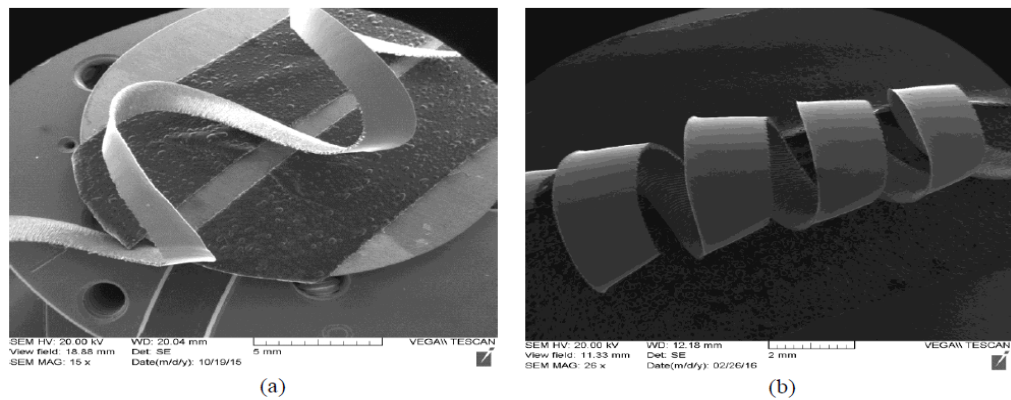


Figure 56: SEM image of chips during roughing operation for uncoated tools: (a) general chip breaker profile (b) positive chip breaker profile

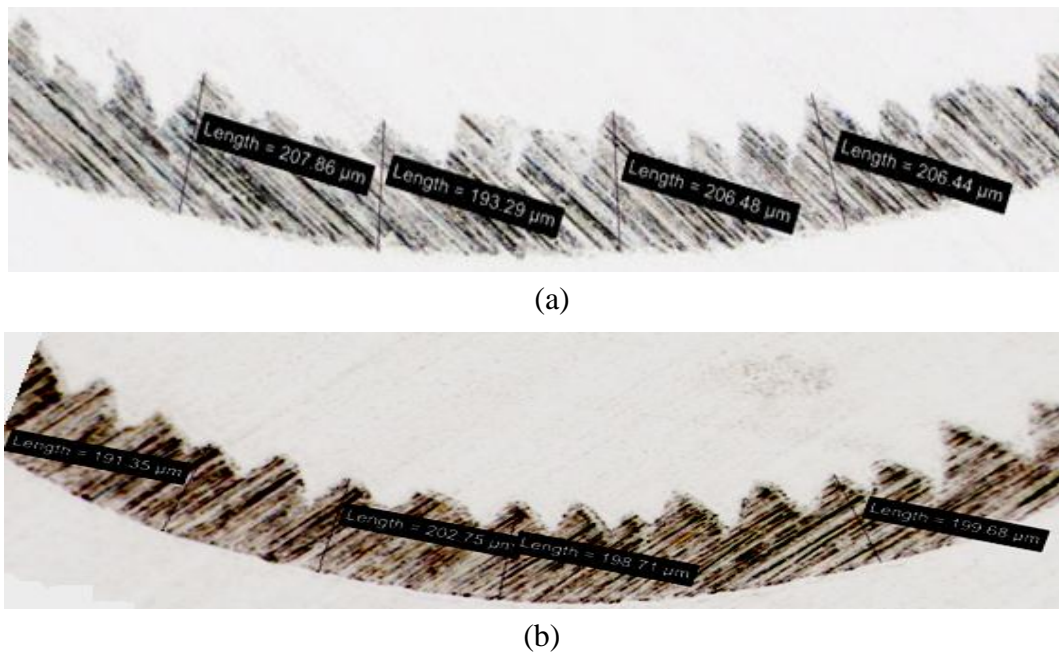


Figure 57: Chip cross-section for positive chip breaker tool: (a) Uncoated (b) TiB_2 coated tool

Table 33: Calculated chip thickness ratio, shear plane angle and ratio of radial force to tangential force for different chip breaker profiles

<u>Tool</u>	<u>Chip Breaker Profile</u>	<u>Uncut Chip Thickness, t (mm)</u>	<u>Average Chip Thickness, t_c (mm)</u>	<u>Chip Thickness Ratio, r</u>	<u>Tool Rake Angle, α (degrees)</u>	<u>Shear Plane Angle, ϕ (degrees)</u>	<u>F_R/F_T</u>
Uncoated	General	0.15	0.264	0.568	12	32.215	0.386
TiB ₂	General	0.15	0.249	0.602	12	33.923	0.362
Uncoated	Positive	0.15	0.204	0.738	12	40.411	0.236
TiB ₂	Positive	0.15	0.198	0.757	12	41.313	0.233

Figure 57 shows the cross-section of the chips when roughing for both uncoated and TiB₂ coated positive chip breaker tools (see Figure 52 for chip cross-section for tools with general chip breaker profiles). Table 33 provides the measured chip thicknesses and the calculated chip thickness ratio, shear plane angle and ratio of radial force to tangential force. As seen in Table 33, the chip thickness of the chips for tools with positive chip breaker profiles are lower than the tools with general chip breaker profiles giving a higher shear plane angle. Hence, it indicates that lower shearing forces are acting on the chips. The cutting force data obtained also compliments this analysis. The ratio of radial force to tangential force is also lower for positive chip breaker profiles as compared to general chip breaker profiles confirming lower friction at the cutting interface.

Therefore based on the aforementioned experimental results and analysis, it can be concluded that tools with positive chip breaker profiles are more effective in machining Ti6Al4V alloys.

4.5.2 Effect of Coating Hardness

Deposition parameters like bias voltage, reactant gases, etc., of the PVD coating process have significant effect on the coating's properties and on how the coating performs. Variations in deposition parameters affect the hardness, residual stresses, etc. of the coating. Hence through optimization of the deposition parameters tool coatings can be made more effective for particular applications. However, defining the optimum deposition parameters was not the focus of the current research. The aim of the current study was to show how the same coating with different deposition parameters can have significantly different tool performance for a particular application, in this case Ti6Al4V machining. Hence, details of the deposition parameters are not reported in this thesis.

To study the effect of different deposition parameters, tool wear studies were conducted for three roughing tools of CNMP432 type (positive chip breaker profile) with TiB₂ coating obtained from three different companies. The characteristic investigated was the tool hardness due to its dominant effect on tool wear. The studies done so far in the current research were with TiB₂ coating with a low hardness (15.5 GPa-measured). TiB₂ coating supplied by the two other companies had higher hardness (39.23 GPa-as reported by the companies). To avoid confusion, the following naming will be used from this point onwards:

- ❖ TiB₂ coating with low hardness from one company → TiB₂-LHC
- ❖ TiB₂ coating with high hardness from other two different companies → TiB₂-Company A and TiB₂-Company B respectively

Figure 58 compares the tool life of the roughing tools with TiB₂ coatings from the three companies.

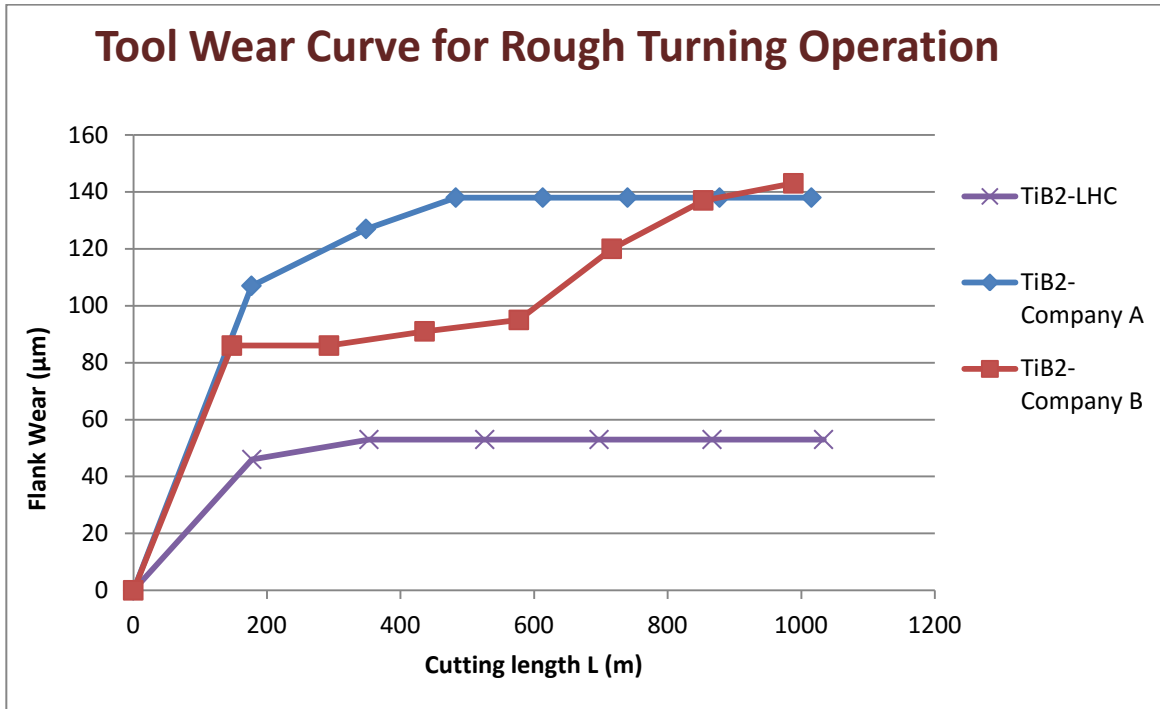


Figure 58: Tool wear curve for rough turning of three different TiB₂ coated tools with positive chip breaker profile

The tool wear studies reveal that the tool with the lower hardness coating outperformed the tools with the higher hardness coatings. As discussed earlier, TiB₂ coated tools form lubricious B₂O₃ tribo-oxide that act as liquid lubricant during machining of Ti6Al4V alloy. Therefore, for all the TiB₂ coated tools, formation of B₂O₃ tribo-oxide are apparent. However, the performances of the tools are distinctly different despite B₂O₃ tribo-oxide formation indicating that wear resistance of the tools depend on other factors as well and not only on tribofilm formation. In this particular study, hardness of the TiB₂ coating played a dominant role in determining tool performance.

Coating with high hardness tends to be brittle, have high residual stresses and low adhesion to substrate [73]. As a result, fracture and delamination of the coating is prominent in high hardness coatings. On the other hand, low hardness coatings exhibit lower shear strength and thus shear more easily under load allowing for lower coefficient of forces and high lubricity at contact interfaces [81]. Prengel et al. [76] have shown that the PVD TiB_2 coating with a hardness of 26.97 GPa is effective in turning A390 aluminium alloy compared to $TiAlN$ and TiN coated tools where tool wear is predominantly abrasive with high built up edge formation. In the case of $Ti6Al4V$ alloy machining, where built up edge is prominent, the lower hardness coating is thus more suitable and is able to lower friction between the interfaces thus reducing tool wear. The above tool wear studies support this fact.

4.6 Tool Wear Studies for End Milling Operation

From all the experimental studies and results analysis of turning operations for $Ti6Al4V$ alloy, the coatings that showed a significant improvement of tool life was the TiB_2 coated tool with the lower hardness (TiB_2 -LHC) and the CrN/WN coated tool. Hence, tool life studies were conducted for end milling operations with the uncoated, TiB_2 -LHC coated and CrN/WN coated four flute end mills to investigate the effectiveness of the coating in milling operations. For end milling of $Ti6Al4V$, in addition to typical flank and rake wear, chipping of the tool is significant. This can be related to the fact that the end milling process is an interrupted machining operation. Each tooth of the tool is actually cutting for only a very small part of the cycle and is therefore exposed to cyclic

mechanical and thermal loads. These cyclic loads together with built up edge formation during Ti6Al4V machining promote tool edge chipping. Therefore, during tool life studies an account of chipping on the flank faces and rake faces of the tools were kept. Figure 59-Figure 62 illustrates the average flank wear, rake wear, flank chipping and rake chipping of the four fluted uncoated, TiB₂-LHC coated and CrN/WN coated end mill. The results show that the performance of the uncoated and coated tools is very similar with only slight differences. Chipping of the tool seems random and is not uniform in each tooth.

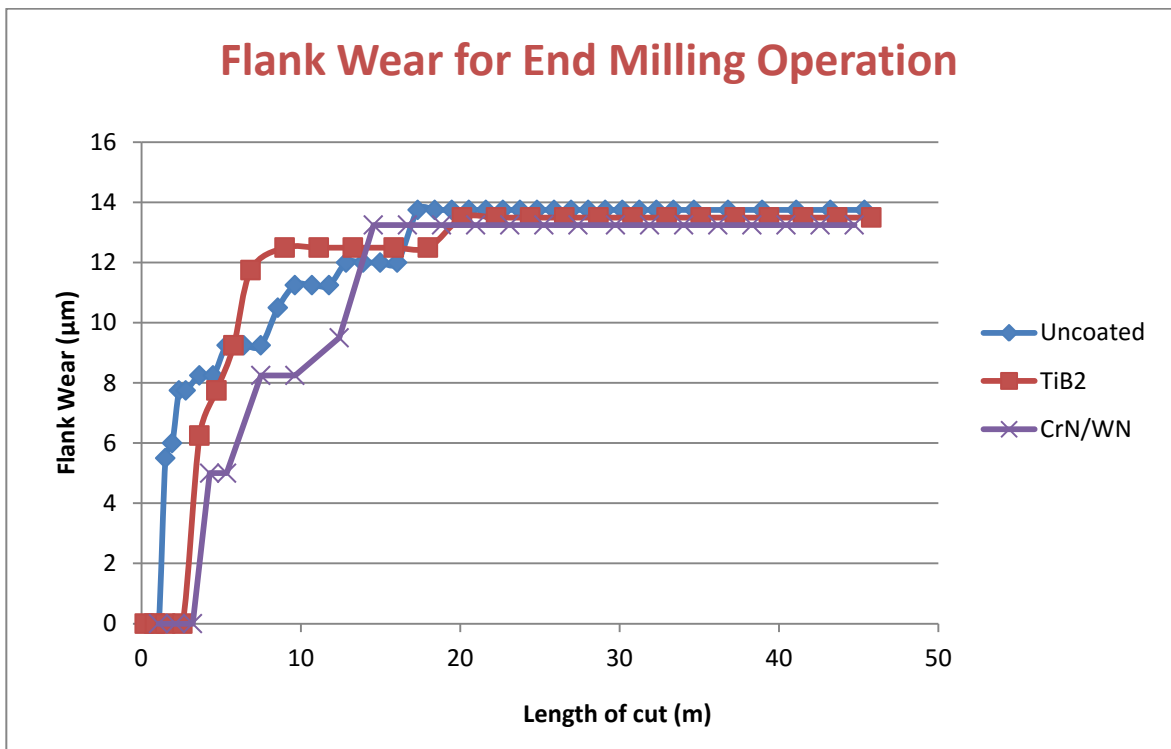


Figure 59: Average flank wear of uncoated, TiB₂-LHC and CrN/WN coated tool during end milling operation

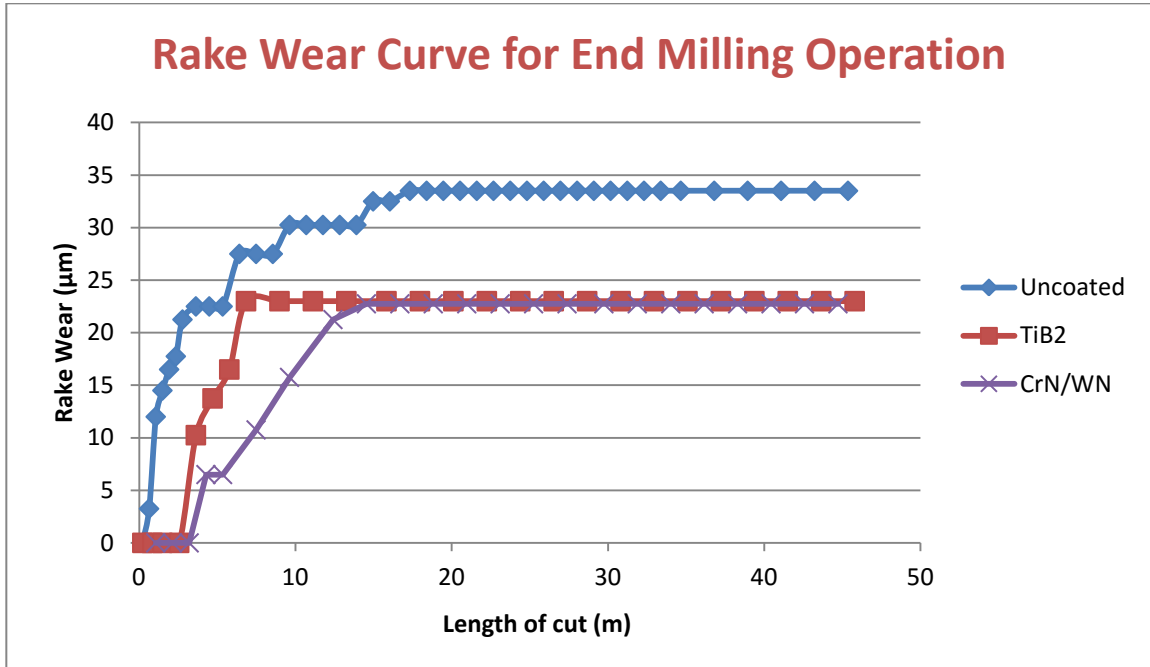


Figure 60: Average rake wear of uncoated, TiB₂-LHC and CrN/WN coated tool during end milling operation

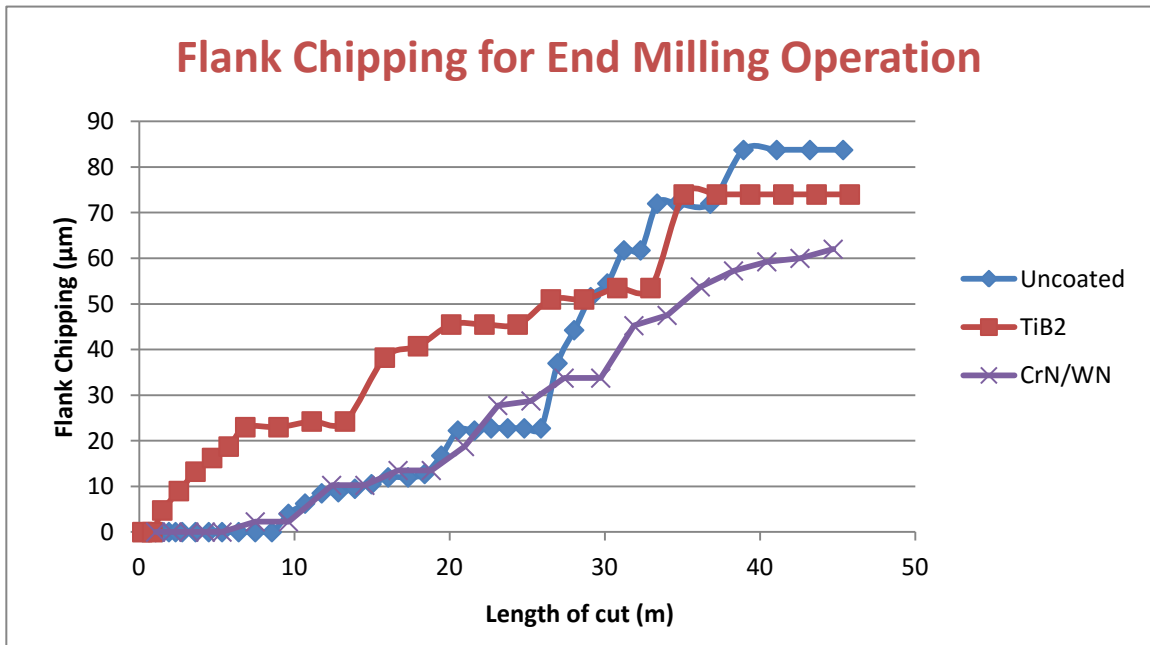


Figure 61: Average flank chipping of uncoated, TiB₂-LHC and CrN/WN coated tool during end milling operation

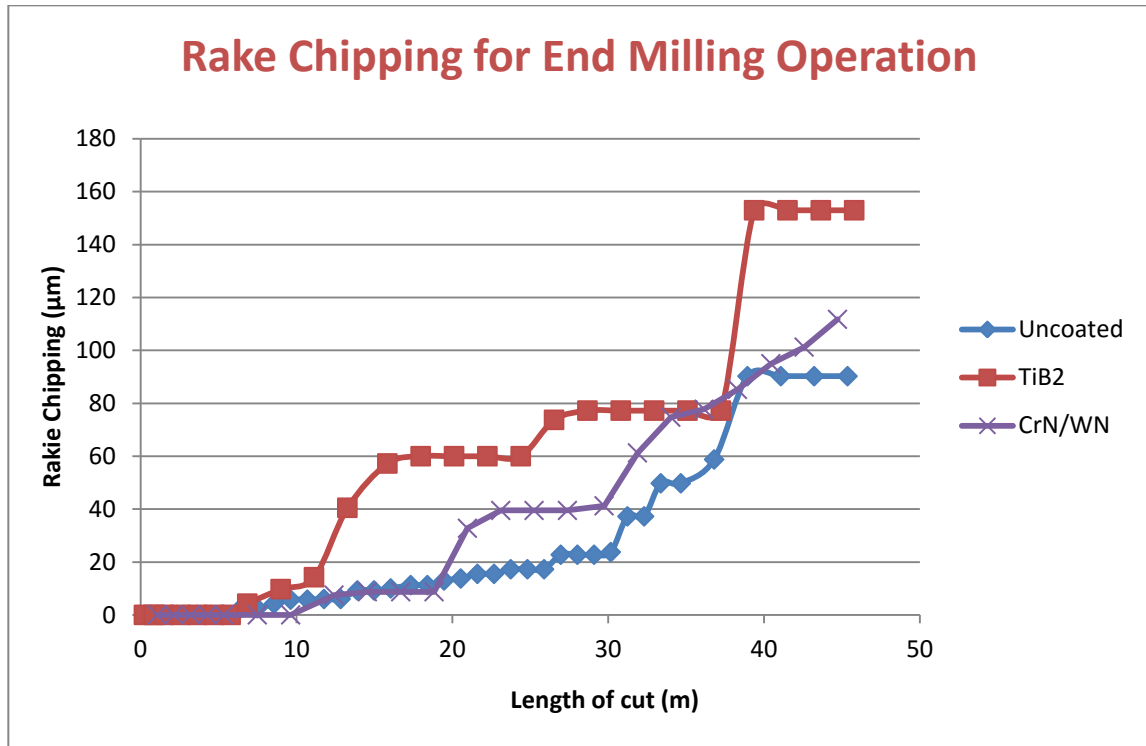


Figure 62: Average rake chipping of uncoated, TiB₂-LHC and CrN/WN coated tool during end milling operation

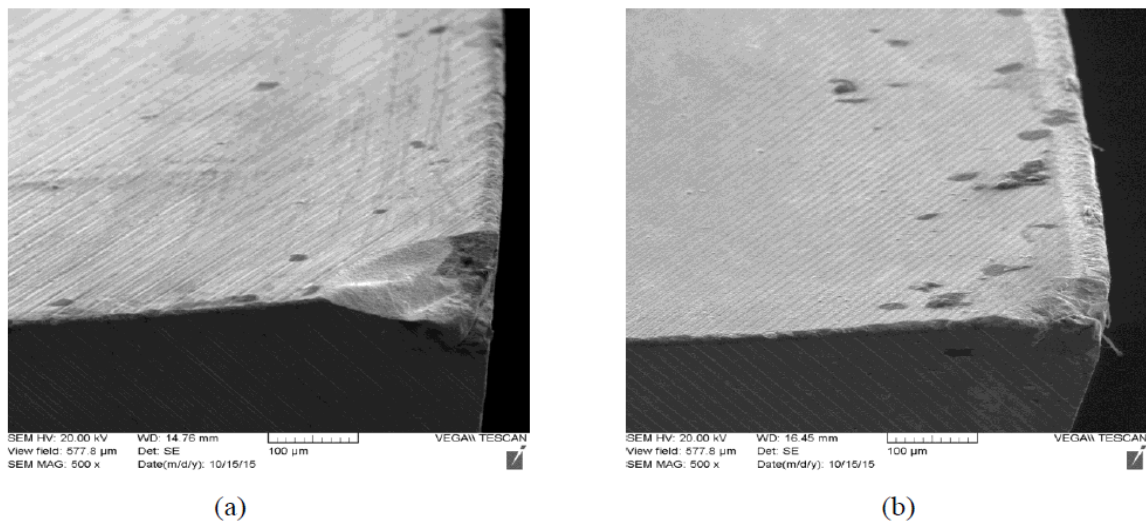


Figure 63: SEM image of one tooth of the worn four flute end mill tool after 50 m cut: (a) Uncoated (b) TiB₂-LHC coated

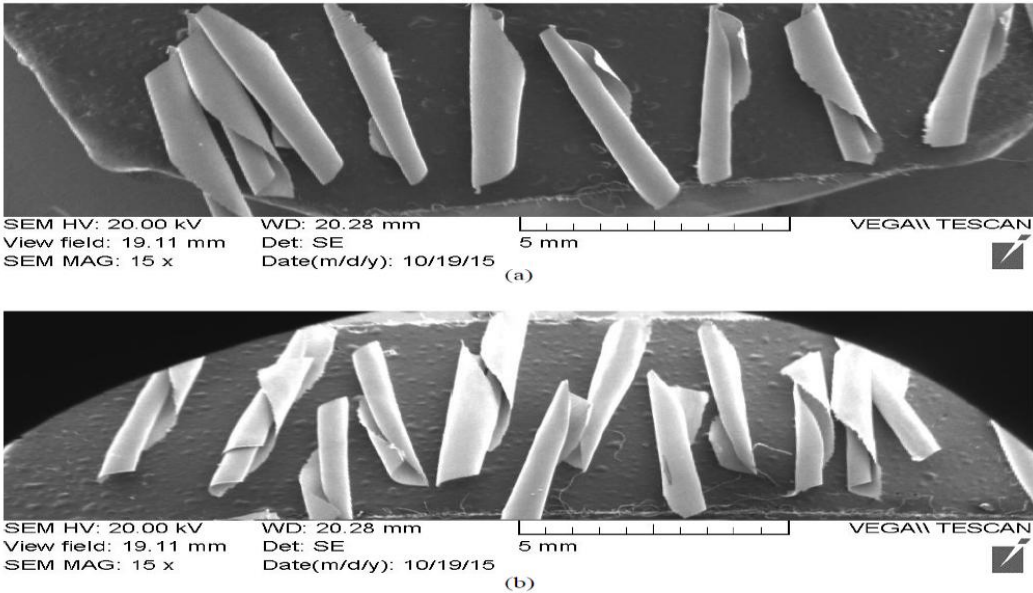


Figure 64: SEM image of chips during end milling for:
(a) uncoated tool (b) TiB₂-LHC coated tool

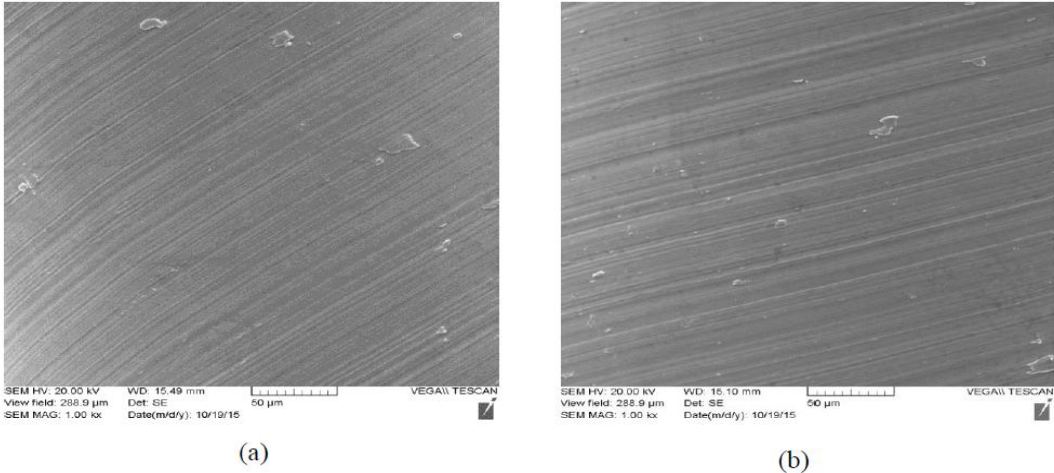


Figure 65: SEM image of chip under-surface morphology:
(a) Uncoated tool and (b) TiB₂-LHC coated tool

SEM analyses of the teeth and chips of the uncoated and TiB₂-LHC coated end mills were carried out. Figure 63 shows the SEM image of one tooth of the uncoated and TiB₂-LHC coated end mill. It shows that chipping of the tool occurs at the tip. This occurs mainly due to the constant generation and breakage of built up edge at the tip. It should be noted here that although the SEM image shows larger chipping for the uncoated tool for this particular tooth, this is not the case for all the teeth and the average chipping for both the tools is fairly similar. Figure 64 and Figure 65 compares the shapes and under-surface morphology of the chips for uncoated and TiB₂-LHC coated end mills. There is no distinct difference between the chip shapes and roughness. Hence it can be said that although TiB₂-LHC coated tools showed significant tool life improvement for turning operations, it is not that effective in end milling. This may be due to the intermittent nature of the cutting process that happens in end milling. In end milling, each tooth is actually engaged for a part of the cutting cycle and is therefore exposed to repeated heating and cooling. Therefore, since tribofilm formation is very temperature dependant, the B₂O₃ tribo-oxide formation is probably not as efficient as in continuous cutting processes like turning and fails to effectively address the built up edge formation during end milling.

Chapter 5: Conclusion

In this research, several self-adaptive PVD coatings have been investigated in an attempt to reduce tool wear during machining of Ti6Al4V alloy. Detailed experimental studies and analyses were carried out to understand the effectiveness and behaviour of the coatings. Special attention was given to the tribofilm generation which is characteristic of self-adaptive coatings. Tribofilm generation studies have not been made in relation to Ti6Al4V machining in the past before. The research can be broken down into five stages. Firstly, experimental studies and analyses were carried out to identify the benchmark tool between uncoated and TiAlN coated tools for rough turning operations against which all other coatings will be tested. Secondly, tool life studies of a variety of coatings were conducted for both rough and finish turning operations and the coatings that outperform the benchmark tool were identified. Thirdly, detailed analyses were carried out on selected best coatings to understand the tribofilm formation and how it affects tool wear. Fourthly, the performance effects of the chip breaker profile of the cutting tools on tool wear were investigated. Finally, the best identified coatings for turning operation was implemented in end milling operation to investigate whether the coating was effective in milling processes as well or not. Based on the results of the current research, following conclusions can be drawn:

1. Tool life studies for uncoated and TiAlN coated straight grade cemented carbide tools reveal that uncoated straight grade cemented carbides are better in rough turning of Ti6Al4V alloy. Tool wear in both rake and flank face is higher for the TiAlN coated tool. Intensive sticking of workpiece material is observed on the TiAlN coated tool as compared to the uncoated tool. Elemental mapping and XPS results suggest that the formation of a solid lubricious WO_2 tribofilm contributes to better performance of the uncoated tools. For TiAlN coated tools such tribo-oxide formations are less probable due to the shielding effect of the coating left on the oxidized tool.
2. Experimental tool life studies comparing different coatings against an uncoated tool for both rough turning and finish turning operations showed that TiCrAlBN, TiAlN/WN, CrWN/WN, CrWN, CrN/WN-WC, CrC/WC and CrWC/CrWN coated tools perform worse than uncoated tools. Whereas the TiB_2 coated tool gave the best performance followed by CrN/WN and CrN/ZrN coated tools respectively.
3. The TiB_2 coated tool gave at least a 65% lower tool wear rate as compared to the uncoated tool over a cutting length of 3000 m for rough turning.
4. CrN/WN coated tool gave at least 44% lower tool wear as compared to the uncoated tool for a cutting length of 3000 m for rough turning.
5. SEM images of the uncoated and TiB_2 coated tool showed significant built up edge formation on the uncoated tool as compared to the TiB_2 coated tool. XPS studies of the built up material showed similar chemical composition for both

uncoated and TiB₂ coated tool. This confirmed that the built up material is mainly coming from the workpiece. EDS and XPS studies performed on the worn TiB₂ coated tool revealed that the coating tribo-oxidizes to form a liquid lubricious B₂O₃ phase reducing friction at the tool-chip and tool-workpiece interfaces decreasing BUE formation and tool wear significantly. This finding is unique and effectively describes why TiB₂ coated tools gives higher tool performance. Such tribofilm generation studies have not been made in the past. Generation of lubricious B₂O₃ tribo-phase is 4.1 times higher on the rake face compared to the flank face as temperature on the rake face is typically higher.

6. Lower built up edge formation is observed on CrN/WN coated tool compared to the uncoated tool. XPS analyses showed that in addition to the W-O tribo-oxides formation, significant amount of Cr-O tribo-oxides are also formed on the worn CrN/WN coated tool. Cr oxides have lubricating properties and thus are able to reduce friction decreasing tool wear.
7. Cutting force comparisons between uncoated and TiB₂ coated tools disclosed that lower cutting forces are registered for TiB₂ coated tool in all directions (radial, feed and tangential). Approximately a 9% reduction in average forces was observed for the TiB₂ coated tool. This complimented tool life and XPS studies and reconfirmed that TiB₂ coating is able to reduce friction due to formation of liquid B₂O₃ lubricant.
8. Curlier chips with smoother undersurface were produced with the TiB₂ coated tool as compared to the uncoated tool indicating the effectiveness of the coating in

providing better frictional characteristics at the contact interfaces. The thickness of the chips for TiB₂ coated tool was lower than the uncoated tool giving a higher shear plane angle. Hence, it indicated that lower shearing forces were acting on the chips complimenting the cutting force data. The ratio of radial force to tangential force was also found to be lower for the TiB₂ coating confirming a reduction of friction during cutting.

9. XRD and nano-indentation tests revealed that TiB₂ coating had compressive residual stress and lower hardness which were shown to be beneficial for lowering friction at contact interfaces.
10. Experimental studies with different chip breaker profiles revealed that tools with positive chip breaker profile (Kennametal CNMP432 insert type) significantly reduces tool wear and BUE formation as compared to tools with a general chip breaker profile (Kennametal CNMG432 insert type). Uncoated tools with positive chip breaker profile gave at least a 33% lower tool wear rate as compared to the uncoated tool with general chip breaker profile over a cutting length of 3000 m for rough turning. This study is unique and effects of chip breaker profiles on tool wear for Ti6Al4V machining have not been conducted in the past.
11. Investigation of cutting forces showed a significant reduction in cutting forces for tools with a positive chip breaker profile as compared to their counter parts with general chip breaker profile. A reduction of 27% in average cutting forces was observed for uncoated tool with the positive chip breaker profile as compared to uncoated tool with the general chip breaker profile.

12. The chips for tools with the positive chip breaker profile were much curlier and smaller indicating smaller tool-chip contact area and reduced friction. The thicknesses of the chips for tools with the positive chip breaker profiles were also lower indicating higher shear plane angles. Hence, lower shearing forces act on the chips. The ratio of radial force to tangential force was found to be lower as well for positive chip breaker profiles.
13. Tool wear investigations between the lower hardness TiB_2 coating and higher hardness TiB_2 coatings showed that the lower hardness coating outperforms the higher hardness coatings. This was due to the fact that low hardness coating exhibited lower shear strength and thus shears more easily under load allowing for a lower coefficient of friction and higher effective lubricity at the contact interfaces. This finding explains why some previous researchers observed higher tool wear with TiB_2 coating compared to uncoated carbide tools.
14. Experimental studies for end milling operations revealed that performance of uncoated tool, TiB_2 -LHC coated and CrN/WN coated tool were similar. Chipping of the tool was significant for all test cases. Hence, the coatings were not as effective as they were in the turning operation. This could be related to the intermittent cutting nature of end milling. The repeated heating and cooling of the tool in end milling possibly hampered the efficient formation of the lubricious liquid B_2O_3 tribo-oxides and self-lubricating solid Cr-O and W-O tribo-oxides in the case of the TiB_2 -LHC and CrN/WN coatings respectively.

Chapter 6: Future Work

Based on the findings of the current research, the following recommendations are made which can further this research:

1. It was established that tribofilms affect tool life significantly. Hence, they might also have a subsequent impact on surface integrity of the workpiece. Surface integrity studies should therefore be conducted to better understand the relationship between the tribofilms formation, surface quality and resulting material microstructure of the workpiece.
2. Other multilayer coatings with different alloying elements that can generate tribofilms must be experimented with in an attempt to further improve tool life.
3. In the current study, chip breaker profile was shown to affect tool wear during Ti6Al4V machining. Hence, the effect of other tool geometry e.g. different rake angle should also be studied.
4. Effect of cutting conditions e.g. cutting speed should also be studied.
5. Further studies with different multilayer and bi-layer coatings should be conducted for milling operations. Special attention should be given to tool chipping that was observed in the current research during milling operations.
6. Advanced and accurate methods of measuring temperatures must be developed to measure the cutting temperatures as temperature plays a significant role in tribofilm formation.

7. Vibration and dynamic studies should be included to study their impact on tool life and overall performance of the tool especially for milling operations as this might give some insight into why chipping of the tool occurs.

References

- [1] R. R. Boyer, “An overview on the use of titanium in the aerospace industry,” *Mater. Sci. Eng.*, vol. 213, pp. 103–114, 1996.
- [2] T. M. Arif, “Impact of tribosystem compatibility on tool wear and surface integrity (M.A.Sc. Dissertaion),” M.A.Sc. Dissertaion, Mechanical Engineering Department, McMaster University, Canada, 2015.
- [3] S. Miller, “Advanced materials means advanced engines,” *Interdiscip. Sci. Rev.*, vol. 21, no. 2, pp. 117–129, 1996.
- [4] K. D. Bouzakis, N. Michailidis, G. Skordaris, E. Bouzakis, D. Biermann, and R. M’Saoubi, “Cutting with coated tools: Coating technologies, characterization methods and performance optimization,” *CIRP Ann. - Manuf. Technol.*, vol. 61, no. 2, pp. 703–723, 2012.
- [5] *Australian Standard, Appendix B P35*. .
- [6] Y. C. Yen, J. Söhner, B. Lilly, and T. Altan, “Estimation of tool wear in orthogonal cutting using the finite element analysis,” *J. Mater. Process. Technol.*, vol. 146, no. 1, pp. 82–91, 2004.
- [7] M. C. Shaw, *Metal Cutting Principles*, Second Edi. Oxford University Press, Inc., 2005.
- [8] U. Khandey, “Optimization of surface roughness, material removal rate and cutting tool flank wear in turning using extended taguchi approach,” National Institute of Technology, Rourkela, India, 2009.

- [9] L. Ning, “Nano-multilayered Self-adaptive Hard PVD Coatings for Dry High Performance Machining,” PhD Dissertaion, Mechanical Engineering Department, McMaster University, Canada, 2007.
- [10] H. A. Jehn, “Multicomponent and multiphase hard coatings for tribological applications,” *Surf. Coatings Technol.*, vol. 131, no. 1–3, pp. 433–440, 2000.
- [11] German S. Fox-Rabinovich and A. I. Kovalev, “Self-Organization and Structural Adaptation during Cutting and Stamping Operations,” in *Self-organization during Friction*, CRC Press, Taylor and Francis Group, Boca Raton, NW, USA, 2006.
- [12] G. Fox-Rabinovich, I. Gershman, M. Hakim, M. Shalaby, J. Krzanowski, and S. Veldhuis, “Tribofilm Formation As a Result of Complex Interaction at the Tool/Chip Interface during Cutting,” *Lubricants*, vol. 2, no. 3, pp. 113–123, 2014.
- [13] E. O. Ezugwu, J. Bonney, and Y. Yamane, “An overview of the machinability of aeroengine alloys,” *J. Mater. Process. Technol.*, vol. 134, no. 2, pp. 233–253, 2003.
- [14] X. Yang and C. Richard Liu, *Machining Titanium and Its Alloys*, vol. 3, no. 1. 1999.
- [15] H. B. B. and F. H. F. J. R. Myers, “Corrosion Behavior and Use of Titanium and Its Alloys,” *J. Miner. Met. Mater. Soc.*, vol. 36, no. 10, pp. 50–60, 1984.
- [16] A. R. Machado and J. Wallbank, “Machinig of titanium and its alloys-a review,” *Proc Instn Mech Engrs, Part B J. Eng. Manuf.*, vol. 204, pp. 53–60, 1990.

- [17] A. Hosseini and H. A. Kishawy, “Cutting Tool Materials and Tool Wear,” in *Machining of Titanium Alloys*, vol. 37, no. 4, Metals Forming, Machining and Tribology, 1985, pp. 27–35.
- [18] Y. Honnorat, “Issues and breakthrough in the manufacture of turboengine titanium parts,” *Mater. Sci. Eng. A*, vol. 213, no. 1–2, pp. 115–123, 1996.
- [19] E. O. Ezugwu and Z. M. Wang, “Titanium alloys and their machinability,” *J. Mater. Process. Technol.*, vol. 68, no. 3, pp. 262–274, 1997.
- [20] M. M. Schwartz, *Encyclopedia of materials, parts, and finishes*, 2nd ed. CRC Press LLC, 2002.
- [21] R. Gaddam, “Effect of Boron and Hydrogen on Microstructure and Mechanical Properties of Cast Ti-6Al-4V,” Lulea University of Technology, 2011.
- [22] X. Yang and C. Richard Liu, *Machining Titanium and Its Alloys*, vol. 3, no. 1. 1999.
- [23] E. M. Trent, *Metal Cutting*, 2nd ed. Butterworths & Co (Publishers) Ltd., 1984.
- [24] M. Fitzsimmons and V. K. Sarin, “Development of CVD WC-Co coatings,” *Surf. Coatings Technol.*, vol. 137, no. 2–3, pp. 158–163, 2001.
- [25] S. H. I. Jaffery and P. T. Mativenga, “Wear mechanisms analysis for turning Ti-6Al-4V-towards the development of suitable tool coatings,” *Int. J. Adv. Manuf. Technol.*, vol. 58, no. 5–8, pp. 479–493, 2012.
- [26] R. Komanduri and B. F. V. O. N. Turkovich, “New observations on the mechanism when machining titanium alloys of chip formation,” vol. 69, pp. 179–188, 1981.

- [27] M. Rahman, Y. S. Wong, and a. R. Zareena, “Machinability of Titanium Alloys,” *JSME International Journal Series C*, vol. 46, no. 1, pp. 107–115, 2003.
- [28] A. Pramanik, M. N. Islam, A. Basak, and G. Littlefair, “Machining and Tool Wear Mechanisms during Machining Titanium Alloys,” *Adv. Mater. Res.*, vol. 651, no. February 2016, pp. 338–343, 2013.
- [29] D. Ulutan and T. Ozel, “Machining induced surface integrity in titanium and nickel alloys: A review,” *Int. J. Mach. Tools Manuf.*, vol. 51, no. 3, pp. 250–280, 2011.
- [30] A. Hosseini, H. A. Kishawy, and H. M. Hussein, “Machinability of Titanium and Its Alloys,” in *Machinability of Advanced Materials*, ISTE Ltd and John Wiley & Sons, Inc., 2014, pp. 95–118.
- [31] B. M. Kramer, “On tool materials for high speed machining,” *J. Eng. Ind.*, vol. 109, no. 2, pp. 87–91, 1987.
- [32] F. Nabhani, “Machining of aerospace titanium alloys,” *Robot. Comput. Integr. Manuf.*, vol. 17, no. 1–2, pp. 99–106, 2001.
- [33] A. K. M. N. Amin, A. F. Ismail, and M. K. Nor Khairusshima, “Effectiveness of uncoated WC–Co and PCD inserts in end milling of titanium alloy—Ti–6Al–4V,” *J. Mater. Process. Technol.*, vol. 192–193, pp. 147–158, Oct. 2007.
- [34] S. H. I. Jaffery and P. T. Mativenga, “Wear mechanisms analysis for turning Ti-6Al-4V-towards the development of suitable tool coatings,” *Int. J. Adv. Manuf. Technol.*, vol. 58, no. 5–8, pp. 479–493, 2012.
- [35] N. Corduan, T. Himbart, G. Poulachon, M. Dessoly, M. Lambertin, J. Vigneau, and B. Payoux, “Wear Mechanisms of New Tool Materials for Ti-6Al-4V High

- Performance Machining,” *CIRP Ann. - Manuf. Technol.*, vol. 52, no. 1, pp. 73–76, 2003.
- [36] A. Hosseini and H. A. Kishawy, “Cutting Tool Materials and Tool Wear,” in *Machining of Titanium Alloys*, vol. 37, no. 4, Metals Forming, Machining and Tribology, 1985, pp. 27–35.
- [37] F. Klocke, *Manufacturing processes 1: Cutting*. 2010.
- [38] Z. C. Lin and D. Y. Chen, “A study of cutting with a CBN tool,” *J. Mater. Process. Tech.*, vol. 49, no. 1–2, pp. 149–164, 1995.
- [39] Z. a. Zoya and R. Krishnamurthy, “Performance of CBN tools in the machining of titanium alloys,” *J. Mater. Process. Technol.*, vol. 100, no. 1, pp. 80–86, 2000.
- [40] A. Chakraborty, K. K. Ray, and S. B. Bhaduri, “Comparative Wear Behavior of Ceramic and Carbide Tools During High Speed Machining of Steel,” *Mater. Manuf. Process.*, vol. 15, no. 2, pp. 269–300, 2000.
- [41] P. A. Dearnley and A. N. Greason, “Evaluation of principal wear mechanisms of cemented carbides and ceramics used for machining titanium alloy IMI 318,” *Mater. Sci. Technol.*, vol. 2, no. 1, pp. 47–58, 1986.
- [42] N. Narutaki, A. Murakoshi, S. Motonishi, and H. Takeyama, “Study on Machining of Titanium Alloys,” *CIRP Ann. - Manuf. Technol.*, vol. 32, no. 1, pp. 65–69, 1983.
- [43] Â. De, J. Pe, J. I. Llorente, J. A. Sa, L. N. Lo, and Â. Meca, “Advanced cutting conditions for the milling of aeronautical alloys,” vol. 100, pp. 1–11, 2000.
- [44] M. Rahman, Z.-G. Wang, and Y.-S. Wong, “A Review on High-Speed Machining of Titanium Alloys,” *JSME Int. J. Ser. C*, vol. 49, no. 1, pp. 11–20, 2006.

- [45] H. J. SIEKMANN, “How to machine titanium,” *Tool Eng.*, vol. 34, no. 1, pp. 78–82, 1955.
- [46] R. Edwards, *Cutting tools*. Institute of Materials, London, 1993.
- [47] R. M. Freeman, “The machining of titanium and some of its alloys,” Ph.D Thesis, University of Birmingham, UK, 1974.
- [48] A. Ikuta, K. Shinozaki, H. Masuda, and Y. Yamane, “Consideration of the adhesion mechanism of Ti alloys using a cemented carbide tool during the cutting process,” vol. 127, pp. 251–255, 2002.
- [49] B. M. Hartung, P.D. dan Kramer, “Tool wear in machining titanium,” *Ann. CIRP*, vol. 30, no. 1, pp. 75–80, 1982.
- [50] W. A. Bryant, “Cutting tool for machining titanium and titanium alloys,” US Patent 5,718,541, 1998.
- [51] Y. Naerheim and E. M. Trent, “Diffusion wear of cemented carbide tools when cutting steel at high speeds,” no. December, pp. 548–556, 1977.
- [52] P. A. Dearnley and E. M. Trent, “Wear mechanisms of coated carbide tools,” *Met. Technol.*, vol. 9, no. 1, pp. 60–75, 1982.
- [53] A. Jawaid, C. H. Che-Haron, and A. Abdullah, “Tool wear characteristics in turning of titanium alloy Ti-6246,” *J. Mater. Process. Technol.*, vol. 92–93, pp. 329–334, 1999.
- [54] Y. Su, N. He, L. Li, and X. L. Li, “An experimental investigation of effects of cooling/lubrication conditions on tool wear in high-speed end milling of Ti-6Al-4V,” *Wear*, vol. 261, no. 7–8, pp. 760–766, 2006.

- [55] W. Min and Z. Youzhen, “Diffusion wear in milling titanium alloys,” *Mater. Sci. Technol.*, vol. 4, pp. 548–553, 1988.
- [56] M. Lee, “The failure characteristics of cutting tools machining titanium alloys at high speed,” *Adv. Process. Methods Titan.*, pp. 275–287, 1981.
- [57] S. K. Bhattacharya, A. R. Machado, E. O. Ezugwu, and I. R. Pashby, “Milling Low Alloy and Martensitic Stainless Steels With Cemented Carbide Insert Face Mills,” in *8 CBECIMAT, Campinas, Brazil*, 1988.
- [58] M. A. Ezugwu EO, “Face milling of aerospace materials,” in *Proceedings of the 1st international conference on behaviour of materials in machining*, 1988, pp. 3–11.
- [59] W. A. Bryant, “Cutting insert for milling titanium and titanium alloys,” 5,984,593, 1999.
- [60] W. Min and Z. Youzhen, “Investigation on Tool Wear Mechanisms in Milling of Titanium Alloys,” in *16th NAMRC: North American Manuf. Res. Conf.*, 1988, pp. 190–194.
- [61] C. H. Che-Haron, “Tool life and surface integrity in turning titanium alloy,” *J. Mater. Process. Technol.*, vol. 118, no. 1–3, pp. 231–237, 2001.
- [62] M. Nouari and H. Makich, “On the Physics of Machining Titanium Alloys: Interactions between Cutting Parameters, Microstructure and Tool Wear,” *Metals (Basel)*, vol. 4, no. 3, pp. 335–358, 2014.

- [63] G. A. Ibrahim, C. H. Che Haron, and J. A. Ghani, "Tool Wear Mechanism in Continuous Cutting of Difficult-to-Cut Material under Dry Machining," *Adv. Mater. Res.*, vol. 126–128, pp. 195–201, 2010.
- [64] P. Pawar, S. Joshi, A. Tewari, and S. Joshi, "Tool wear mechanisms in machining of titanium alloys," no. 345, pp. 4–8, 2012.
- [65] T. Burger, Uli, Kuttolamadom, Mathew, Bryan, April, Mears, Laine and Kurfess, "Volumetric flank wear characterization for titanium milling insert tools," *Proc. 2009 ASME Int. Manuf. Sci. Eng. Conf.*, pp. 1–8, 2009.
- [66] T. Cselle and A. Barimani, "Today's applications and future developments of coatings for drills and rotating cutting tools," *Surf. Coatings Technol.*, vol. 76–77, no. PART 2, pp. 712–718, 1995.
- [67] F. H. F. D. Eylon, S. Fujishiro, Pamela J. Postans, "High-temperature titanium alloys—a review," *J. Miner. Met. Mater. Soc.*, vol. 36, no. 11, pp. 55–62, 1984.
- [68] L. Settineri and M. G. Faga, "Nanostructured Cutting Tools Coatings for Machining Titanium," *Mach. Sci. Technol.*, vol. 12, no. 2, pp. 158–169, 2008.
- [69] A. Jawaid, S. Sharif, and S. Koksai, "Evaluation of wear mechanisms of coated carbide tools when face milling titanium alloy," *J. Mater. Process. Technol.*, vol. 99, no. 1–3, pp. 266–274, Mar. 2000.
- [70] E.O. Ezugwu and Z.M. Wang, "Tool life and workpiece surface integrity evaluation when machining Ti6Al4V with PVD coated tools," *Surf. Modif. Technol.*, vol. IOM 10, pp. 414–426, 1997.

- [71] Z. M. Wang and E. O. Ezugwu, "Performance of PVD-Coated Carbide Tools When Machining Ti-6Al-4V[©]," *Tribol. Trans.*, vol. 40, no. 1, pp. 81–86, 1997.
- [72] T. Özel, M. Sima, A. K. Srivastava, and B. Kaftanoglu, "Investigations on the effects of multi-layered coated inserts in machining Ti-6Al-4V alloy with experiments and finite element simulations," *CIRP Ann. - Manuf. Technol.*, vol. 59, no. 1, pp. 77–82, 2010.
- [73] R. Cherukuri and P. Molian, "Lathe Turning of Titanium Using Pulsed Laser Deposited, Ultra-Hard Boride Coatings of Carbide Inserts," *Mach. Sci. Technol.*, vol. 7, no. 1, pp. 119–135, 2003.
- [74] C. H. C. Haron, A. Ginting, and H. Arshad, "Performance of alloyed uncoated and CVD-coated carbide tools in dry milling of titanium alloy Ti-6242S," *J. Mater. Process. Technol.*, vol. 185, no. 1–3, pp. 77–82, 2007.
- [75] B. D. Beake, J. F. Smith, a. Gray, G. S. Fox-Rabinovich, S. C. Veldhuis, and J. L. Endrino, "Investigating the correlation between nano-impact fracture resistance and hardness/modulus ratio from nanoindentation at 25-500°C and the fracture resistance and lifetime of cutting tools with Ti_{1-x}Al_xN (x = 0.5 and 0.67) PVD coatings in milling operat," *Surf. Coatings Technol.*, vol. 201, no. 8, pp. 4585–4593, 2007.
- [76] H. G. Prengel, P. C. Jindal, K. H. Wendt, a. T. Santhanam, P. L. Hegde, and R. M. Penich, "A new class of high performance PVD coatings for carbide cutting tools," *Surf. Coatings Technol.*, vol. 139, no. 1, pp. 25–34, 2001.

- [77] J. Rao, T. Rose, M. Craig, and J. R. Nicholls, “Wear Coatings For High Load Applications,” *Procedia CIRP*, vol. 22, pp. 277–280, 2014.
- [78] A. Devillez, F. Schneider, S. Dominiak, D. Dudzinski, and D. Larrouquere, “Cutting forces and wear in dry machining of Inconel 718 with coated carbide tools,” *Wear*, vol. 262, no. 7–8, pp. 931–942, 2007.
- [79] J. M. Castanho and M. T. Vieira, “Effect of ductile layers in mechanical behaviour of TiAlN thin coatings,” *J. Mater. Process. Technol.*, vol. 143–144, no. 1, pp. 352–357, 2003.
- [80] S. S. Gill, J. Singh, H. Singh, and R. Singh, “Investigation on wear behaviour of cryogenically treated TiAlN coated tungsten carbide inserts in turning,” *Int. J. Mach. Tools Manuf.*, vol. 51, no. 1, pp. 25–33, 2011.
- [81] A. Erdemir, “Solid Lubricants and Self-Lubricating Films,” in *Modern Tribology Handbook, Two Volume Set*, CRC Press, 2000.
- [82] S. M. Aouadi, H. Gao, a. Martini, T. W. Scharf, and C. Muratore, “Lubricious oxide coatings for extreme temperature applications: A review,” *Surf. Coatings Technol.*, vol. 257, pp. 266–277, 2014.
- [83] A. Erdemir, “A crystal chemical approach to the formulation of self-lubricating nanocomposite coatings,” *Surf. Coatings Technol.*, vol. 200, no. 5–6, pp. 1792–1796, 2005.
- [84] A. Biksa, K. Yamamoto, G. Dosbaeva, S. C. Veldhuis, G. S. Fox-Rabinovich, A. Elfizy, T. Wagg, and L. S. Shuster, “Wear behavior of adaptive nano-multilayered

- AlTiN/MexN PVD coatings during machining of aerospace alloys,” *Tribol. Int.*, vol. 43, no. 8, pp. 1491–1499, 2010.
- [85] G. Montay, A. Cherouat, A. Nussair, and J. Lu, “Residual Stresses in Coating Technology,” *J. Mater. Sci. Technol.*, vol. 20, no. Suppl. 1, 2004.
- [86] F. Klocke, *Manufacturing processes 1: turning, milling, drilling*, no. 7858. Springer, 2011.
- [87] R. L. Vaughn, *Modern Metals Machining Technology*. 1966.
- [88] *Modern Metal Cutting, A Practical Handbook*. Sandvik Coromant.
- [89] H. K. Tönshoff, B. Denkena, T. Friemuth, and C. Spengler, “Influence of different grinding processes on coating adhesion on cutting tools,” *Proc. 3rd Int. Conf. – Coat. Manuf. Eng. EUREKA Partnering Event*, pp. 3–16, 2002.
- [90] G. Boothroyd and W. A. Knight, *Fundamentals of machining and machine tools*, Third. CRC Press, Taylor and Francis Group, Boca Raton, NW, USA, 2006.